Dissertation

submitted to the

Combined Faculty of Natural Sciences and Mathematics

of the Ruperto Carola University Heidelberg, Germany

for the degree of

Doctor of Natural Sciences

Presented by

M.Sc. Sevinç Gücüm

born in: Gebze/Turkey

Oral examination: 11.06.2021

Modeling hypo-*N*-glycosylation in medaka, *Oryzias latipes*, to decipher mechanisms of Congenital Disorders of Glycosylation

Referees: Prof. Dr. Ingrid Lohmann
Prof. Dr. Sabine Strahl

Abstract

Glycosylation is one of the most abundant forms of ubiquitous co- and posttranslational modifications affecting protein stability, transportation, and function. The most common type of glycosylation is *N*-glycosylation, which refers to the addition of glycans to the Nitrogen of Asparagine. Mutations of enzymes involved in this pathway give rise to Congenital Disorders of Glycosylation (CDG) by generating hypomorphic alleles rendering glycosylation enzymes with partial activity. Since animal models of CDGs mostly rely on mutations leading to complete loss of function, the human situation is not recapitulated. Here, we present two distinct hypo-*N*-glycosylation fish models to address the effects of reduced glycosylation on animal physiology and at the molecular level.

The alg2^{hypo} model was generated by introducing a well-defined mutation of alpha-1,3/1,6-mannosyltransferase 2, *Alg2*, from an ALG2-CDG patient allele into the orthologous region of medaka (*Oryzias latipes*) via CRISPR/Cas9 targeted genome editing. Under homozygosity, this model displayed multisystemic phenotypes closely resembling patient symptoms, including reduction in white matter, motor development abnormalities and craniofacial dismorphism. *N*-glycome analysis revealed a total reduction in *N*-glycan occupancy both in whole medaka and patient fibroblast samples, which in turn led to changes in protein abundance. Accordingly, mass spectrometry of both whole hatchling and dissected eye samples showed reduction in proteins responsible for photoreceptor signaling, as well as upregulation of proteins responsible for nucleotide-sugar metabolism, *N*-glycosylation machinery, vesicle trafficking and protein folding. Immunofluorescence analysis revealed rod cell death leading to a condition called retinitis pigmentosa or night blindness seen among patients with other CDG types. Finally, mRNA injections into alg2^{hypo} line synthesized from both medaka and human full-length *Alg2* coding sequences rescued the multisystemic phenotypes and overcame early-juvenile lethality.

In a second model, phosphomannomutase 2 (Pmm2) enzyme was depleted by an engineered degron, deGradFP, to create a proxy for PMM2-CDG model by reducing the enzyme amount to different levels via auxin induction. To this end, Pmm2 was tagged endogenously in its C-terminal end with GFP and was successfully depleted when F-box protein, TIR1, was ectopically expressed together with an auxin-induced degron (AID) fused to a GFP nanobody binding to GFP tagged proteins.

All in all, this study presents two different medaka models of hypo-*N*-glycosylation to study the mechanism behind multisystemic disease phenotypes seen among CDG patients. Both models serve as promising platforms for pre-clinical studies, such as drug-screening and gene therapy approaches to develop novel therapeutic avenues for treating symptoms of CDGs.

Zusammenfassung

Glykosylierung gehört zu den häufigsten Formen ubiquitärer co- und posttranslationaler Modifikationen, die sowohl die Proteinstabilität, als auch deren Transport und Funktion beeinflusst. Der überwiegende Typ ist hierbei die Addition eines Glykans an das Stickstoffatom der Aminosäure Asparagin, was als N-Glykosylierung bezeichnet wird. Mutationen in Enzymen eben jenes Signalwegs bedingen sogenannte angeborene Erkrankungen der Glykosylierung (CDG), bei denen hypomorphe Allele die Aktivität der Glykosylierungsenzyme verringern. Da Tiermodelle von CDG in der Regel auf Mutationen basieren, die kompletten Funktionsverlust nach sich ziehen, wird die klinische Situation nicht ausreichend rekapituliert. In dieser Studie präsentieren wir zwei unterschiedliche auf dem Fischmodell Medaka (Oryzias latipes) basierte hypo-N-Glykosylierungsmodelle zur Untersuchung der Effekte eines reduzierten Glykosylierungslevel auf die Physiologie sowie dessen molekulare Konsequenz.

Das Modell alg2^{hypo} wurde durch die Insertion einer gut definierten Mutation der alpha-1,3/1,6-Mannosyltransferase 2, Alg2, die einem Patientenallel entstammt, in die orthologe Region des Medaka Genoms mittels CRISPR/Cas9 gerichteter Genom-Editierung generiert. Im homozygoten Zustand weist das Modell multisystemische Phänotypen auf, die ähnlich dem klinischen Bild sind, wie unter anderem die Reduktion weißer Gehirnmasse, Abnormalitäten in der motorischen Entwicklung und kraniofaziale Dysmorphismen. Die Analyse des *N*-Glykoms des Medaka Larvenlysats, sowie dem Lysat primärer Patientenfibroblasten ergab eine Reduktion der totalen *N*-Glykan Proteinbelegung, die zu einer Änderung der totalen Proteinabundanz führte. Im Einklang damit zeigten massenspektrometrische Analysen des Proteinlysats ganzer Larven sowie des Lysat isolierter Larvenaugen eine Reduktion an Proteinen die im Photorezeptor-Signalweg involviert sind, wohingegen eine Hochregulierung von Proteinen des Nukleotid-Zucker Metabolismus, des Vesikeltransports, und der Proteinfaltung zu beobachten war. Weiterführende Analysen des Auges anhand von Immunfluoreszenz offenbarten das Absterben der Stabzellen, auch als retinitis pigmentosa oder Netzhautdystrophie bekannt, was so auch in CDG Patienten mit anderem Mutationsspektrum vorzufinden ist. Letztlich konnte das Krankheitsbild der alg2^{hypo} Linie erfolgreich durch mRNA Injektionen der kompletten vom Fisch- oder humanen Allel synthetisierten, kodierenden *Alg2* Sequenz behandelt und die juvenile Lethalität überkommen werden. In einem zweiten Modell wurde das Enzym Phosphomannomutase 2 (Pmm2) mittels eines Degron-Systems, deGradFP, depletiert, was zusätzlich eine Reduktion der Enzymabundanz zu unterschiedlichen Leveln via der Induktion durch Auxin ermöglichte. Hierzu wurde Pmm2 an seinem C-terminus mit GFP fusioniert und konnte abgebaut werden sobald das F-Box Protein TIR1 ektopisch gemeinsam mit einem Auxin-induzierbaren Degron (AID) exprimiert wurde, welches mit einem GFP-Nanobody der GFP markierte Proteine bindet fusioniert war.

Alles in allem beschreibt diese Thesis die Generierung zweier Medaka hypo-N-Glykosylierungsmodelle zum Studium der molekularen Mechanismen die den multisystemischen Phänotypen wie sie in CDG Patienten vorzufinden sind unterliegen. Beide Modelle repräsentieren vielsprechende Plattformen für präklinische Studien, wie zum Beispiel Hochdurchsatz-Wirkstoffscreenings oder Gentherapieverfahren zur Entwicklung neuartiger therapeutischer Ansätze zur Behandlung von CDG.

Table of Contents

Abbreviations

AID	auxin-induced degron
ALG	Asparine linked glycosylation or alpha-1,3/1,6-mannosyltransferase
***C*-**	Carbon
Cas9	CRISPR-associated system 9
CDG	Congenital Disorders of Glycosylation
CMZ	ciliary marginal zone
ConA	concanavalin A
CRISPR	clustered regularly interspaced short palindromic repeats
CUL1	cullin 1
DAPI	4’,6-diamidino-2-phenyindole
DMEM	Dulbecco's Modified Eagle Medium
DNA	deoxyribonucleic acid
Dol	dolichol
dph	days post hatch
dpi	days post injection
ds	double-stranded
E	exon
ER	Endoplasmic Reticulum
ERAD	ER-associated protein degradation
ERT2	estrogen receptor
F	phenylalanine
FCS	fetal calf serum
FP	forward primer
Fuc	fucose
GAG	glycosaminoglycans
Gal	galactose
GalNac	*N*-acetygalacosamine
GCL	ganglion cell layer
gDNA	genomic DNA
GFP	green fluorescent protein
Glc	glucose

GlcA	glucuronic acid
GlcNAc	*N*-acetylglucosamine
H	Histidine
HDR	homology-directed repair
HF	homology flank
hpf	hours post fertilisation
hpi	hours post injection or induction (depends on the context)
hr	hour/s
hs	*Homo sapiens (human)*
IdoA	iduronic acid
IF	immunofluorescence
INL	inner nuclear layer
IPL	inner plexiform layer
L	Leucine
LLO	lipid-linked oligosaccharide
LoxP	locus of X-over P1
Man	mannose
mCherry	monomeric Cherry
min	minute/s
mM	millimolar (10^{-3} Molar)
MPI	mannose phosphate isomerase
MRM	multiple reaction monitoring
mRNA	messenger RNA
MS	mass spectrometry
N (Ans)	Asparagine
***N*-**	Nitrogen
Na-NAA	naphthaleneacetic acid sodium salt
NAA	naphthaleneacetic acid
NaOH	sodium hydroxide
ng	nanogram (10^{-9} gram)
NHEJ	non-homologous end joining
NR	neural retina
***O*-**	Oxygen
ol	*Oryzias latipes (medaka)*

ONL	outer nuclear layer
OPL	outer plexiform layer
P	phosphate
PCR	polymerase chain reaction
Pmm2	phosphomannomutase 2
PP	pyrophosphate
R	Arginine
Rbx	ring box 1
RNA	ribonucleic acid
RP	retinitis pigmentosa
RP	reverse primer
RPE	retinal pigmented epithelium
RT	room temperature
RT-PCR	reverse transcription polymerase chain reaction
S (Ser)	Serine
sec	second/s
sgRNA	single guide RNA
Sia	sialic acid
SKP1	S-phase kinase associated protein 1
ss	single-stranded
ssODN	single-stranded oligodeoxynucleotide
st	developmental stage
T (Thr)	Threonine
TIR1	transport inhibitor response 1
TUNEL	terminal deoxynucleotidyl transferase dUTP nick end labeling
UPR	unfolded protein response
W (Trp)	Tryptophan
WGA	wheat germ agglutinin
xCGE-LIF	multiplexed capillary gel electrophoresis with laser-induced fluorescence detection
Xyl	xylose
αDG	alpha- dystroglycan
µl	microliter (10^{-6} liter)
µM	micromolar (10^{-6} Molar)

1

Introduction

1.1 Glycosylation

Glycosylation is a co- and posttranslational modification, in which oligosaccharides or glycans are covalently attached to proteins or lipids (Goreta et al. 2012; Moremen et al., 2014). It is a well conserved and ubiquitous pathway found in all domains of life. Glycosylation plays an important role in terms of protein folding, quality control, cell-cell adhesion and interaction, pathogen invasion and tumor metastasis (Moremen et al., 2014; Wang & Quanyong et al., 2020). With the addition of 10 different monosaccharides including mannose (Man), fucose (Fuc), galactose (Gal), glucose (Glc), sialic acid (SA), *N*- acetylgalactosamine (GalNAc), *N*-acetylglucosamine (GlcNAc), glucuronic acid (GlcA), iduronic acid (IdoA), and xylose (Xyl), more than thousands of different combinations of complex glycan structures can be created by each cell. In mammalian cells, approximately 700 proteins are estimated to catalyze reactions for glycan assembly, about 200 of which are glycosyltransfrerases using either nucleotide or lipid linked-sugars to build up glycans (Moremen et al., 2014), which makes glycosylation one of the most complex types of post translational modifications.

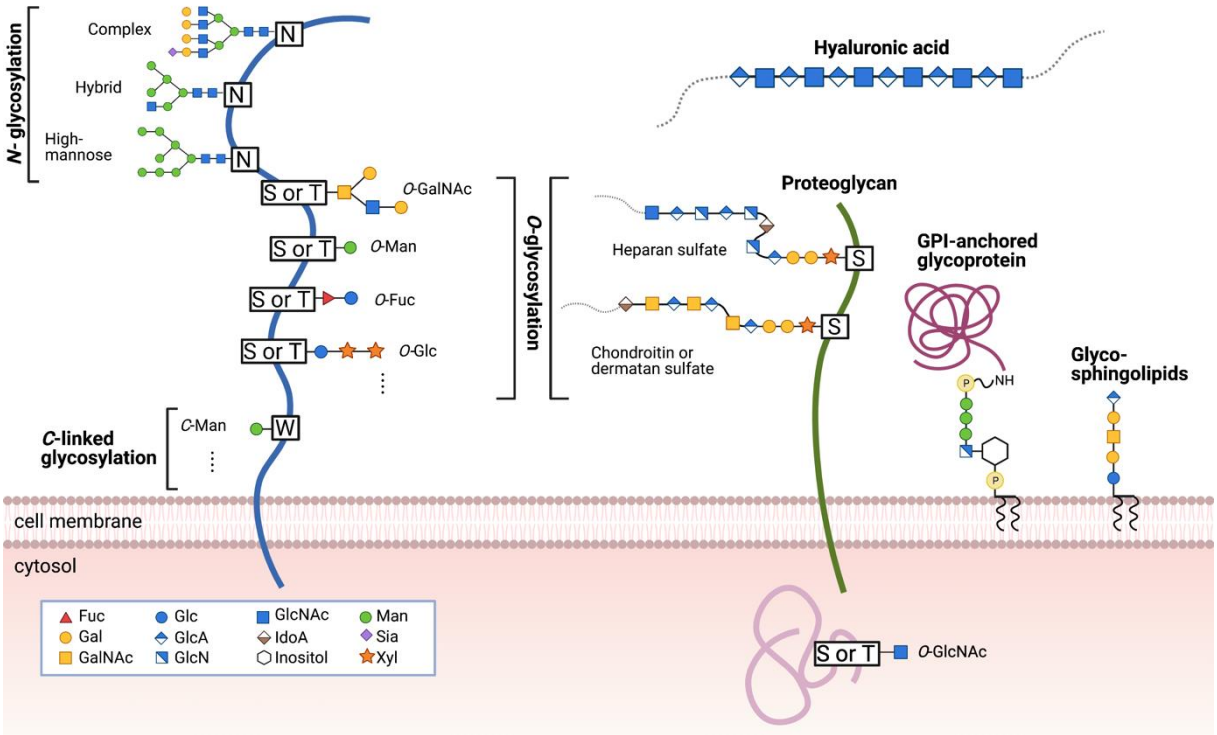

Figure 1: Schematic overview of different glycosylation types
Protein glycosylation involves majorly *N*-glycosylation attached to Asparagines (N), followed by *O*-glcysoylation attached to Serines (S) or Threonines (T). Some type of *O*-glycosylated proteins localizes to cytosol and nucleus. Proteins can be attached to cell membrane via GPI anchors. *C*-glycosylation exists as a more rare form of protein glycosylation that is attached to Tryptophan (W) amino acid. Major glycosylated lipid on the cell membrane is spingholipid, giving rise to glycosphingolipids. Hyaluronic acids exists as the only non-attached glycan, which localizes to extra cellular matrix (ECM). *Fuc: Fucose; Gal: Galactose; GalNAc: N-acetylgalacosamine; Glc: Glucose; GlcA: glucuronic acid; GlcN: Glucosamine; GlcNAc: N-acetylglucosamine; IdoA:Iduronic acid; Man: Mannose; Sia: Sialic acid; Xyl: Xylose; GPI: glycosyl-phosphatidylinositol (Adapted from (Reily et al. 2019)).*

There are 6 main types of glycosylation: *N*-linked, *O*-linked, and *C*-linked glycosylation, glypiation, and phosphoglycosylation as protein glycosylation and sphingolipid glycosylation as lipid glycosylation (Moremen et al., 2014; Wang & Quanyong et al., 2020) (**Figure1**). *N*-linked glycosylation is the most common type of protein glycosylation and its name derives from the attachment of the GlcNAc residue of glycans to Asn of polypeptide chains via amide (Nitrogen-Carbon) linkage. *O*-linked glycosylation is very diverse and its name indicates the attachment of a variety of mono- and oligosaccharides (GalNAc, GlcNAc, Xyl, Man, glycosaminoglycans (GAG) etc.) to mostly Serine (Ser) or Threonine (Thr), or rarely to Tyrosine (Tyr), Hydroxylysine (Hyl) or Hydroxyproline (Hyp) residues via glycosidic (Oxygen-Carbon) bond. In particular, the attachment of one or more GAG to serine residues gives rise to proteoglycans such as heparan sulfate, heparin, chondroitin, and dermatan sulfates (Lindahl, Couchman, Kimata, & Esko, 2009). *C*-mannosylation is an unusual Carbon-Carbon linkage of mannose to Trp side chains (Reily et al., 2019). Glypiation refers to the addition of glycosyl-phosphatidylinositol (GPI) to a protein for its localization to the cell membrane via a so called GPI-anchor (Puig, Altmeppen, & Glatzel, 2014; Tsai, Liu, & Seeberger, 2012). Phosphoglycosylation is the addition of carbohydrates to Serine residue of proteins via phosphodiester bond (Haynes, 1998). In addition to protein glycosylation, transfer of glycans to ceramide of sphingolipids, which generates glycosphingolipids on the cell membrane is the most common type of lipid glycosylation (Reily et al., 2019). Of note, hyaluronic acid exist as the only type of none-attached glycan neither to proteins or to lipids, but its structure resembles the one of GAGs (Moremen et al., 2014). Other rare glycosylation types such as *S*-linked and *C*-linked glycosylation (other than mannosylation) also exist (Jayaprakash & Surolia, 2017).

1.2 *N*-glycosylation

More than half of all proteins are known to be glycosylated, of which *N*-glycosylation represents the largest fraction with approximately 90%, considering the proteome of all

organisms from metazoan to viruses (Apweiler et al., 1999). *N*-glycosylation involves glycosyltransferases and glucosidases from the Endoplasmic Reticulum (ER) to covalently attach mannoses and glucoses onto lipid linked oligosaccharides (LLOs), trim *N*-glycans and transfer them on proteins as well as glycosyltransferases from the golgi to further mature glycoproteins. As a result, so-called 'complex glycan trees' or LLOs are assembled in a step-wise manner (Helenius & Aebi, 2004).

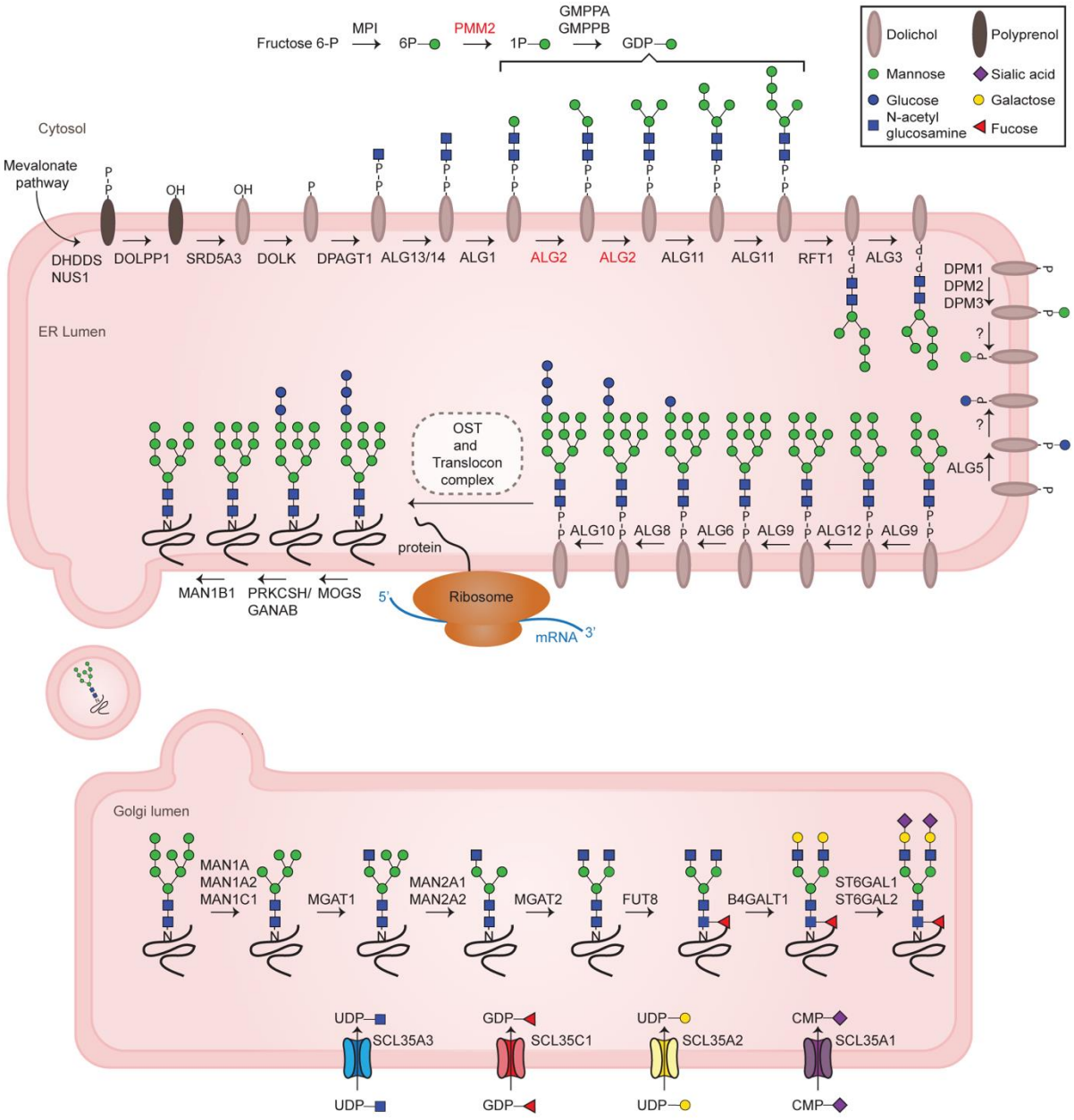

Figure 2: Schematic representation of *N*-glycosylation pathway
Enzymes involved in building up of glycans and transfer of those onto the proteins are shown. N-glycosylation starts in the cytosol with the production of GDP-mannose, which is used as substrate for the enzymes indicated with parenthesis. First 5 mannoses are added and then the *N*-glycans are flipped into the ER lumen by a flippase (RFT1). Next, 4 mannoses and 3 glucoses are transferred onto N-glycans, which are then transferred on the Asparagine residue of the proteins. Those are transported to golgi via vesicles and further trimming and addition of galactose, fucose, and sialic acids take place. *Enzymes used for disease modeling in this thesis are written in red. P: phosphate; GDP: Guanosine*

diphosphate; UDP: Uridine diphosphate; CMP: Cytidine monophosphate monophosphate (Adapted from (Ng and Freeze 2018)).

N-glycosylation starts in the cytosol with the production of GDP-mannose and at the ER-membrane with dolichol-phosphate mannose (Dol-P-man) and dolichol-phosphate glucose (Dol-P-Glc) as substrates of reactions catalyzed by mannosyltransferases and glucosyltransferases (**Figure 2**). It continues with the addition of 2 GlcNAc on dolichol-pyrophosphate (Dol-PP) embedded in the ER membrane, followed by addition of 5 mannoses from GDP-mannoses to LLOs via Asparagine Linked Glycosylation (ALG) enzymes, generating $Man_5GlcNAc_2$-Dol-PP. Thereafter, this *N*-glycan is flipped into the ER lumen via a flippase and 4 more mannoses from Dol-P-Man and 3 glucoses from Dol-P-Glc are added to LLOs to create $Glc_3Man_9GlcNAc_2$-Dol-PP. Eventually, oligosaccharyltransferases catalyze the covalent attachment of glycans via attaching GlcNAc of *N*-glycan to the nitrogen of Asn in some of the Asn-X-Ser/Thr motifs of many secreted and membrane embedded proteins (X is any amino acid except Proline). *N*-glycosylated proteins are trimmed further in the ER via glucosidases as a quality control for successful *N*-glycosylation. Proteins are then transferred to the golgi apparatus via vesicle trafficking and are further trimmed and/or other monosaccharides, such as fucose, galactose, and sialic acids are added on the *N*-glycans to mature the glycoproteins. When the proteins are properly glycosylated, they are trafficked to the cell membrane or secreted to the extracellular matrix via golgi vesicles. Proper *N*-glycosylation ensures proper protein folding, stability, solubility, interactivity, transport and signaling (Helenius & Aebi, 2004).

1.3 Congenital Disorders of Glycosylation (CDG)

Congenital Disorders of Glycosylation (CDG) is a group of rare genetic diseases affecting patients with mutations in glycosylation genes. Most of the CDGs are due to defects in *N*-glycosylation (Cylwik et al., 2013). CDG is categorized into 2 groups according to which type of enzyme is mutated in the *N*-glycosylation pathway. Accordingly, mutations occurring in cytosolic and ER-resident enzymes responsible for the assembly and transfer of *N*-glycans give rise to CDG-type Ix, whereas mutations of enzymes responsible for trimming and processing of *N*-glycans in the ER and golgi result in CDG type IIx (x is any letter depending on when the particular CDG type was discovered) (**Figure 2**) (Hennet & Cabalzar, 2015; Jaeken & Carchon, 2001).

As *N*-glycosylation is a conserved pathway occurring in every cell of the body, dysregulations consequently manifest in multisystemic disease phenotypes affecting many different organs and tissues such as liver, heart, intestine, eyes, brain, muscles, blood etc (Freeze, 2007; Jaeken & Carchon, 2001; Kjaergaard, Schwartz, & Skovby, 2001). Multisystemic feature of CDGs makes the diagnosis difficult, so molecular tests play an important role in pinpointing the actual cause of disease phenotypes. To this end, the diagnosis of the patients is done both via exome sequencing and the measurement of glycosylation patterns of serum transferrin via isoelectric focusing (Freeze, Schachter, & Kinoshita, 2017; Jaeken, 2003). The normal glycoprotein structure of serum transferrin contains 4 sialic acid residues attached to two *N*-glycan sites (Asn413 and Asn611). Since sialic acids are negatively charged, a shift in the band pattern toward the cathode indicates either reduced *N*-glycan attachment or aberrant glycan processing (Butler et al., 2003). Changes in this *N*-glycosylation patterning result from compound heterozygote missense mutations of *N*-glycosylation genes, in which patients inherit two distinct mutations from their parents (Bogdańska et al., 2021; Haeuptle & Hennet, 2009; Matthijs et al., 1998). Patients mostly carry hypomorphic alleles, in which there is still a residual enzyme activity of less than 50%, whereas parents as carriers with 50% or higher activity does not have any phenotype (Westphal et al., 2001; Yuste-Checa et al., 2015). Severity of the phenotypes mostly correlates with the residual enzyme activity (Freeze, 2002; Grünewald, 2009; Imtiaz et al., 2000). However, mechanism behind changes in enzyme activity and its downstream effects leading to CDG disease phenotypes are not well understood. To this end, I generated disease models of an ER-resident enzyme, *asparagine linked glycosylation 2 (alg2)* and a cytosolic *N*-glycosylation enzyme *phosphomannomutase 2 (pmm2)* to model the disease mechanism of the most common form of CDGs, namely *N*-linked CDGs.

1.4 Alpha-1,3/1,6-Mannosyltransferase or Asparagine-Linked Glycosylation 2 (ALG2) and ALG2-CDG (CDG Type Ii)

ALG2 is one of the ER-resident mannosyltransferases and it uses GDP-mannose as a substrate to catalyze the transfer of the second and the third mannose onto LLOs, namely $Man_1GlcNAc_2$-Dol-PP and $Man_2GlcNAc_2$-Dol-PP, to form $Man_3GlcNAc_2$-Dol-PP. It can transfer mannoses in either 1,3 or 1,6 position, thus it serves as a branching enzyme (Engel, 2018; Kämpf et al., 2009). Mutations in *Alg2* give rise to CDG-Type Ii (or ALG2-CDG) and myasthenic syndrome. ALG2-CDG is one of the rarest forms of all CDGs with worldwide 9 patients from 5 families reported so far (Cossins et al., 2013; Monies et al., 2014; Thiel et al., 2003). The rarity of the

disease alone illuminates the indispensability of proper enzyme function during embryonic development and survival.

In this thesis, *Alg2* maternal mutant allele from one of the well described ALG2-CDG patients (Thiel et al., 2003) was used to study the function of *N*-glycosylation during vertebrate development. The patient carried a compound heterozygote *Alg2* allele with a single nucleotide deletion, *del1040G*, leading to an early stop codon as maternal and a single nucleotide substitution, *G393T*, as paternal allele. Interestingly, transcripts of the paternal allele were neither detected in samples of the father nor in patient, arguing for the instability of paternal mRNA, while the maternal allele was found to be stably expressed. The patient carrying the mutations was born without abnormalities and until the age of 2-months was thought to develop normally. However, the patient started displaying multisystemic phenotypes rapidly thereafter, exhibiting first vision abnormalities including bilateral coloboma of the iris, unilateral cataract, and irregular nystagmus. At 4-months old, infantile spasms and hypsarrhythmia started occurring, followed by retarded myelinization at the 5th month, which eventually came to a stand-still at the 8th month. Moreover, mental and motor development were impaired and the liver showed borderline enlargement. Molecular analysis of patient fibroblasts shed light on the mechanism of ALG2-CDG. In this line, the inability of ALG2 to elongate short LLOs was shown with rescue experiments. Accordingly, overexpression of wild-type ALG2 protein in patient fibroblasts revealed an accumulation of LLOs upstream of ALG2, including $Man_1GlcNAc_2$-PP-dolichol and $Man_2GlcNAc_2$-PP-dolichol in mock-transduced cells compared to wild-type allele transduced cells, indicating reduced enzyme activity of truncated ALG2 protein (Thiel et al., 2003).

1.5 Phosphomannomutase 2 (PMM2) and PMM2-CDG (CDG Type Ia)

PMM2, previously called ALG4, is a cytosolic enzyme catalyzing isomerization of mannose-6-phosphate to mannose-1-phosphate (Roos et al., 1994). The integrity of Pmm2 protein is important for all types of glycosylation as it is catalyzing the upstream reaction of GDP-Man and dolichol phosphate mannose (Dol-P-Man), which are substrates for most of the glycan syntheses, including *N*-glycans, GPI-anchors, *O*-mannose, and *C*-mannose (Freeze, Eklund, Ng, & Patterson, 2012). Mutations in *Pmm2* gene leads to CDG- Type Ia (PMM2-CDG), which is the most common form of all CDGs with more than 1000 cases worldwide (Péanne et al., 2018). Patients carry mostly hypomorphic alleles and the most common mutant alleles to date

are *R141H* and *F119L* (Kjaergaard et al., 2001; Thiel et al., 2006). As for other CDG types, patients display multisystemic phenotypes such as developmental delay, liver disease, failure to thrive, ataxia, coagulopathy, strabismus, cerebellar atrophy, retinitis pigmentosa etc. (Jaeken, 2010; Matthijs et al., 1997; Verheijen et al., 2020). The severity of the patient phenotypes varies from mild to very severe with neonatal death (Grünewald, 2009).

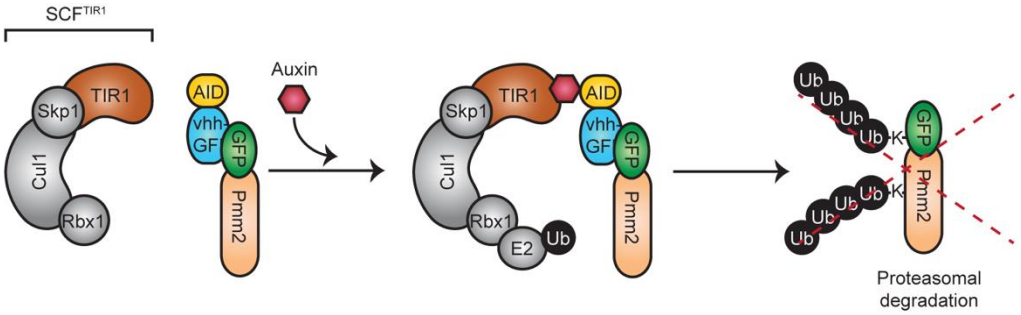

Figure 3: Schematic representation of Pmm2 degradation via deGradFP
TIR1 is an F-box protein that is able to recognize auxin. AID is an auxin inducible degron and vhh-GFP4 is an anti-GFP nanobody. deGradFP requires ectopic expression of TIR1 and AID-vhhGFP4 fusion proteins for degradation of endogenous GFP labeled Pmm2 protein. In the presence of auxin, TIR1 recruits auxin bound AID-vhh-GFP4, which binds to Pmm2-GFP. Recruitment of E2 ligase leads to ubiquitination of both Pmm2 and GFP at their lysine (K) residues for their proteasomal degradation *(Adapted from (Daniel et al. 2018)).*

In this thesis, I aimed to reduce the quantity of Pmm2 to different levels by targeting the enzyme with a degron in order to establish a model as a proxy for different levels of enzyme activity. Engineered degrons initially used an F-box protein fused to GFP nanobody, vhhGFP4 (Caussinus, Kanca, & Affolter, 2011), for targeted depletion of GFP labeled proteins. The degron system was engineered even further to induce degradation of GFP labeled proteins in an auxin inducible way, termed deGradFP (Daniel et al., 2018). In this case, an F-box protein that can specifically recognize auxin, TIR1, was ectopically expressed in cells together with an auxin-inducible degron (AID) fused to GFP nanobody (vhhGFP4). The latter binds to TIR1 only when auxin is present, while TIR1 forms the SKP1-CUL1-F-Box (SCF) complex of the E3 ubiquitin ligase for ubiquitinating and degrading specifically GFP labeled proteins. To this end, I endogenously labeled Pmm2 at its C-terminus end with GFP and employed deGradFP with auxin induction to set Pmm2 degradation at different levels (**Figure 3**). By that, I aimed to study the impact of Pmm2 degradation in a dose-dependent manner on the development of multisystemic phenotypes with a special focus on central nervous system abnormalities.

1.6 Central Nervous System (CNS) Abnormalities Among CDG Patients

Although CDG is a multisystemic disorder, most of the disease phenotypes revolve around neurological abnormalities including cognitive disabilities, psychomotor retardation, epileptic seizures, hypotonia, ataxia, polyneuropathy, and stroke-like events. CNS abnormalities leading to those phenotypes include midline brain structure and volume anomalies, myelination disorders, cortical malformations, venous sinus thrombosis, and neuronal migration defects, the latter of which is the most commonly seen abnormality among all (Paprocka, Jezela-Stanek, Tylki-Szymańska, & Grunewald, 2021; Schiller, Rosewich, Grünewald, & Gärtner, 2020).

Mutations in *N*-glycosylation enzymes give rise to the majority of the CDG types. The most common form of CDGs due to *N*-glycosylation defects is PMM2-CDG, followed by ALG6-CDG (CDG-Type Ic), SRD5A3-CDG (CDG-Iq), and ALG1-CDG (CDG-Ik). PMM2-CDG manifest itself with many neurological symptoms such as intellectual disabilities, cerebellar atrophy/hypoplasia, seizures, microcephaly, hypotonia, stroke-like episodes and strabismus. ALG6-CDG, as the second most common *N*-linked CDG, leads to clinical features such as developmental delay, axial hypotonia, strabismus, and seizures. SRD5A3-CDG and ALG1-CDG, on the other hand, manifest themselves with intellectual disability, brain malformations, cerebellar atrophy, hypoplasia, cerebellar ataxia microcephaly, and epileptic seizures. Ocular abnormalities include coloboma, nystagmus, optic nerve atrophy, cataract, glaucoma, and even blindness (Dupré et al., 2010; Morava et al., 2010). Since the other types of CDGs are rare, it is tough to generalize the neurological symptoms. However, other patients display phenotypes similar to aforementioned symptoms.

O-linked glycosylation gives rise to the second most common type of CDGs (Freeze et al., 2012). The major carrier of *O*-glycans is alpha-dystroglycan (αDG), which connects muscle cells to laminin, an extracellular matrix protein. Defects in αDG lead to α-dystroglycanopathies (Praissman & Wells, 2014). The clinical spectrum of α-dystroglycanopathy is broad, ranging from very severe musculo-oculo-encephalopathies, such as Walker Warburg syndrome, muscle-eye-brain disease, and Fukuyama congenital muscular dystrophy, to milder forms of limb-girdle muscular dystrophy (Godfrey, Foley, Clement, & Muntoni, 2011). Patients suffering from α-dystroglycanopathies display congenital brain malformations, cerebellar hypoplasia, and white-matter changes (Clement et al., 2008). Epilepsy due to neuronal

migration errors is likely, since αDG under normal conditions provides a neuronal migration stop signal (Vuillaumier-Barrot et al., 2012). All in all, due to variant neurological as well as the multisystemic feature of CDGs in general, the cell culture systems alone would not be sufficient to study disease mechanism. To this end, it is crucial to establish organismal models since some cell types might have higher levels of vulnerability to the mutations in glycosylation genes, rendering them more susceptible to disease phenotypes.

1.7 Model Organisms Used to Study CDGs

Highly conserved protein sequences and functions of glycosylation enzymes throughout all eukaryotes allows for the generation of disease models to study the function of glycosylation in a variety of model organisms, from yeast to mouse (Gámez et al., 2020). Yeast mutagenesis screens enabled researchers to study the functions of glycosylation genes, whereas yeast complementation assays as a tool are commonly used to validate the patient mutations (Frank et al., 2004; Ng et al., 2016; Roos et al., 1994; Thiel et al., 2003). However, model organisms used to study the function of those enzymes commonly relied on the generation of null alleles, which lead to embryonic lethality (Balakrishnan et al., 2019; DeRossi et al., 2006; Ioffe & Stanley, 1994; Stanley, 2016; C. Thiel et al., 2006; Thiel & Körner, 2011) except for some cases in in which null alleles were viable (Sarkar et al., 2006).

To overcome the embryonic lethality in animal models and to be able to mimic the patient scenario, many attempts have been made to create hypomorphic alleles either by knock-down approaches or the introduction of human mutant alleles to the orthologous region. Knock-down studies, so far, relied on zebrafish models, in which enzyme levels were reduced with morpholino injections to block translation of target mRNAs (Corey & Abrams, 2001). For instance, the MPI-CDG model of zebrafish morpholinos led to 50% embryonic lethality at 4dpf with multisystemic abnormalities among survivors including small eyes, dismorphic jaws, pericardial edema, and small liver, which could be rescued via mannose supplementation (Chu et al., 2013). A Pmm2-CDG model of morpholino injected zebrafish was viable with craniofacial defects and impaired motility (Cline et al., 2012). However, recent research showed that morpholino injected fish models led to more severe phenotypes than the knock-out lines. Furthermore, mutant lines showed compensatory upregulation of genes leading to the rescue of the mutant line, showing clear differences between knock-down and knock-out studies, underlining the importance of choosing the right model to answer the question of interest (El-

Brolosy et al., 2019; Rossi et al., 2015). Comparably only a few studies attempted to introduce patient alleles to create hypomorphic animal models, such as PMM2-CDG mouse models. The generation of the most common compound heterozygote *Pmm2* patient allele *R141H/F119L* with the mouse ortholog alleles of *R137H/F115L* led to the death of many of the mice prenatally (50.9% survival at postnatal Day 65). Surviving progeny displayed significantly stunted growth, accumulation of cytoplasmic hyaline bodies in the liver, and decreased wall thickness in the heart (Chan et al., 2016).

CDG patients are mostly born with an uneventful pregnancy and good birth weight although some rare occasions of prenatal diagnosis were reported (Grünewald, 2009; Kleijer et al., 2011; Malhotra et al., 2009). Multisystemic phenotypes start as early as postnatally, rendering embryonically lethal model organisms not suitable to study the disease mechanism. As the null alleles of glycosylation genes are majorly embryonically lethal and morpholino knock-down studies have features different than naturally occurring mutant alleles, animal models carrying hypomorphic alleles are needed for disease modelling of CDG symptoms.

1.8 Medaka, *Oryzias latipes*, as a New Model Organism to Study CDGs

Medaka, *Oryzias latipes,* is a small freshwater fish habituating to rice paddies mainly in Japan, but also in eastern China and Korea. Medaka adults are sexually dimorphic, meaning that the gender of the fish can be identified from the shape of the dorsal fin. Medaka females lay 30-50 eggs during fertilization, which allows fast generation and screening of many mutant lines. Development of the embryos is extrauterine and embryos are transparent, allowing for the observation of the embryonically lethal or early onset phenotypes without euthanizing or operating the mother. On the other side, development of medaka is temperature dependent and as the temperature decreases, the development rate slows down, which allows for a higher resolution of developmental processes by fine-tuning of the developmental time. At 28 degrees Celsius, *in vitro* raised embryos develop to hatching stage in 8 days and reach to adulthood in 2-3 months (Wittbrodt et al., 2002). These all together making medaka an easy-to-handle and more convenient model organism compared to the mouse models, especially to study the vertebrate development.

The extent to which genetic manipulations can be applied is important for the use of model organisms for molecular biology approaches. Most of the genetic manipulation techniques work in medaka including irradiation or *N*-ethyl-*N*-nitrosourea (ENU) treatment (Shima & Shimada, 1994; Shima & Shimada, 1991), foreign DNA injections into the cytoplasm of embryo or eggs (Boon Ng & Gong, 2011; Grabher & Wittbrodt, 2007), enhancer and gene traps (Froschauer et al., 2012; Grabher et al., 2003), morpholinos to block mRNA translation (Carl et al., 2002), and targeted genome editing technologies such as zin-finger nucleases and CRISPR/Cas9 (Ansai & Kinoshita, 2014; Guan et al., 2014; Jinek et al., 2012). The latter is crucial in terms of studying the function of a single gene causing disease phenotype in human. Medaka was used to study the cellular mechanism of several human diseases including polycystic kidney disease, Gaucher disease, and nonalcoholic steatohepatitis via morpholino injections, ENU treatment and high-fat diet feeding regimen, respectively (Hashimoto et al., 2009; Matsumoto et al., 2010; Uemura et al., 2015). As a result, mutant medaka displayed the pathological phenotypes resembling human symptoms. These results taken together with ability of easy genetic manipulations, fast generation time, high number of progeny and transparency of medaka present it as a promising model organism for studying disease phenotypes and for the design of new and effective therapies.

All in all, importance and necessity of glycosylation is evident from the rarity of the patients reported so far. Although it is one of the most abundant forms of post-translational modifications and it is highly crucial for organismal survival, function of glycosylation during vertebrate development and mechanism of multisystemic CDG phenotypes have not yet been addressed in a molecular level. To this end, this thesis models the most common form of glycosylation and presents two medaka models displaying reduced *N*-glycosylation levels generated by two different approaches to study the function of *N*-glycosylation during vertebrate development.

2

Aims and Approaches

The aim of this study was to investigate the role of *N*-glycosylation on vertebrate development under physiological and pathological conditions. To this end, following steps were aimed to be achieved:

1. **Generation of ALG2-CDG and PMM2-CDG models of medaka**

   by employing CRISPR/Cas9 targeted genome editing and homology directed repair to integrate a specific patient allele into the *alg2* locus and to insert *GFP* at the C-terminus of *pmm2*.

2. **Characterization of the multisystemic phenotypes under hypo-*N*-glycosylation**

   by assessing the consequences of hypo-*N*-glycosylation at the macroscopic level by gross morphological analyses, as well as at the cellular level by means of histology.

3. ***N*-glycome and proteome analysis for the identification of molecular determinants driving the disease phenotype**

   by analyzing *N*-glycan occupancy of total protein from both medaka and patient fibroblast, as well as unbiased mass spectrometry of whole medaka hatchlings and enucleated eyes.

4. **Rescue of multisystemic phenotypes by genetic manipulations and nutritional therapies**

   by overexpressing Alg2 protein via microinjections of mRNAs synthesized from both medaka and human full-length coding sequences and supplementing *alg2* medaka model with D-mannose and D-glucose.

3

Chapter 1

3.1 Results

This section is dedicated to the results produced throughout this thesis. Please refer to the "Contributions" section for the details of the contributions of collaborators, colleagues, and internship students.

3.1.1 Employing CRISPR-Cas9 targeted genome editing to create a precise patient-based *alg2* allele in medaka

Given that complete loss of function mutations of glycosylation enzymes in human leads to early embryonic lethality (Freeze et al., 2017) and, hence, patients carry hypomorphic alleles led us to create an *in vivo* model of ALG2-CDG by mimicking a previously published (Thiel et al., 2003) *Alg2* human allele. High conservation of ALG2 protein sequence throughout eukaryotes and ease of genetic manipulations in fish models enabled us to use more simple forms of model systems, such as *Oryzias latipes* or medaka, for disease modelling (**Figure 4A and 4B**). Accordingly, the ALG2 protein conservation between medaka and human is 63.7% in terms of sequence identity and the mutation site is well preserved (Bateman, 2019) (**Figure 4A, red bar**).

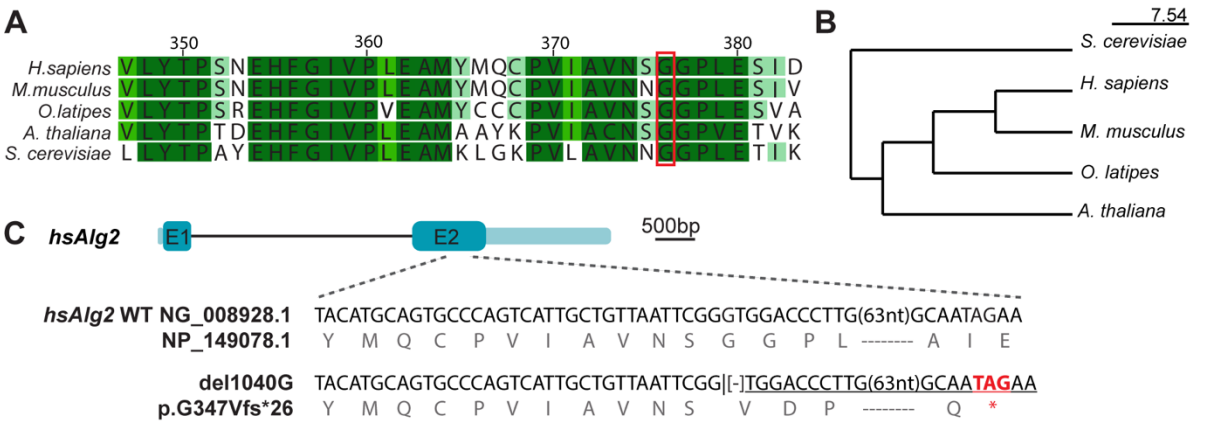

Figure 4: Protein sequences at the mutation site of the *hsAlg2* allele is highly conserved throughout eukaryotes

(A) Protein sequences at the C-terminus of ALG2 enzyme is highly conserved from yeast to human. *Darker green: highest conservation, lighter green: least conservation, white: conservation in at most two species among five. For alignment of the protein sequences T-Coffee algorithm and for conservation*

calculation Percentage Identity (PID) was used. Red bar: mutation site of the human maternal allele modeled in this thesis; Letters are abbreviations of amino acids.
(B) Phylogenetic tree according to the whole ALG2 protein sequence conservation confirms medaka (*O. latipes*) as a close relative to human and mouse in terms of protein sequence conservation. *Tree construction method: Average Distance; Distance Measurement: Percentage Identity (PID). Scale bar: 7.54 amino acid changes per 100 amino acids.*
(C) *hsAlg2* maternal allele carries 1 nucleotide deletion at the C-terminus end leading to an early stop codon. *Underline: frameshift; red asterix: stop codon; square brackets: deletion; dashed lines: skipped sequences; bar inside nucleotide sequence: mutation start site; E: exon; light blue: untranslated regions (UTRs); Scale bar: 500bp.*

The modelled human allele was compound heterozygote, meaning that the patient carried different mutated alleles from each parent. Here, only the maternal allele was used as the base of the fish model since the transcript from the paternal allele was shown to be non-stable in the patient sample (Thiel et al., 2003). The maternal allele had a deletion of a single Guanosine at the C-terminus end of the gene, *Δ1040G,* which led to an early stop codon at the C-terminal end (**Figure 4C**). Precise editing of the medaka genome for integration of a single base pair deletion together with a restriction recognition site (StuI site) was accomplished with CRISPR/Cas9 targeted genome editing. To this end, medaka zygotes were injected with 2 guide RNAs, Cas9 mRNA, single stranded oligodeoxynucleotide (ssODN) with the designed mutation, and GFP mRNA as an injection tracer (**Figure 5A**). Some of the injected embryos were pooled (5-10 embryos) and genotyped to test efficient integration in the F0 generation. The rest of the fish were raised to adulthood and outcrossed to a wild-type fish to screen for the germ line transmission of the allele. Individuals with successful integration, as well as other CRISPR derived mutants, were screened in F1 generation. This screening revealed several alleles in the germline including a 2 amino acid deletion (c.999-1004del translating into p.N334_S335del), a complete deletion after double stranded break (c.1002_1218+5delinsTCTG translating into p.(S335Lfs*8)), and the intended integration of the ssODN and generation of an early stop codon at the C-terminal end (c.1006-1011delinsTAAGG translating into p.G336*) (**Figure 5B**).

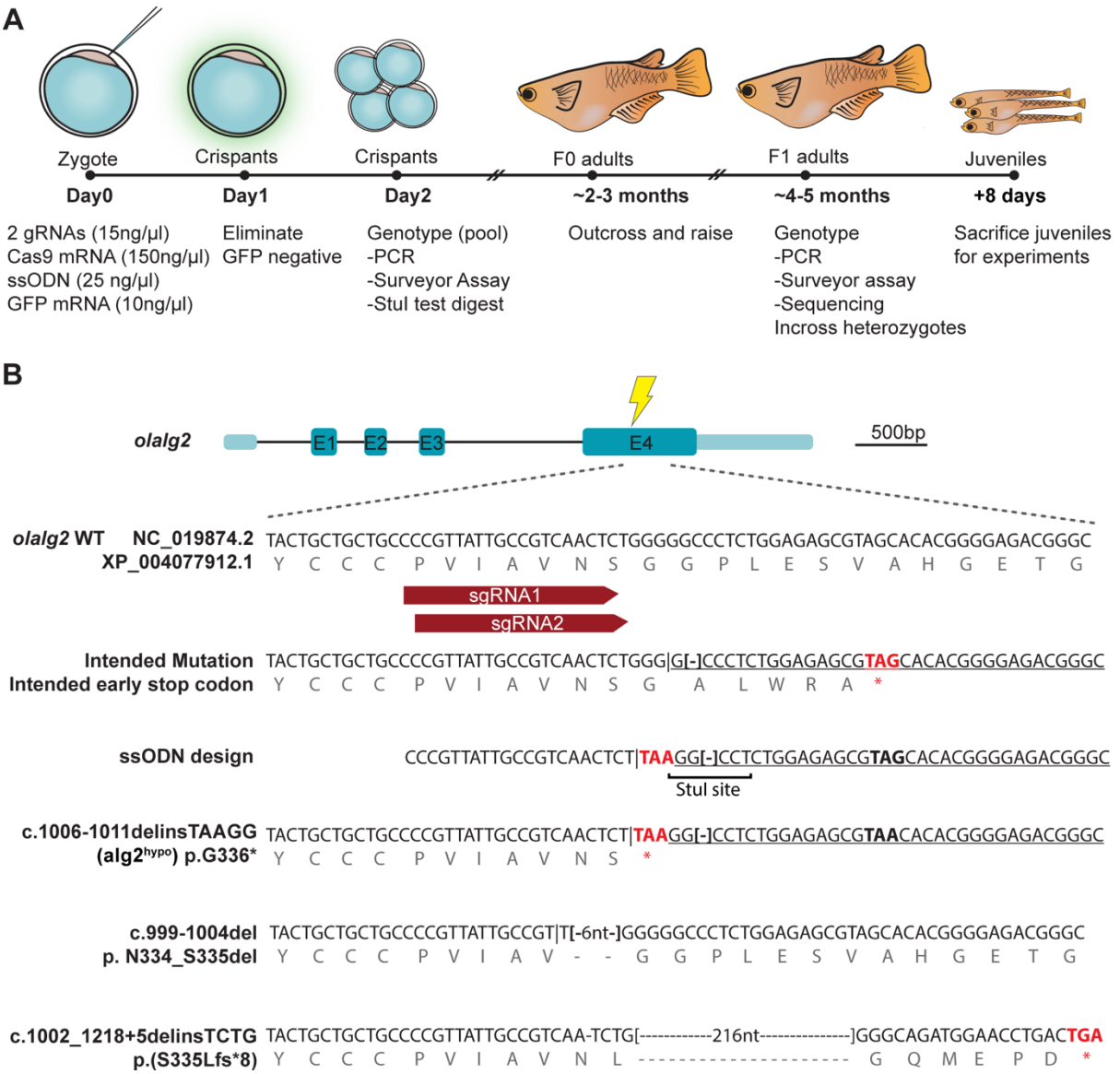

Figure 5: Schematic representation of *in vivo* CRISPR/Cas9 genome editing in medaka for precise knock-in and resultant alleles

(A) Embryos were injected with the injection mixture at one-cell stage, zygote. GFP expression was used for screening of successful injection. Crispants were genotyped for the successful integration and raised to adulthood. Those adults were outcrossed to wild-type fish and alleles that could survive under heterozygosity were raised. Those fish were incrossed for the analysis of homozygotes at the juvenile stage. *Note: timeline is not to scale*.

(B) Schematic representation of the medaka *alg2* gene depicting the C-terminus of the gene and protein sequences in wild-type and in case of the respective mutations. "Intended mutation" represents the hypothetical sequence if 1bp deletion is introduced, as in human allele, to the orthologous region of *alg2* gene in medaka. "ssODN design" is the commercial single stranded sequence bearing an early stop codon and StuI test digest site. "alg2^{hypo} (c.1006-1011delinsTAAGG)" allele represents ssODN integration into alg2 medaka endogenous locus. Below this allele, "2 amino acid deletion allele (c.999-1004del)" and "C-terminal truncation allele (c.1002_1218+5delinsTCTG)" are presented. *Underline: frameshift; red asterix: stop codon; square brackets: deletion; dashed lines: skipped sequences; bar inside nucleotide sequence: mutation start site; E: exon; light blue: untranslated regions (UTRs); bar: 500bp.*

3.1.2 *alg2* C-terminal mutant alleles lead to multisystemic phenotypes under homozygosity

Interestingly, none of the fish carrying either of the three alleles showed any symptoms until stage 39 (Iwamatsu, 2004) under homozygosity, meaning that until the hatching stage the homozygous fish were indistinguishable from their wild-type counterparts. At the end of stage 39 and the beginning of stage 40, all 3 alleles led to similar multisystemic phenotypes under homozygosity (**Figure 6A to C**). Heterozygotes, however, remained indistinguishable from their wild-type siblings. The early stop codon allele, from here on referred to as alg2^{hypo}, and the 2 amino acid deletion alleles were both viable for only 2-4 days after hatching. Of note, the mutation leading to a large deletion at the C-terminus often led to embryonic lethality at stage 39 although some of the siblings could hatch and survive as in the other alleles (survival not quantified) (**Figure 6C**). Morphologically, the multisystemic phenotypes manifested themselves by a gradually slowing and eventually arrested blood flow, blood clogging, edemas, especially around the heart and the eyes, (nearly) tubular heart lobes, shortened snout, and seizures (not shown) for all three alleles. The most characteristic phenotype to distinguish homozygote fish from the rest was the slow blood flow and eventually beating of the heart devoid of red blood cells, which was clogged in the several spots of the body including thymus and the tail. The yolk was not digested and the swim bladder was not filled with air. Hatched fish were mostly stationary and displayed severely impaired motility, as evidenced by swimming in upward circles. All in all, the here established *alg2* fish model was resembling patient-like phenotypes in terms of their multisystemic nature and shortened life span.

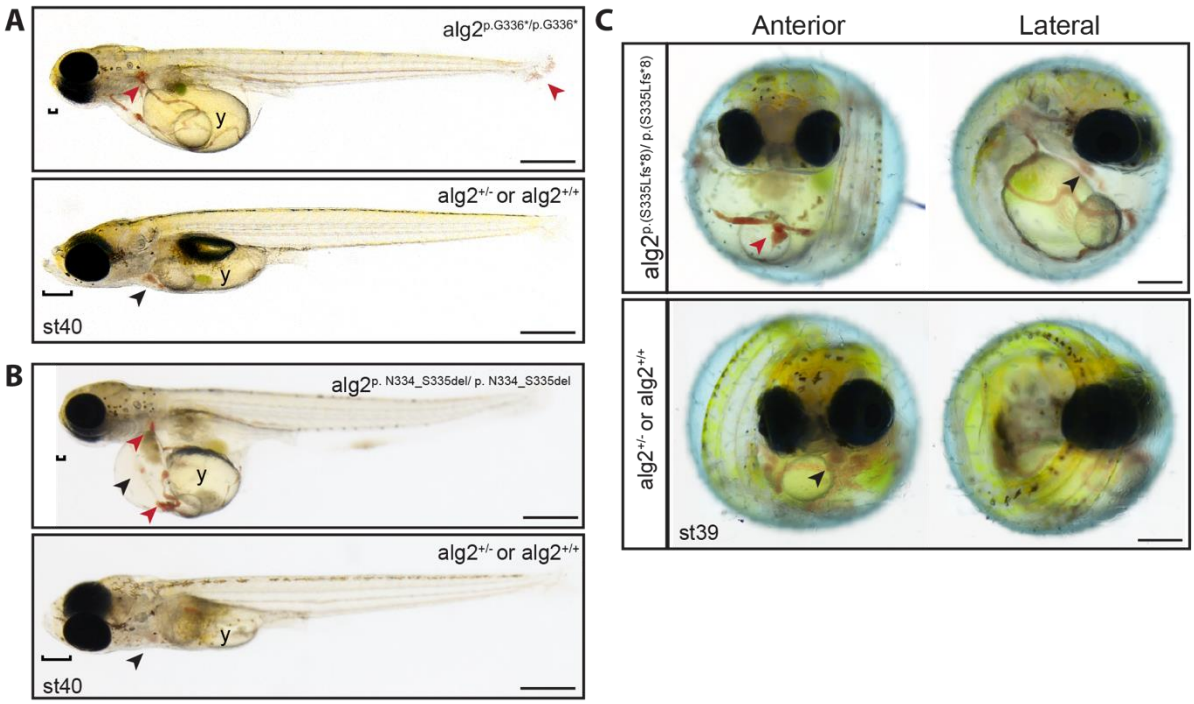

Figure 6: Mutations at the C-terminus end of *alg2* lead to multisystemic phenotypes
Multisystemic phenotypes under homozygosity of the Alg2:p.G336*, or alg2^{hypo} *(adjusted from (Gücüm et al., 2020))***(A)**, 2 amino acid deletion Alg2:p.N334_S335del **(B)**, and C-terminal truncation Alg2:p.S335Lfs*8 **(C)** allele include shortened snout (square brackets), blood clogging/clotting (red arrowhead), tubular heart (black arrowhead) and edemas around the heart and the eyes. *y: yolk. Scale bar: 0.5 mm.*

I further examined the gross morphological changes of the mutants at the microscopic level via histology. Transverse sections through the homozygote juvenile body indicated abnormalities in several organs including eye, brain, and heart. Organs were generally smaller compared to wild-type siblings, indicating developmental defects. In the eye, the outer nuclear layer (ONL) adjacent to retinal pigmented epithelium (RPE) was shorter compared to the wild-type siblings (**Figure 7A-A'**). White matter in the brain was reduced in size and gray matter was more dispersed into the white matter leading to gray matter heterotropia. The ventricle opening, on the other side, was widened, and, hence, left a distance between the lobes of midbrain and optic tectum as well as left and right hindbrain (**Figure 7B-B' and 7C-C'**). Although all the organs, including the heart, developed normal until stage 39, heart of the mutant fish thinned and the chambers were not apparent at stage 40, meaning that the heart became more tubular (**Figure 7D-D' and 7I-I'**). Morphological abnormalities were not observed neither in spleen (data not shown), nor intestine and liver via histology (**Figure 7E-E'**).

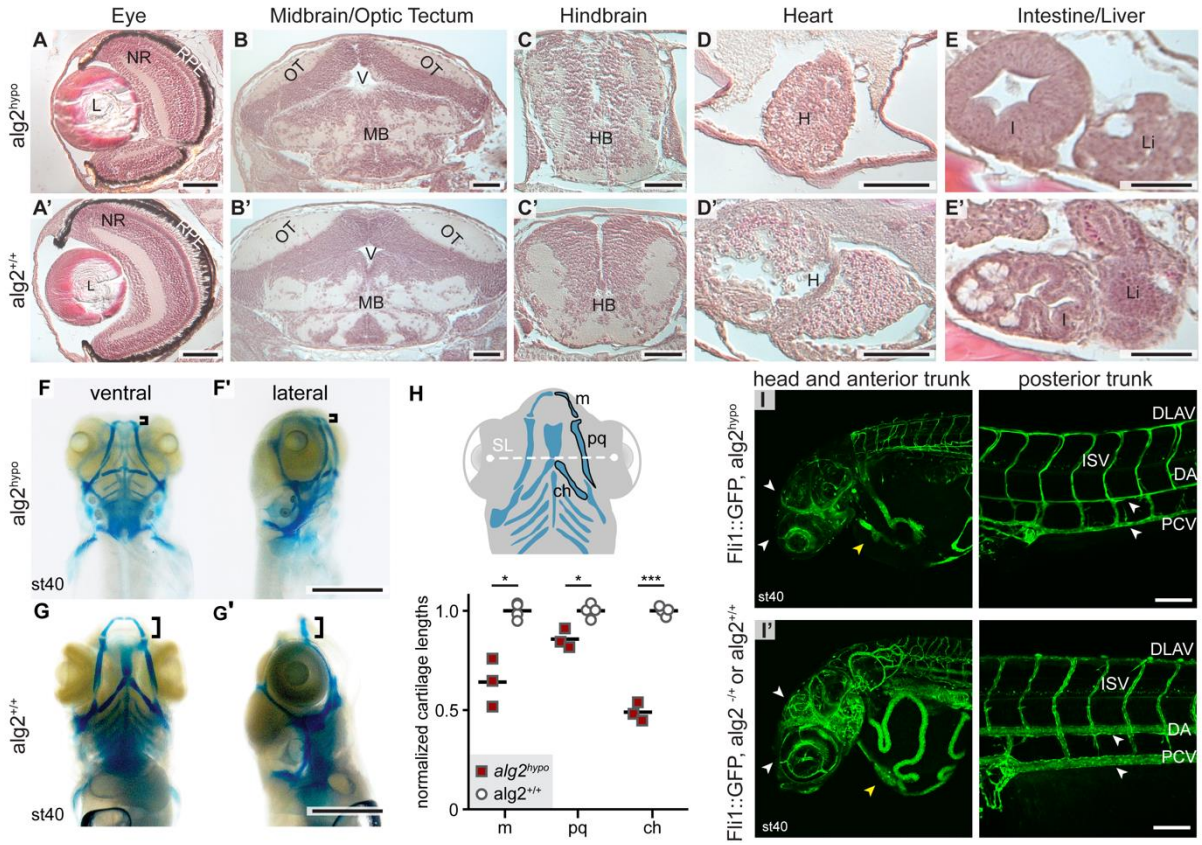

Figure 7: Characterization of multisystemic phenotypes confirms multiorgan and tissue abnormalities

(A to E') Hematoxylin and eosin staining of transverse sections of alg2^{hypo} and wild-type siblings revealed shortened ONL and smaller eyes (A-A'), reduced white matter and gray matter heterotropia (B-C'), tubular heart (D-D'), but normal intestine and liver (E-E'). *NR: Neural retina; RPE: Retinal pigmented epithelium; OT: Optic tectum; MB: Midbrain; V: Brain ventricle; HB: Hindbrain; H: Heart; I: Intestine; Li: Liver. Scale bar: 50µm*

(F to G') Alcian blue staining of alg2^{hypo} fish showed reduced cartilage length and thickness at stage 40. *Square brackets: Meckel's cartilage. Scale bar: 0.5mm*

(H) Schematic representation (upper panel, ventral view) of craniofacial cartilages and quantification (lower panel) of the cartilage lengths normalized to distance between lenses (*standard length, SL*) and mean of that of the wild-type reveals significant reduction of all three cartilage structures in mutant compared to wild-type. *m: Meckel's cartilage; pq: palatoquadrate; ch: ceratohyal cartilage. Two-tailed nonparametric Student's T-test; * <0.05; *** < 0.001.*

(I-I') Confocal imaging of vessel structures of alg2^{hypo} medaka shows severe vessel thinning (arrowheads) and ruptures at stage 40. *Yellow arrowhead: heart; DA: Dorsal aorta; PCV: Posterior cardinal vein; DLAV: Dorsal longitudinal vessel; ISV: Intersegmental vessel. Scale bar: 0.25mm*
(Figure adjusted from (Gücüm et al., 2020)).

Since patients often display craniofacial dismorphisms (Luderman, Unlu, & Knapik, 2017), the craniofacial cartilage morphology of mutant medaka was investigated, as fish do not display calcification or bone formation at this stage. Alcian blue staining revealed cartilage thinning and significant shortening of head cartilages. The reduction in jaw size was caused by significantly shorter Meckel's cartilage ($p = 0.02$), palatoquadrate ($p = 0.03$) and ceratohyal ($p < 0.001$) cartilages compared to stage-matched wild-type siblings (**Figure 7F to H).** As one of the characteristic features of the mutants is slow blood flow and eventual blood clogging (or

potentially clotting) and patients often suffer from blood clotting (Brum, 2013; "Congenital Disorders of Glycosylation", 2015) associated with the endothelial cell abnormalities (Yau, Teoh, & Verma, 2015), the morphology of the blood vessels was analyzed. To this end, *alg2* mutants were crossed to *Fli1::GFP* reporter line, allowing for endothelial cell-specific fluorescent labelling *in vivo*. Severe vessel thinning was observed in the mutants, which was pronounced in the posterior cardinal vein and dorsal aorta and could potentially cause the observed slow blood flow and clogging (**Figure 7I-I'**).

3.1.3 Reduction in the Alg2 enzyme activity (or level) leads to reduced *N*-glycan occupancy, or hypo-*N*-glycosylation

Reducing enzyme activity or abundance should cause a deficiency of the product from the reaction catalyzed by the enzyme. Since the first substrate of Alg2 is $Man_1GlcNAc_2$-PP-Dol, mutant fish would presumably display reduced levels of all downstream *N*-glycans in the ER- and golgi-resident *N*-glycosylation cascade, including high-mannose type and complex-type *N*-glycans. Hence, the mutant fish would exhibit a decrease in *N*-glycan occupancy of the proteins. To test this hypothesis, I employed lectin blotting and multiplexed capillary gel electrophoresis with laser-induced fluorescence detection (xCGE-LIF).

Given that different lectins have the capacity to recognize different sugar structures, Concanavalin A (Con A) was used to detect mannose and wheat germ agglutinin (WGA) to detect *N*-acetylglucosamine. Lectin blots against ConA measured total mannose occupancy, which is not exclusive to *N*-glycans, but also found in *O*- glycans and *C*-mannoses. Nevertheless, mutants showed only 72% mannosylation compared to the wild-type. WGA binds to acetylated glucoses and recognizes more specifically *N*-glycans, but also some of the *O*-glycans. Lectin blot against WGA showed a reduction in glucosylation level to 83% of the wild-type siblings (**Figure 8A**). Both lectin blots, hence, revealed similarly reduced protein glycosylation, pointing towards lower enzyme activity, which results in hypoglycosylation. To put these findings in a more clinically relevant perspective, lectin blots were performed for cultured primary fibroblast of the ALG2-CDG patient (*by Lars Beedgen, Thiel Lab, University Clinic Heidelberg, Germany*). Surprisingly, we did not observe differences for neither mannose nor acetylated glucose levels between the control and patient fibroblast sample (102 %; Con A, 94 %; WGA blot) (**Figure 8B**), adding to the notion that different cell types show different susceptibilities towards perturbed glycosylation and, thus, highlighting the importance of using *in vivo* models for hypoglycosylation studies.

To further address how the *N*-glycan occupancy of medaka alg2^{hypo} variant and fibroblasts of the ALG2-index patient was impacted, we performed an extended *N*-glycan analysis by xCGE-LIF *(in collaboration with Rapp Lab, Max-Planck Institute, Magdeburg)*. This approach enabled the identification and relative quantification of individual *N*-glycan structures via normalization to an internal standard allowing the direct quantitative comparison between samples of different origin like fish and human **(Appendix Table 1)** (Hennig et al., 2016). The evolutionary conservation of the complex glycosylation machinery resulted in a high structural similarity of the *N*-glycan profile of wild-type medaka hatchlings and control human fibroblasts. In the medaka wild-type *N*-glycan fingerprint (**Fig 8C, black**), 57 % represented complex- type *N*-glycans that were predominantly Neu5Ac-sialylated. The remaining 41 % of the *N*- glycome comprised of high-mannose-type *N*-glycans ranging from Man5 to Man9 structures and hybrid-type *N*-glycans were present with only 2.5 %. In contrast, in the alg2^{hypo} *N*-glycan fingerprint (**Fig 8C, red**) a severe hypo-*N*-glycosylation was apparent by an overall reduction of 61 % in the levels of *N*-glycosylation (**Figure 8C and 8E**). This hypoglycosylation affected all *N*-glycan structures to a comparable extent with only minor qualitative differences.

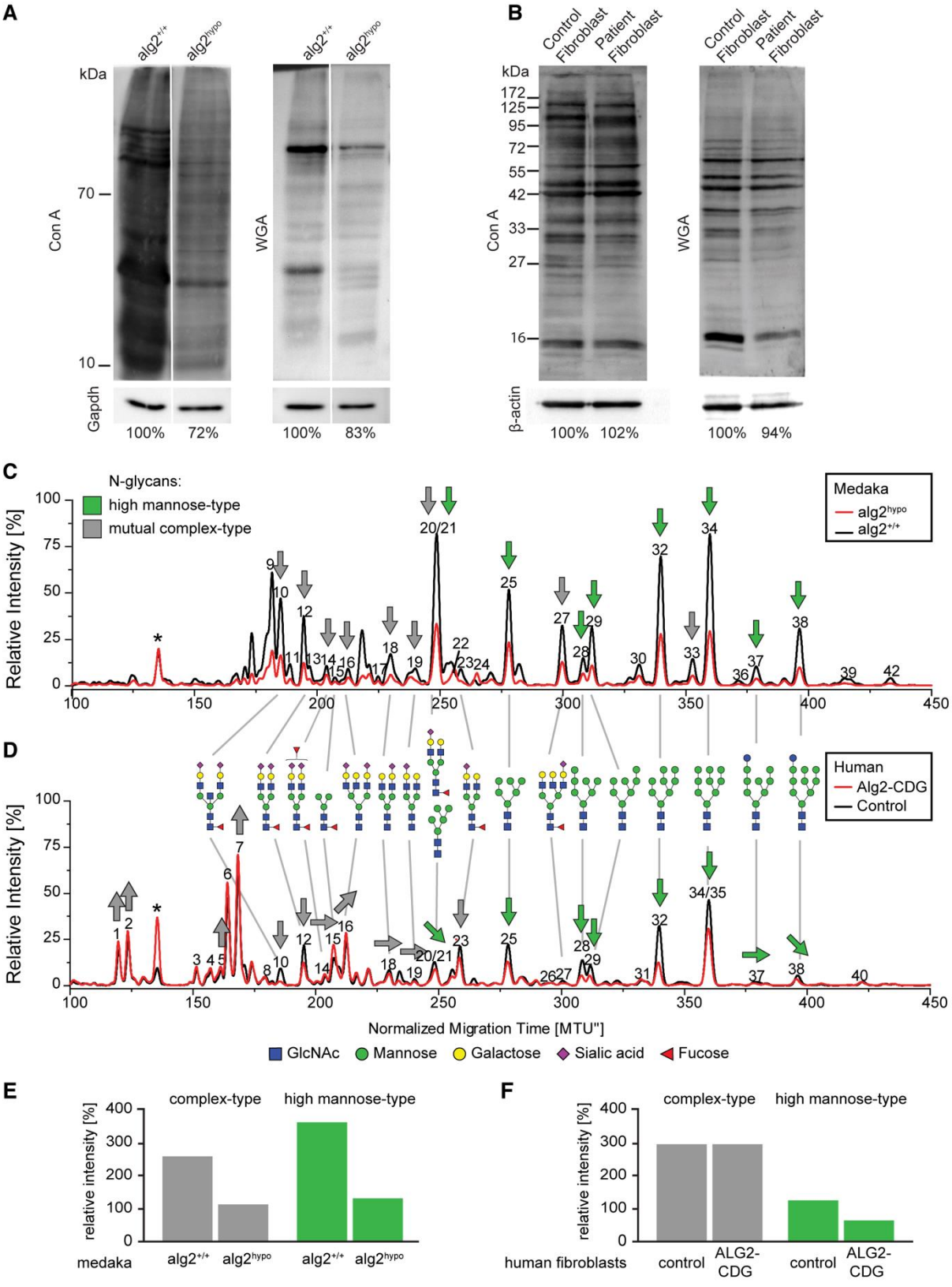

Figure 8: xCGE-LIF quantifying *N*-glycan occupancy identifies both medaka and human mutations as hypomorphic alleles

(A) Lectin blots of total fish lysate blotted against ConA and WGA, binding to mannose and acetylated-glucoses, respectively, showed hypoglycosylation in medaka alg2^{hypo} variant.

(B) Lectin blots of the patient fibroblast lysate blotted against ConA and WGA showed similar levels of glycosylation in the patient fibroblast compared to the control samples *(Data produced by Lars Beedgen, Thiel Lab, Univeristy Clinic Heidelberg, Germany)*
(C and D) Multiplexed capillary gel electrophoresis with laser-induced fluorescence detection (xCGE-LIF) both for whole medaka hatchlings (C) and human fibroblast samples (D) showed hypo-*N*-glycosylation. *Arrows indicate trend of the N-glycan signal in the mutants relative to the wild-types, up: higher in mutant and down: lower in mutant. Numbers indicate the N-glycan structures listed in Appendix Table 1. Black line: wild-type or control; red line: mutant or patient sample; asterix: x-axis normalization peak (Data produced jointly with Valerian Grote, Max-Planck Institute, Magdeburg, Germany)*
(E and F) Overall quantification of the electropherogram in (C) and (D), respectively, for complex- and high-mannose-type *N*-glycans *(Data produced jointly with Valerian Grote, Max-Planck Institute, Magdeburg, Germany)*
(Figure adjusted from (Gücüm et al., 2020))

The *N*-glycan fingerprint of the human fibroblast control sample (**Figure 8D, black**) revealed that, similar to fish, 68 % of the *N*-glycome was composed of complex type *N*-glycans with a substantial proportion of multi-antennary structures. The remainder consisted of high-mannose type *N*-glycans (29 %) and hybrid-type structures (3 %). Similar to the medaka samples, the majority of complex-type *N*-glycans in the human fibroblasts were characterized by a terminal sialylation. The *N*-glycan fingerprint from fibroblasts of the human ALG2 index patient (**Fig 8D, red**) showed few qualitative changes in its *N*-glycome compared to the control. Consistent with our findings in the medaka animal model, the human fibroblasts of the ALG2-CDG patient revealed a general hypo-*N*-glycosylation, although less pronounced. High-mannose-type glycosylation was reduced by 48 %, while complex type *N*-glycans showed only marginal changes (0.5 %) (**Figure 8D and 8F**).

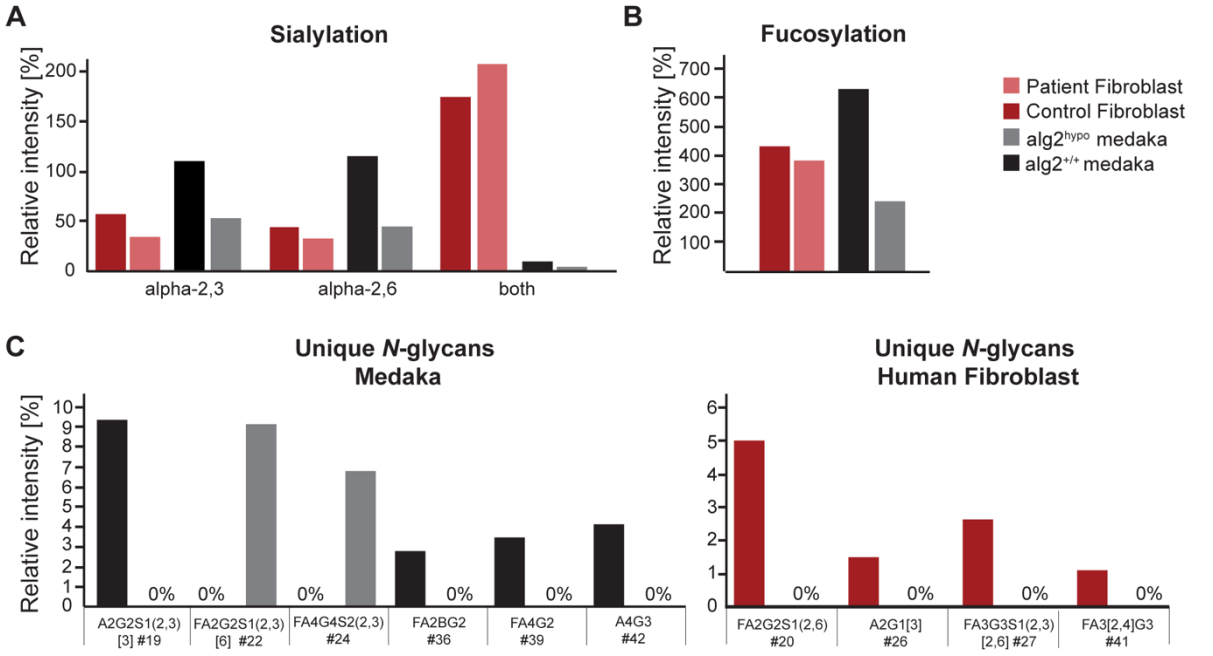

Figure 9: xCGE-LIF indicates reduced sialylation and fucosylation and as well unique *N*-glycans
(A-B) Levels of sialylation(A) and fucosylation(B) were reduced in alg2^{hypo} and human fibroblast sample compared to wild-type medaka and control fibroblast, respectively.
(C) *N*-glycans exclusive to either medaka mutant or wild-type allele (left) and patient or control fibroblast (right) show generation of unique *N*-glycans in medaka mutants. *Numbers refer to the N-glycans in Appendix Table 1 (Data produced jointly with Valerian Grote, Max-Planck Institute, Magdeburg, Germany).*

Besides hypo-*N*-glycosylation, overall sialylation and fucosylation levels were reduced in the medaka animal model as well as in the patient fibroblast (**Figure 9A and 9B**). Moreover, the medaka model showed unique *N*-glycan structures, namely FA2G2S1(2,3) and FA4G4S2(2,3) (**Appendix Table 1; Figure 9C-left**), which is a phenomenon that can also be observed in the tissue samples of CDG patients (Freeze, 2007). However, those unique *N*-glycans were not observed from the patient fibroblast sample. (**Figure 9C-right**). All in all, our analysis revealed that both, the human ALG2:p.G347Vfs*26 (*Δ1040G)* and the medaka Alg2:p.G336* (or alg2^{hypo}) alleles resulted in a hypo-*N*-glycosylation, and hence, suggested Alg2:p.G336* as a hypomorphic model.

3.1.4 Unbiased proteomics assay points towards a putative downregulation of phototransduction pathway and upregulation of protein-processing machinery

Glycosylation is an important and necessary post-translational modification for proper protein folding. Misfolded proteins are sensed by the cell and either refolded by chaperons or sent for proteasomal degradation for recycling of amino acids (Hetz, 2012; Rao & Bredesen, 2004). This would imply reduction in the quantity of certain proteins upon hypo-*N*-glycosylation. To test this hypothesis, we performed an unbiased proteomics on whole medaka hatchling lysis (*in collaboration with Ruppert Lab, Zmbh, Heidelberg University, Germany*). Each alg2^{hypo} and wild-type samples were normalized to their total protein and finally, alg2^{hypo} was normalized to its wild-type counterpart to compare protein amounts quantitatively. This approach did not allow for the analysis of proteins below the detection limit of the mass spectrometer in either of the groups. To this end, we included an exclusive protein list from alg2^{hypo} and as well as wild-type samples (**Figure 10A and 10C**).

As a pilot experiment, whole hatchling samples were measured via label-free LC-MS, which detected 6378 protein groups, which was reduced to 2190 protein groups upon filtering for protein groups identified by site, reverse sequences, potential contaminants, and at least 2 valid values. However, chemical labeling detected 2594 protein groups from whole hatchling, which was reduced to 1222 upon same filtering steps as in label-free technique. All in all, chemical

labeling reduced the number of detected proteins 1.8 times after filtering. Coverage of the LC-MS was not increased by increasing the amount of protein loaded in the column from 2µg to 8µg (data not shown).

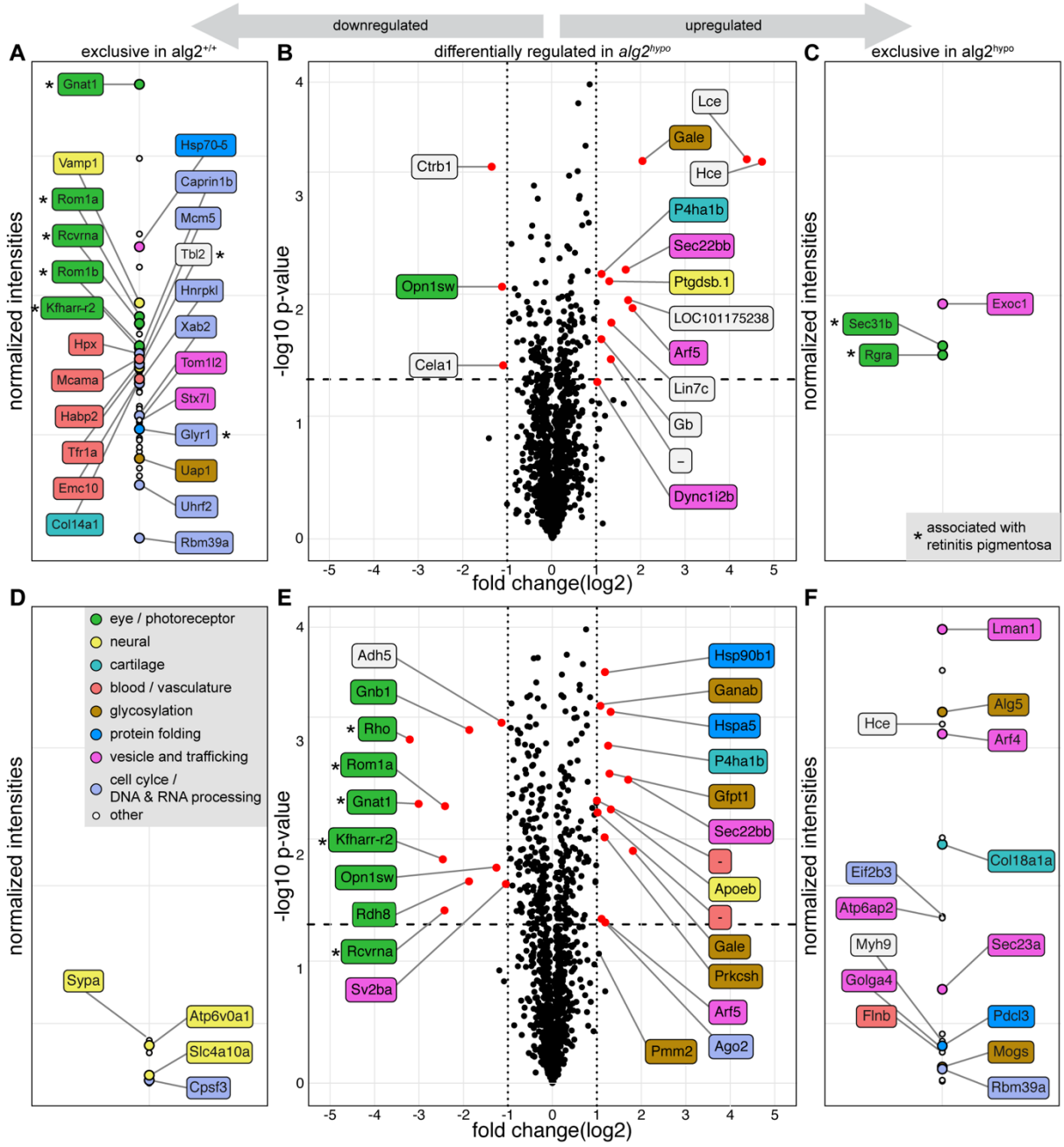

Figure 10: Mass Spectrometry analysis of medaka samples indicates a putative downregulation in the phototransduction pathway and points towards rod cell degeneration (upper panel: whole hatchling; lower panel: eyes)

(A, D) Intensity plots of proteins exclusively detected in wild-type samples amounted to 56 proteins from whole hatchling samples (A) and 7 from enucleated eye samples (D).

(B, E) Volcano plots of protein expression fold change of alg2^{hypo} normalized to wild-type medaka reveals distinct changes reminiscent of the multisystemic phenotypes. Proteins with significant ($p < 0.05$, dashed line) and more than 2-fold change (dotted lines) are indicated (red dots) and labelled.

(C, F) Intensity plot of proteins exclusively detected in alg2^{hypo} mutant samples amounted to 3 proteins from whole hatchling samples (C), 19 proteins from enucleated eye samples (F).

(All data produced jointly with Roman Sakson, ZMBH, Heidelberg, Germany; Figure adjusted from (Gücüm et al., 2020)).

Analysis of total protein extracts from alg2^{hypo} and wild-type hatchlings (stage 40, de-yolked, three replicates with six hatchlings each) upon isotopic labelling on the peptide level by dimethylation (Boersema et al., 2009) did reveal distinct differences, but not a global regulation of protein levels. Analysis of the proteome of alg2^{hypo} mutant (**Figure 10A to C**) uncovered 15 proteins with a significant ($p < 0.05$) differential abundance differing more than 2-fold (**Figure 10B**) in comparison to wild-type controls, out of which 12 were upregulated and 3 were downregulated in the alg2^{hypo} mutant fish. We identified the secreted metalloendopeptidases, low (lce) and high (hce) choriolytic enzymes (19 and 22-fold upregulation, respectively), as the top upregulated proteins followed by UDP-glucose 4-epimerase (Gale). The latter catalyzes two distinct interconverting reactions: UDP-galactose (UDP-Gal) from and to UDP-Glc, as well as *N*-acetylgalactosamine (GalNAc) from and to GlcNAc (Daenzer, Sanders, Hang, & Fridovich-Keil, 2012). All four nucleotide sugars serve as substrates for glycan synthesis. The remaining upregulated proteins are related to endopeptidases or play a role in vesicle transport, heme binding, or collagen synthesis. The three downregulated proteins were a putative violet sensitive opsin and two proteins containing peptidase S1 domain (**Figure 10B**). As mentioned previously, we found 56 proteins exclusive for wild-type (**Figure 10A**) and three for alg2^{hypo} samples (**Figure 10C**). Those proteins grouped into classes involved in vesicle trafficking, regulation of blood and circulatory system, protein folding as well as proteins with described and predicted functionality in neuronal and especially eye and photoreceptor related activity. Some of those eye related proteins (both from eye and whole hatchling) are associated with rod cell degeneration, namely retinitis pigmentosa (RP): Rho (Dryja, 1990; White, Hauswirth, Kaushal, & Lewin, 2007), Kfharr-r2 (Sippel, DeStefano, Berson, & Dryja, 1996), Gnat1(Carrigan et al., 2016), Pmm2 (Matthijs et al., 1997), Glyr1, Sec31b, and Rgra (Stelzer et al., 2016) ***(This paragraph was paraphrased from** (Gücüm et al., 2020)**).***

Remarkably, although proteomics analysis was performed on whole hatchlings, we found a prominent cluster of proteins related to retinitis pigmentosa to be regulated. To better understand the changes within the mutant eyes, we performed an unbiased proteomics approach on enucleated eyes (four replicates, 30 eyes each) of alg2^{hypo} and wild-type hatchlings at stage 40. The analysis identified 23 differentially expressed proteins ($p < 0.05$) with more than 2-fold change and 26 proteins exclusively found in wild-type or mutant samples (**Figure 10D to 10F**), while global protein levels were not changed. Differentially regulated and exclusive proteins revealed distinct cellular pathways to be affected by hypo-*N*-glycosylation. Alg2^{hypo} mutants displayed downregulation of proteins involved in the phototransduction pathway specific to

photoreceptor cells while proteins of the glycosylation machinery involving protein processing in the ER and protein folding enzymes, as well as vesicle trafficking proteins were found to be upregulated *(This paragraph was paraphrased from (Gücüm et al., 2020))*.

3.1.5 Analysis of the marker expression in eye shows rod cell degeneration and, hence, confirms retinitis pigmentosa

The prevalent downregulation of photoreceptor proteins in whole hatchling and eye-specific proteomics strongly suggested photoreceptor abnormalities. Similar to human eyes, ONL of medaka is composed of rod and cone cells. Previous histological examinations showed a shortened photoreceptor layer in the alg2^{hypo} (**Figure 7A-A'**). Closer examination of the transverse sections through mutant eyes showed a single layer of cells in ONL instead of two layers with shortened rods or cones (**Figure 11A-A'**). The analysis of a possible single layer with both cell types or one missing cell type was not performed. However, immunofluorescent markers revealed a severe decrease in the rhodopsin expression in rod cells, meaning that majority of the rod cells were missing, whereas cone cells (Zpr1) were not affected (**Figure 11B**). To understand whether reduction in the rhodopsin expression was due to the inability of cells to be maintained or to be differentiated, TUNEL apoptosis assay was performed on transverse eye sections, revealing apoptotic cells that were exclusive to the rod cell layer through the whole eye, both in the center and the periphery (**Figure 12**). This finding indicates that the rod photoreceptors were initially formed during development and post-embryonic growth, but were not maintained and were rather eliminated by apoptosis, a condition known as retinitis pigmentosa or night blindness. Of note, heat shock protein A5 (Hspa5), which is a facilitator of ER-associated protein degradation (ERAD) and initiator of the unfolded protein response (UPR) (Wang, Lee, Liem, & Ping, 2017) was upregulated in the proteomics assay from the mutant eye samples (**Figure 10E**). These data combined with the immunofluorescence (IF) strongly suggest induced-ER stress-associated apoptosis, upon prolonged UPR (Fribley, Zhang, & Kaufman, 2009) as the mechanism behind rod cell degeneration.

To further support that the rod cell degeneration was due to a potential maintenance issue rather than a differentiation, we assessed the ciliary marginal zone (CMZ) of the eye for the presence of stem and progenitor cells. For this purpose, alg2^{hypo} fish was crossed to *cndp1::GFP* reporter line to mark the stem cell population (Becker, Lust, & Wittbrodt, 2021) and sections were stained with Rx2 antibody to mark CMZ and photoreceptors (**Figure 13**). All in all, alg2^{hypo} did not display abnormalities regarding stem or progenitor cell morphology, further substantiating

the hypothesis that hypoglycosylation of photoreceptor proteins leads to rod cell degeneration while rod cell differentiation is largely unaffected.

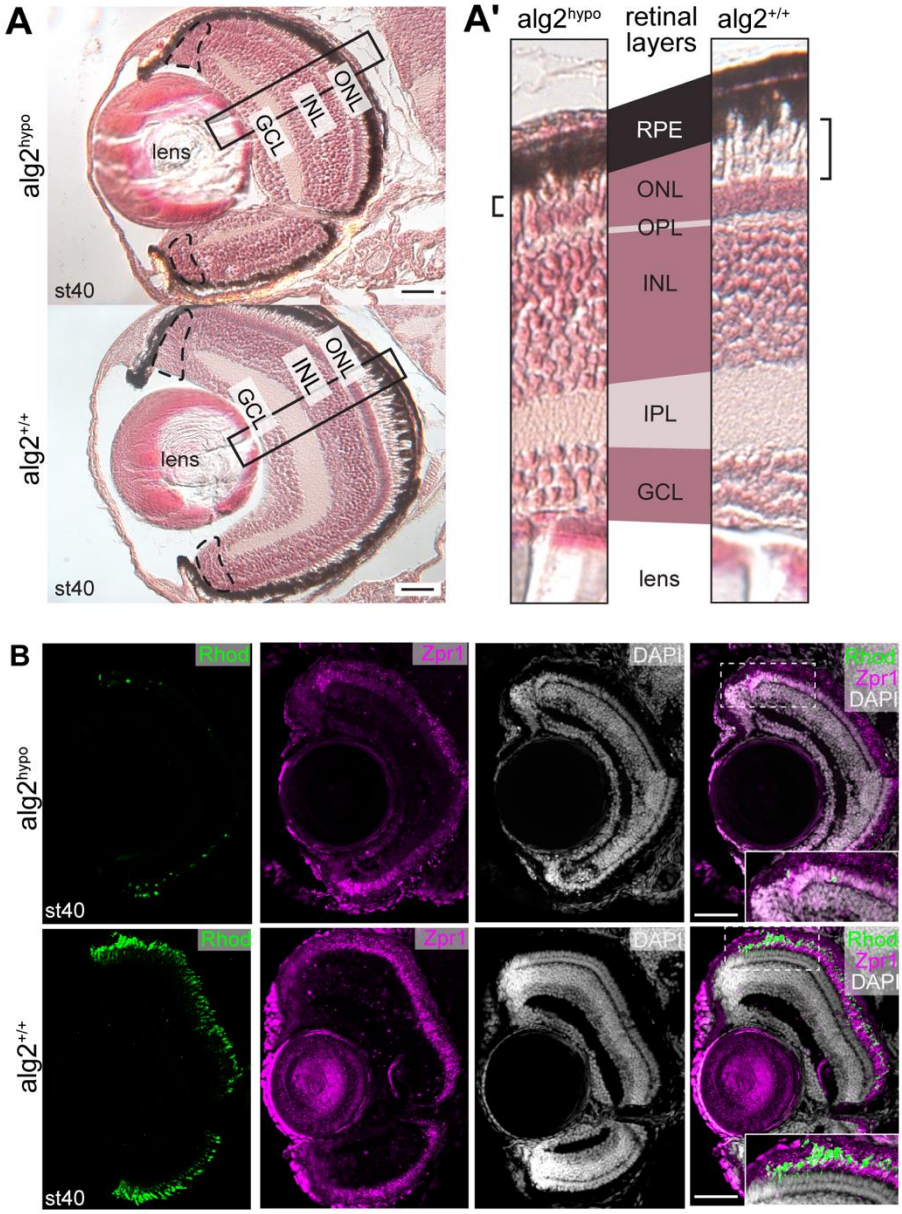

Figure 11: Histology and immunofluorescence on medaka sections suggest rod cell degeneration

(A-A') Hematoxylin and eosin staining on alg2^{hypo} and wild type eyes shows a single layer of photoreceptor in outer nuclear layer (ONL) whereas stem and progenitor or other differentiated cell layers do not show apparent abnormalities. *INL: Inner Nuclear Layer; GCL: Ganglion Cell Layer; RPE: Retinal Pigmented Epithelium; OPL: Outer Plexiform Layer; IPL: Inner Plexiform Layer. Square brackets: Rods and cones of photoreceptor cells. Dashed line: CMZ. Scale bar: 50µm.*
(B) Immunofluorescence on transverse sections of medaka eye indicated reduced rhodopsin (Rhod) expression whereas cone cells (Zpr1) cells were not affected. *Dashed area: outer nuclear layer of dorsal eye. Scale bar: 50µm.*
(Figure adjusted from (Gücüm et al., 2020)).

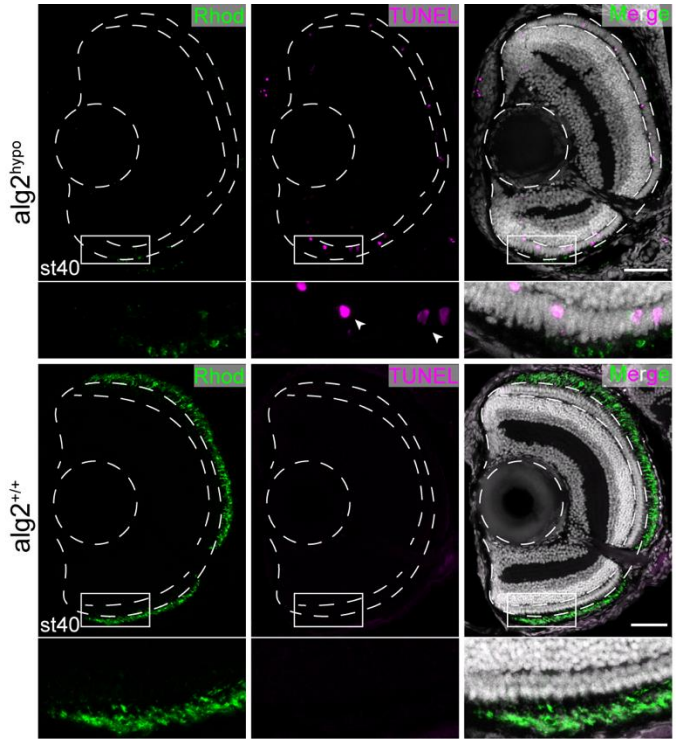

Figure 12: alg2^{hypo} rod cells are apoptotic at stage 40
TUNEL staining of transverse section marks exclusively apoptotic rod cells (arrows) while wild-type hatchlings do not have any apoptosis in the photoreceptor layer. *Dashed area: outer nuclear layer of eye and lens. Squares: Outer nuclear layer of the ventral retina. Scale bar: 50µm.*
(Figure adjusted from (Gücüm et al., 2020)).

Since neuronal cells support their maintenance via synapse formation and a possible synapse loss leads to apoptosis (Fricker et al., 2018), the cells from INL and their synapses to the rod cells were analyzed via marker expression. We found that the morphology or synapse formation of both bipolar cells (PKCα) and non-neuronal Muller glial cells (GS) was not affected in the alg2^{hypo} model (**Figure 14A and B**). Furthermore, ganglion cells (HuC/D, data not shown), horizontal cells judged by their morphology with nuclear DAPI staining, and the axonal projections of the ganglion cells to the optic tectum were not affected by hypoglycosylation (**Figure 15**). Overall, these data suggest that apoptosis of rod cells is due to cell-intrinsic factors, rather than perturbed synaptic communication or support by neuronal or non-neuronal cells in the eye.

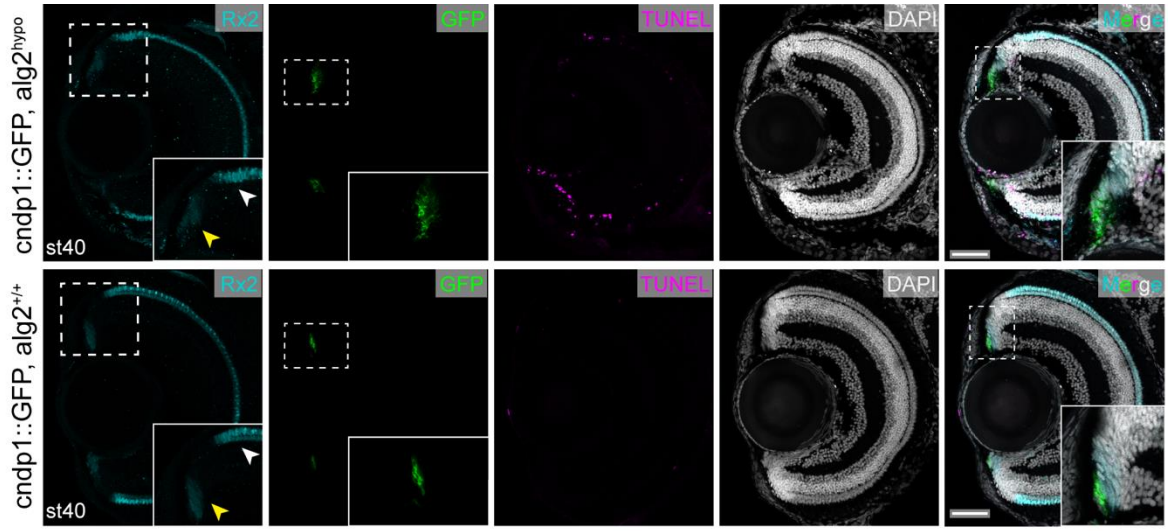

Figure 13: alg2^{hypo} stem and progenitor cells are not affected from hypoglycosylation
Immunofluorescence of the alg2^{hypo} fish in the *cndp1::GFP* background shows normal morphology of the stem and the progenitors in the CMZ (ciliary marginal zone). *Boxes show dorsal eye. Yellow arrowhead: CMZ; white arrowhead: photoreceptor layer; Scale bar: 50µm.*

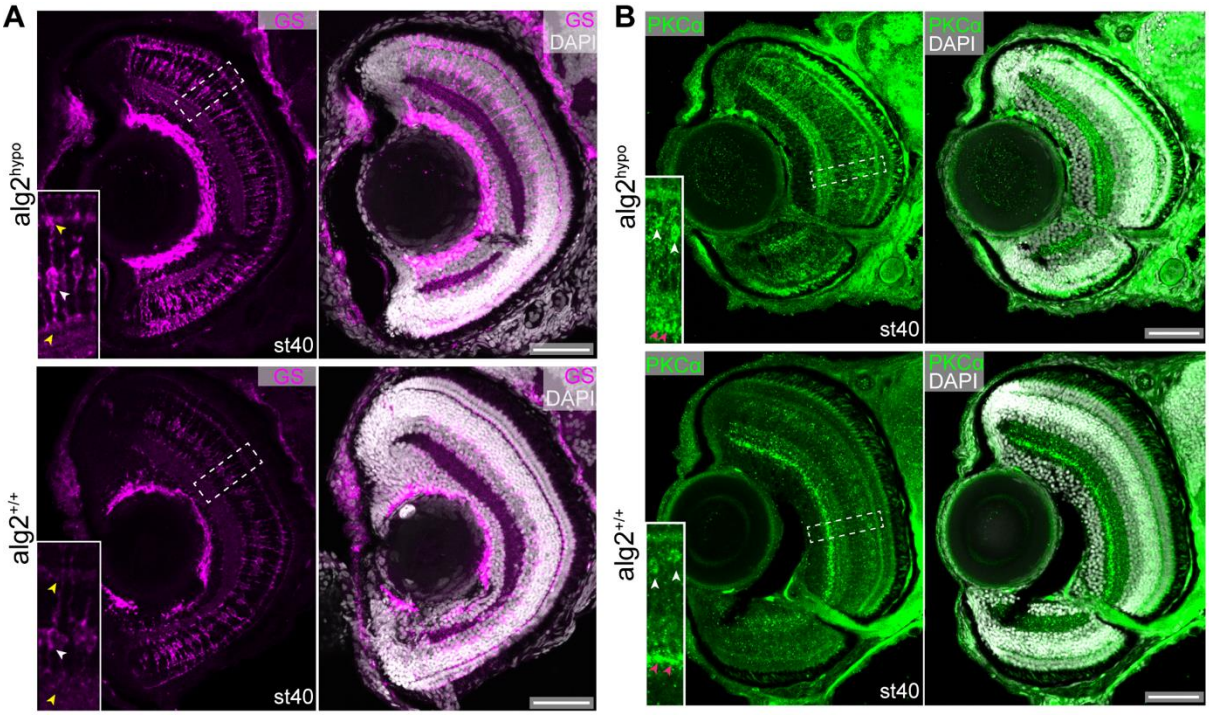

Figure 14: Muller glial cells or bipolar cells in the INL have normal morphology and marker expression in alg2^{hypo} fish
(A) Immunofluorescence of a non-neuronal Muller glial cells (GS) and **(B)** bipolar cells (PKCα) and their cell bodies and axonal and dendritic projections show normal morphology. *Yellow and red arrowhead: dendrites; white arrowheads: cell body. Scale bar: 50µm.*

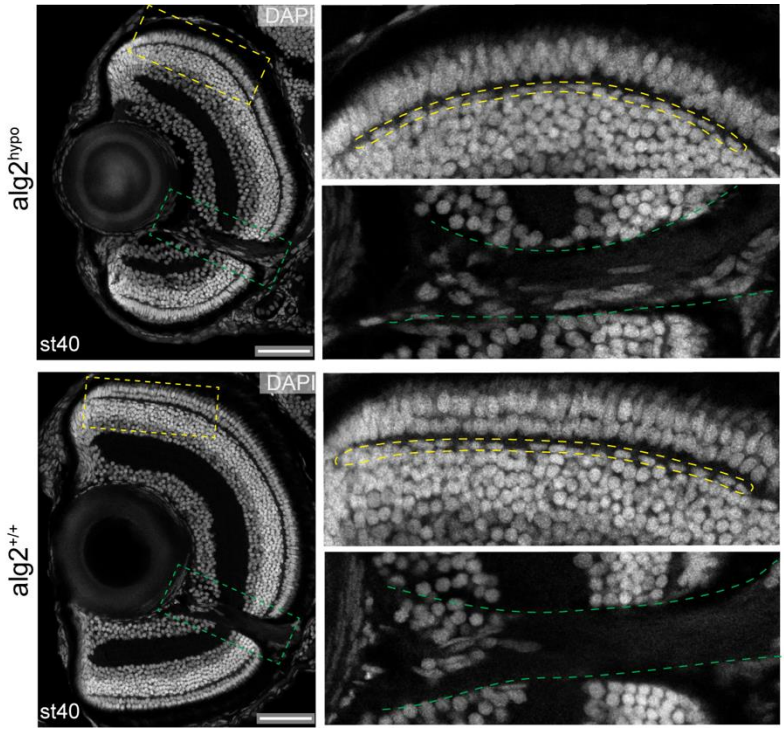

Figure 15: Nuclear staining identifies normal morphology of the horizontal cell and axonal projections to brain.
Transverse sections show that the horizontal cells (yellow) in the INL differentiated and axonal projections (green) are sent to the brain. *Scale bar: 50µm.*

3.1.6 Both medaka and human *Alg2* mRNA rescues the multisystemic phenotypes and survival of the alg2^{hypo} model

Gene therapy is an emerging field for the gene correction of hereditary diseases. As a proof of principle experiment for potential gene correction, alg2^{hypo} fish were injected at zygotic stage with medaka or human *Alg2* mRNA. Both injection schemes resulted in the rescue of the multisystemic phenotypes apparent from gross morphology (**Figure 16A**) and cartilage tissue staining (**Figure 16B and B'**) at the stage when the control injections displayed multisystemic abnormalities. Intriguingly, the life span of the homozygote juveniles was extended until the end point of the experiment, 18dph (**Figure 16C**). Importantly, medaka *alg2* mRNA injections led to the rescue of rod cells in ONL and prevented their degradation (**Figure 16D**). Furthermore, the rescue of the mutants also validated that the multisystemic phenotypes arise specifically from the mutation in the *alg2* allele, but not due to an off-target sgRNA binding site in other regions of the medaka genome.

These results raised the question whether the Alg2 protein is required to overcome a developmental bottleneck through embryonic or post-embryonic development. To address that question, fish were injected with lesser amounts of mRNA, which would result in an earlier

depletion of wildtype Alg2 enzyme. An injection tracer, *GFP* mRNA, was used to assess the dosage of *hsAlg2* mRNA. Interestingly, fish injected with low dose Alg2 mRNA developed multisystemic phenotypes including edema around the eyes and the heart, blood clogging in the vessels, tubular heart, thinned vessels, shortened snout (**Figure 16E**) and difficulty in swimming at 7dph, which is 7 days after the control group died. These preliminary results suggest that the Alg2 enzyme is not only needed to overcome a developmental bottleneck, but required throughout the life of fish to maintain the physiological integrity and cell maintenance.

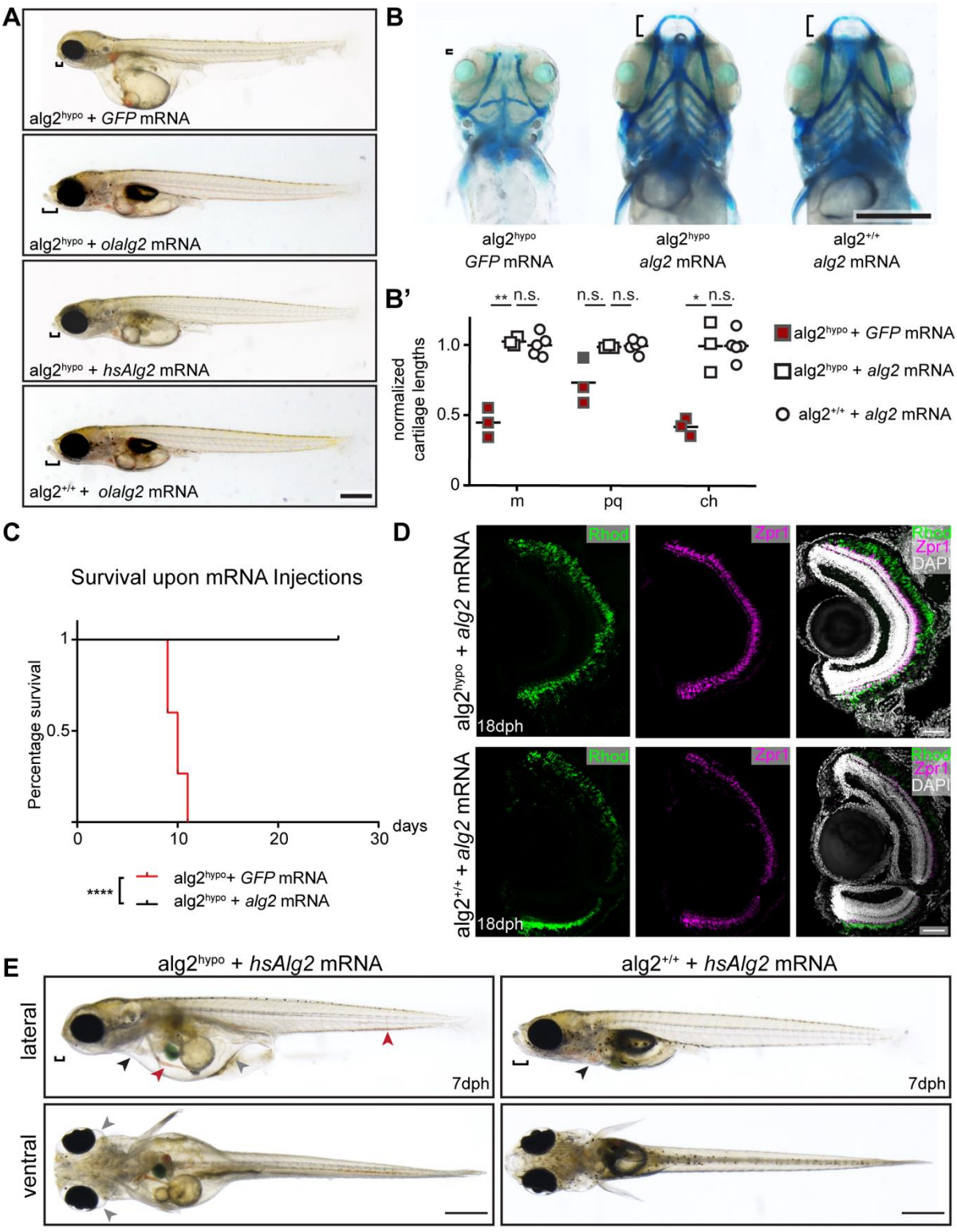

Figure 16: alg2^{hypo} is successfully rescued with both *olalg2* (medaka*)* and *hsAlg2* (human) mRNA injections

(A) *In vitro* synthesized medaka and human *Alg2* mRNAs were injected at one-cell stage and the fish were raised 3 weeks post hatching (18dph). Multisystemic phenotypes were rescued at stage 40 when the control injected fish displayed phenotypes. *n=11 for alg2^{hypo}+ olalg2 injection; n=2 for alg2^{hypo}+hsAlg2 mRNA; n=4 for alg2^{hypo}+GFP mRNA; square brackets: size of the snout. Scale bar: 0.5mm*

(B-B') Alcian blue stainings (B) and quantification of the cartilage lengths (B') showed rescue to the wild-type levels upon mRNA injection. *m: Meckel's cartilage; pq: palatoquadrate; ch: ceratohyal cartilage. Two-tailed nonparametric Student's T-test; * <0.05; ** < 0.01. Scale bar: 0.5mm*

(C) alg2^{hypo} injected with *olalg2* mRNA can survive until the end-point of the experiment (18dph) without displaying multisystemic phenotypes. Only the number of homozygote mutants are displayed in the Kaplan-Meier plot. *Gehan-Breslow-Wilcoxon test, p<0.0001. n=15 for alg2^{hypo}+GFP mRNA and n=11 for alg2^{hypo}+alg2 mRNA.*
(D) Rod cell degeneration is rescued upon *olalg2* mRNA injections at 18dph. *Scale bar: 50µm.*
(E) *hsAlg2* mRNA rescued fish with lower amounts of mRNA injection displayed multisystemic phenotypes 1 week after the control injected homozygote mutant, which is when control group already died. *n=1; Gray arrow: edemas; black arrow: heart; red arrow: blood clogging; square brackets: snout. Scale bar: 0.5mm*
(Figure adjusted from (Gücüm et al., 2020)).

3.1.7 D- mannose supplementation does not rescue alg2^{hypo} fish

Carbohydrate supplementation, such as mannose and galactose, is a method used to ease the symptoms of CDGs (Witters, Cassiman, & Morava, 2017). With this method, concentration of the substrate is increased to shift the balance of the chemical reaction catalyzed by glycosylation enzymes to the product side. To rescue the multisystemic phenotypes, alg2^{hypo} fish and their wild-type or heterozygote siblings were treated with D-glucose (data now shown) or D-mannose supplementation (**Figure 17A**). Toxicity tests showed that at high concentrations, around 500mM, mannose leads to blood clotting and dismorphisms and it also reduces the life-span of the wild-type fish (**Figure 17B**). These results confirmed also that the mannose can penetrate through the chorion as untreated fish displayed similar abnormalitites as the sand paper treated wild-type medaka, which is used to introduce micro-holes on the chorion surface. Moreover, high mannose treatment led to developmental delays (**Figure 17C**). Treatment of fish with D-glucose (data not shown) or D-mannose at its lowest possible concentration, 50mM, did not rescue the multisystemic phenotypes or the survival ability of the alg2^{hypo} fish (**Figure 17D**). The fish that died upon hatching with multisystemic phenotypes were not genotyped as it followed Mendelian segregation (n=16/71 (23%) for 50mM mannose supplementation or n=13/51 (25%) for vehicle control). All in all, this data suggest that nutritional supplementation is not enough to push the activity of the Alg2 enzyme to elevate the levels of downstream *N*-glycan products.

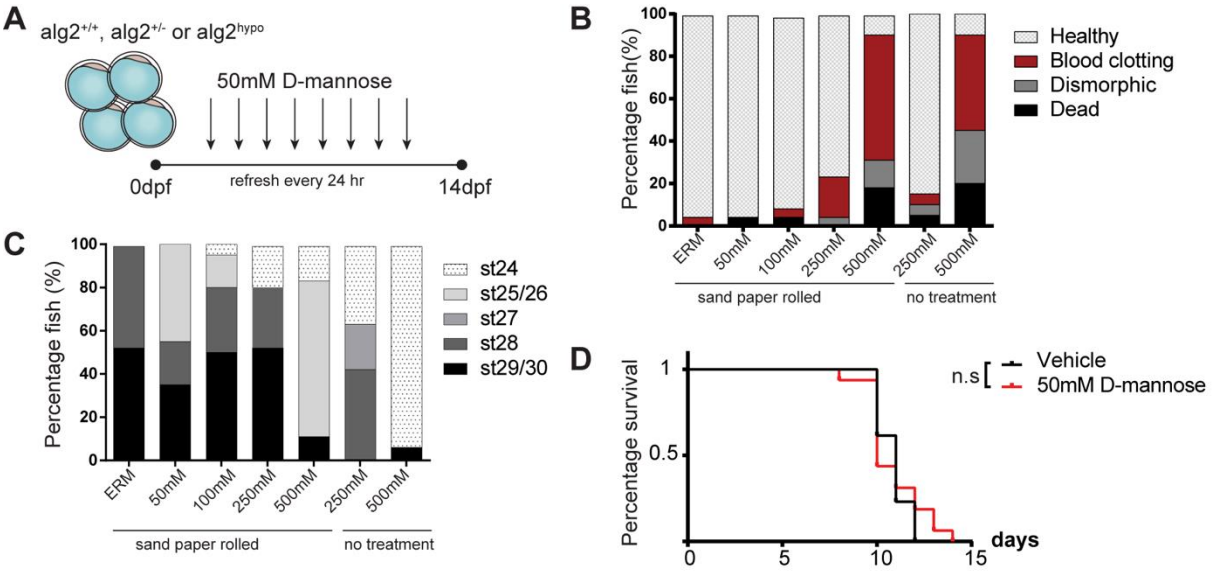

Figure 17: D-mannose supplementation throughout embryonic and juvenile stage did not rescue alg2^{hypo} phenotype.

(A) Scheme representing D-mannose (or D-glucose) treatment until 14dpf. Fish were incubated in 50mM D-mannose dissolved in ERM at 28 °C until the end-point of the experiment. Medium was refreshed every 24hr.

(B-C) Toxicity test reveals that D-mannose is toxic to fish at high concentrations leading to blood clotting and dismorphism (B) as well as developmental delays (C).

(D) Kaplan-Meier plot showing that there is no survival benefit upon D-mannose supplementation. Only fish with multisystemic phenotypes, which eventually died are represented in the Kaplan -Meier plot. *n=16 for 50mM Mannose and n=13 for vehicle control. Gehan-Breslow-Wilcoxon test, p=0.75.*

3.2 Discussion

3.2.1 Effects of C-terminal mutation alleles on the Alg2 enzyme activity remains to be addressed

Congenital disorders of glycosylation (CDG) is a set of diseases seen among patients with mutations in glycosylation genes (Brasil et al., 2018). It affects multiple organs and tissues, including brain, eyes, heart, liver, intestine, muscles, and blood (Freeze, 2007; Jaeken & Carchon, 2001; Kjaergaard et al., 2001). As such, patients can display variant combinations of diseases depending on the mutated gene. Patients carry hypomorphic alleles, meaning that the mutated allele renders enzyme with a residual activity (Freeze et al., 2017). Moreover, patients with mutations in the same gene can bear symptoms of differing severity, although conflicting reports on the correlation between the residual enzyme activity and the severity of the disease exist (Grünewald, 2001; Imtiaz et al., 2000). In this sense, the disease of each patient can be viewed as unique, which also implies that generating a model organism to study all aspects of CDGs is simply not possible, as each model would reflect one set of disease groups emerging due to a particular glycosylation deficiency.

The generation of precisely targeted mutations in our fish model relied on CRISPR/Cas9 mediated double stranded break and homology-directed repair (HDR) mediated insertion. Due to the higher percentage of non-homologous end joining (NHEJ) events for double-stranded DNA break repairs (Yang et al., 2020), we have generated many different alleles among which a 2-amino acid deletion mutant and a C-terminal truncation mutant were raised to homozygosity. Interestingly, the latter led to a higher percentage of embryonic lethality compared to the rest (quantification not shown). This might be due to the fact that *alg2* is regulated on the RNA level, meaning that a truncated form of RNA is leading to its nonsense-mediated mRNA decay and triggering a further instability of the protein (Baker & Parker, 2004). The truncated DNA sequence might also serve as an important regulatory element such as an miRNA binding site for regulation of its activity.

One aspect in this work that still remains elusive is how the mutant alleles affect the enzyme conformation and function. One possibility is that the mutant allele might reduce the enzyme activity by rendering the enzyme catalyzing the reaction slower or less efficient. Unfortunately, addressing the enzyme activity directly has been challenging due to necessity to synthesize the precursor substrates under analytic laboratory conditions (Li et al., 2018) and the isolation of

functional ER-resident enzyme. Alternatively, the *alg2* mutations might reduce the stability of the protein and thereby lead to a reduction of its protein level, as can be observed for the multiple reaction monitoring (MRM) analysis of human ALG2-CDG fibroblast samples (Sakson et al., 2020). To this end, enzyme expression levels at the RNA and protein level can be examined. On the other side, mass spectrometry approaches could be used for a relative quantification since label-free quantification detects levels of medaka Alg2 although it is a low abundant protein (data not shown), however reproducibility of this method was low (Alg2 was detected in 1 out of 4 wild-type samples). However, our dimethyl labeling approach for a more robust and reproducible quantification method could not detect endogenous levels of mannosyltransferases, except for Alg5, as this method is reducing the resolution at least 2-3 times due to loss of sample for further processing and multiplexing of samples (Liu et al., 2017). Furthermore, search of specific Alg2 mass as a targeted-MS approach could not detect Alg2, neither. However, quantification of low-abundant proteins is possible via MRM with optimization of detection parameters with synthetic peptides (Shi et al., 2012).

Although the effects of mutations on the enzyme function was not directly measured, xCGE-LIF was used as an indirect measurement of effects on *N*-glycome as Alg2 is catalyzing the addition of the second and the third mannoses to the growing chain of lipid-linked oligosaccharides. A reduced enzyme activity or level in the alg2^{hypo} model would imply production of lower amounts of *N*-glycans and accumulation of substrates from upstream reactions. Of note, only high-mannose and complex-type *N*-glycans were detected and annotated in xCGE-LIF. Thus, the accumulation of substrates upstream of Alg2 products was not analyzed. However, the effect of hypoglycosylation manifested itself as a reduction of downstream *N*-glycans both in medaka and human fibroblast samples. The observed reduction in *N*-glycans might result from several possible changes in terms of protein glycosylation. First, some of the *N*-glycan sites in each glycosylated protein might be skipped, hence, rendering some *N*-glycan sites unoccupied. Secondly, some of the proteins might not be glycosylated at all, whereas others display glycosylation, as there might be a competition between proteins to be glycosylated. Moreover, combination of the first and the second scenarios might cooccur. The third possible outcome of hypo-*N*-glycosylation is that *N*-glycans might be build up aberrantly due to deficiencies in the pathway. Due to the complex mixture of the input protein samples with and without *N*-glycosylated proteins, addressing *N*-glycan site occupancy via unbiased MS approaches was not possible. Although MS can detect all of the post translationally modified proteins, database search of all the possible combinations of *N*-glycan

sites and types for whole proteome would be impractical. However, experimentally the study of the *N*-glycan sites as well as types for a single peptide or protein could be achieved by overexpression of the tagged protein and its subsequent purification and MS analysis. On the other side, previous publications showed that mutations in the enzymes processing the build-up of *N*-glycans in the ER lead to reduced *N*-glycan site occupancy (Butler et al., 2003; Coddeville et al., 1998; Hülsmeier et al., 2016; Mills et al., 2003), whereas mutations of enzymes responsible from *N*-glycan processing in the golgi lead to aberrant glycan processing (Imtiaz et al., 2000). However, alg2^{hypo} model displayed both reduction in *N*-glycosylation occupancy and aberrant *N*-glycan branching (unique *N*-glycans). The latter might result from the fact that mutations of Alg2 result in regulation of protein levels of *N*-glycan processing enzymes in ER including Mogs, Ganab, and Prkcsh and ER-to-Golgi trafficking proteins such as Sec22b, Dyn1l2, Sec23a, Lman1, and Arf5. Importantly, the xGEC-LIF data did not only reveal the reduction of the *N*-glycan occupancy under hypoglycosylation, but also a high conservation of the glycan types and their relative contributions for human and fish samples.

Lectin blots performed as a supporting assay for xCGE-LIF data showed a discrepancy for the patient fibroblast samples. This might be due to the fact that fibroblast samples are not as susceptible to changes in *N*-glycosylation as the other tissues, which is supported by the xCGE-LIF data, as only high-mannose type structures were found to be reduced, whereas complex-types, which make up for 68% of all the *N*-glycans, were not affected. Since the resolution of lectin blots is limited, the reduction in a subset of glycan structures might not be detected with this strategy. Moreover, lectin blots do not only measure the mannose and *N*-acetylglucosamines from *N*-glycans, but from all other glycosylation types. On the other side, differences between wild-type and alg2^{hypo} medaka samples were observable in both assays. This might again be explained by the complex mixture of different cell types that might have different vulnerabilities towards reduced *N*-glycosylation, leading to a more robust overall reduction of *N*-glycan levels. For a better comparison between medaka and human samples, cultured medaka fibroblast samples would circumvent discrepancies arising from comparing a specific cell type with complex tissues. Yet, fibroblast samples from alg2^{hypo} fish could not be maintained in DMEM with 10% FCS culture conditions whereas heterozygote and wild-type counterparts could be grown (data not shown). This also implies that the phenotype resulting from the *alg2* mutation in fish might result in a stronger phenotype, and hence, a stronger reduction in enzyme activity than the compound heterozygote allele.

Lectin blots and xCGE-LIF serve as a good proxy to show that alg2^{hypo} is a hypomorphic model, but it does not serve as a direct indication of hypomorphicity. One possibility to argue that alg2^{hypo} is a null allele is that the lack of Alg2 enzyme in embryo might be rescued by contribution of yolk until hatching stage as yolk is known to contribute to hormones and enzymes although very little is known about the content of enzymes in fish oocytes/eggs (Brooks, Tyler, & Sumpter, 1997; Kamler, 2008). However, maternal mRNA expression in the cell, which lasts only until very early stages of embryonic development, such as 3hpf of zygotic genome activation in zebrafish (Tadros & Lipshitz, 2009), would not be sufficient to rescue the alg2^{hypo} embryos until hatching unless protein has a slow turnover rate. All in all, for a direct answer to hypomorphicity either an enzyme activity test or a complete null allele of *alg2* under homozygosity has to be analyzed. In addition, rescue experiments with the overexpression of the alg2^{hypo} allele, instead of the wild-type allele, could indicate whether the model carries a real hypomorphic allele.

3.2.2 Susceptibility of certain cell types to hypo-*N*-glycosylation patterns the ALG2-CDG phenotypes

Medaka alg2^{hypo} model was established by mimicking the maternal allele of a patient with multisystemic phenotypes (Thiel et al., 2003). The finding that the fish model did not show any visible phenotype until the hatching stage and that patients seem to develop normally until birth, is strongly suggesting a maternal contribution or a maternal rescue of the loss of enzyme function. Common phenotypes, such as reduced white matter, delayed motor development and craniofacial dismorphism for both human and fish further reiterates the conservation of the *N*-glycosylation pathway across the species and emphasizes the validity of using medaka as a model organism for human disease modelling.

CDG patients are reported to have varying degrees of life expectancy that is mostly shortened due to multisystemic phenotypes, which are also the cause of death, such as bleeding, liver failure, cardiac failure and pneumonia (Bogdańska et al., 2021; Freeze et al., 2017; Kjaergaard et al., 2001; "Congenital Disorders of Glycoyslation", 2015). Similarly, mutant fish are only viable for 2-4 days after hatching, whereas healthy siblings survive up to 1.5 years. Although comparing lifelines between fish and human is not trivial, the fact that the index-patient is about 19 years old and still alive, raises the question whether the fish allele leads to more drastically reduced enzyme activity than the human allele. To this end, it is important to keep in mind that human allele is composed of a compound heterozygote allele, of which the paternal transcript

was shown to be missing from the paternal sample (Thiel et al., 2003). Yet, we do not have any information about the tissue-specific expression of ALG2 paternal and maternal alleles (Andergassen et al., 2017) and whether the paternal allele is stable in other tissues of patient, rendering some tissues with higher enzyme activity levels. Nevertheless, the cause of death in alg2^{hypo} model could be resulting from apoptosis of several tissues and oxygen and food deprivation due to blood flow arrest. Moreover, mutant fish might fail to feed due to shortened snout or failure to catch the food from the surface of the water due to swim bladder and motor development abnormalities. Since Alg2 is also associated with congenital myasthenic syndrome (Cossins et al., 2013), assessment of muscle fiber physiology and swimming behavior assays are of interest for the future characterization of mutants in terms of neuromuscular development. Additionally, this model displays edemas most probably due to vessel thinning or the inability of lymphatic vessels to collect excess liquid from the extracellular matrix. The slow blood flow might be a consequence of these edemas, as well as thinned vessels, or impaired heart function.

Besides common phenotypic features, our fish model showed other multisystemic phenotypes observed among CDG-type I patients, but not reported for the ALG2-index patient specifically. Rod cell degeneration, namely Retinitis Pigmentosa (RP) or night blindness, was a prominent phenotype observed in the fish model, which is also shared by other CDG-type I patients. If not RP, the ALG2-CDG patient displayed other eye abnormalities including, cataract, coloboma of the iris, abnormal vision, and nystagmus. The latter is reported to co-occur with RP in early-onset patients (Verbakel et al., 2018), as our ALG2-index patient. Moreover, retinitis pigmentosa was reported in many patients with mutations in *Pmm2* and *Dhdds*, which are other enzymes of *N*-glycosylation pathway (Lam et al., 2014; Monin et al., 2014; Thompson et al., 2013; Züchner et al., 2011). Thus, RP is an important identifier of CDG-Type I patients and relevant model for studying the role of *N*-glycosylation in cell type maintenance. In line with this, one study showed that in mouse brain, cerebellar granule cells are more sensitive to inhibition of *N*-glycosylation than cortical neurons (CN) either by tunicamycin (a lipid-linked oligosaccharide (LLO) synthesis inhibitor) or *Pmm2* knockdown (Sun et al., 2013). The reason for why some cell types are more susceptible to hypo-*N*-glycosylation rather than the others still remains to be elucidated. One explanation could be that rather than displaying patterns or markers of susceptibility, some cell types might simply express proteins that need to be glycosylated more than the others. Consequently, hypoglycosylation in these cells would lead to elevated levels of misfolded proteins, higher ER-stress and eventual apoptosis. Mapping

whole medaka homozygote mutants for apoptotic cell types and their common features could identify the common denominator for susceptibility of different cell types or tissues under hypo-*N*-glycosylation conditions.

3.2.3 Proteomics analysis has to be combined with the transcriptome data to address mechanism of rod cell apoptosis

Unbiased proteomics performed on eye and whole hatchling samples of alg2 mutant and wild-type via mass spectrometry identified proteins related to sugar metabolism (Gale and Gfpt1) and ER-resident glycosylation (Alg5, Mogs, Prkcsh, Ganab) to be upregulated and proteins related to RP to be downregulated in the mutant. Possible causes of these changes could be grouped under primary or secondary changes as a response to hypoglycosylation. Primary changes would result from a direct change of glycosylation status of a protein, whereas secondary changes would be changes occurring as a response to primary changes (**Figure 18**).

Primary changes can be explained in terms of downregulation due to protein ubiquitination and proteasomal degradation (**Figure 18-I**) or upregulation via escape of proteins from degradation (**Figure 18-V**) process leading to protein accumulation, such as in Alzheimer's disease (Thal & Fändrich, 2015). Importantly, eye samples were not pre-treated with de-glycosylation enzymes, such as PNGaseF to remove *N*-glycans, or other posttranslational modifications from the protein lysates. Mass spectrometry would detect all proteins and their *N*-glycosylated forms, but the database search of the results would not enable detection of the latter since *N*-glycans are very diverse and complex. Thus, an upregulation in the mass spectrometry might simply mean that the non-glycosylated counterpart of the proteins increased with or without the total protein amount has changed (**Figure 18-VI**). To address this issue, protein lysates could be run as PNGaseF treated and untreated counterparts and their relative ratios in both mutant and wild-type samples could be compared to estimate the glycosylation coverage. This analysis would also identify the *N*-glycosylation sites that were affected from hypoglycosylation and would point towards downstream effectors of the *alg2* mutation.

The main cause of the secondary changes, on the other hand, is due to transcriptional changes. This is further supported by MS targets that do not occupy any *N*-glycosylation motif or predicted *N*-glycosylation site (**Appendix Table 2a and 2b**). For instance, levels of mRNA(X) can change due to protein degradation or accumulation of Protein(Y) or as a response to its own changes: Protein(X) (**Figure 18-III-IV)**. The latter case would be identified as a compensatory

up- or downregulation, meaning that the cell would try to make up for its loss or lower its amounts for a healthy homeostasis. In this line, interpretation of a compensatory up- or downregulation from MS data without transcriptomic would require the assumption that glycosylated counterpart of a protein is quantitatively negligible compared to its non-glycosylated counterpart. Lack of *N*-glycosylation sites or occupancy is not only explained in terms of RNA level of changes, but also possible through protein-protein interaction level of regulation of proteome, which can be accepted as another secondary effect (**Figure 18-VII**). For instance, a protein that needs to be glycosylated might form a protein complex with another protein that does or does not need to be glycosylated under hypoglycosylation. Stability or formation of such a persistent complex or oligomer might depend on glycosylation of at least one of the partners. In this line, *N*-glycosylation is reported as an important and necessary process for oligomer separation and monomer stability. For example, protein disulfide isomerase family A member 2 (PDIA2) has three *N*-glycosylation motifs, all of which are occupied with *N*-glycans. Mutation of one of the *N*-glycosylation sites increases the formation of highly stable dimers (Walker et al., 2012). Additionally, *N*-glycosylation is what differs Ribonuclease B (RNaseB) from Ribonuclease A (RNaseA) as they share the same protein sequence and conformation. Yet, oligomerization of RNaseB is hindered by the occupied Asn34 site (Gotte, Libonati, & Laurents, 2003; Jayaprakash & Surolia, 2017). In this line, I found rhodopsin to be upregulated in our MS screening, which has been implicated in photoreceptor instability in *Drosophila* and mouse models. Mechanistically, rhodopsin was shown to form a stable complex with arrestin that induces photoreceptor cell death via apoptosis (Alloway, Howard, & Dolph, 2000; Murray et al., 2009; Chen et al., 2006). While rhodopsin is known to be *N*-glycosylated (Murray et al., 2015), arrestin is not reported to have occupied *N*-glycosylation sites, despite containing *N*-glycosylation motifs. These findings make it intriguing to speculate that such protein-protein complex formation might occur in rod cells under hypo-*N*-glycosylation conditions, which in turn may mediate a mechanism of protein-protein interaction induced apoptosis of rod cells.

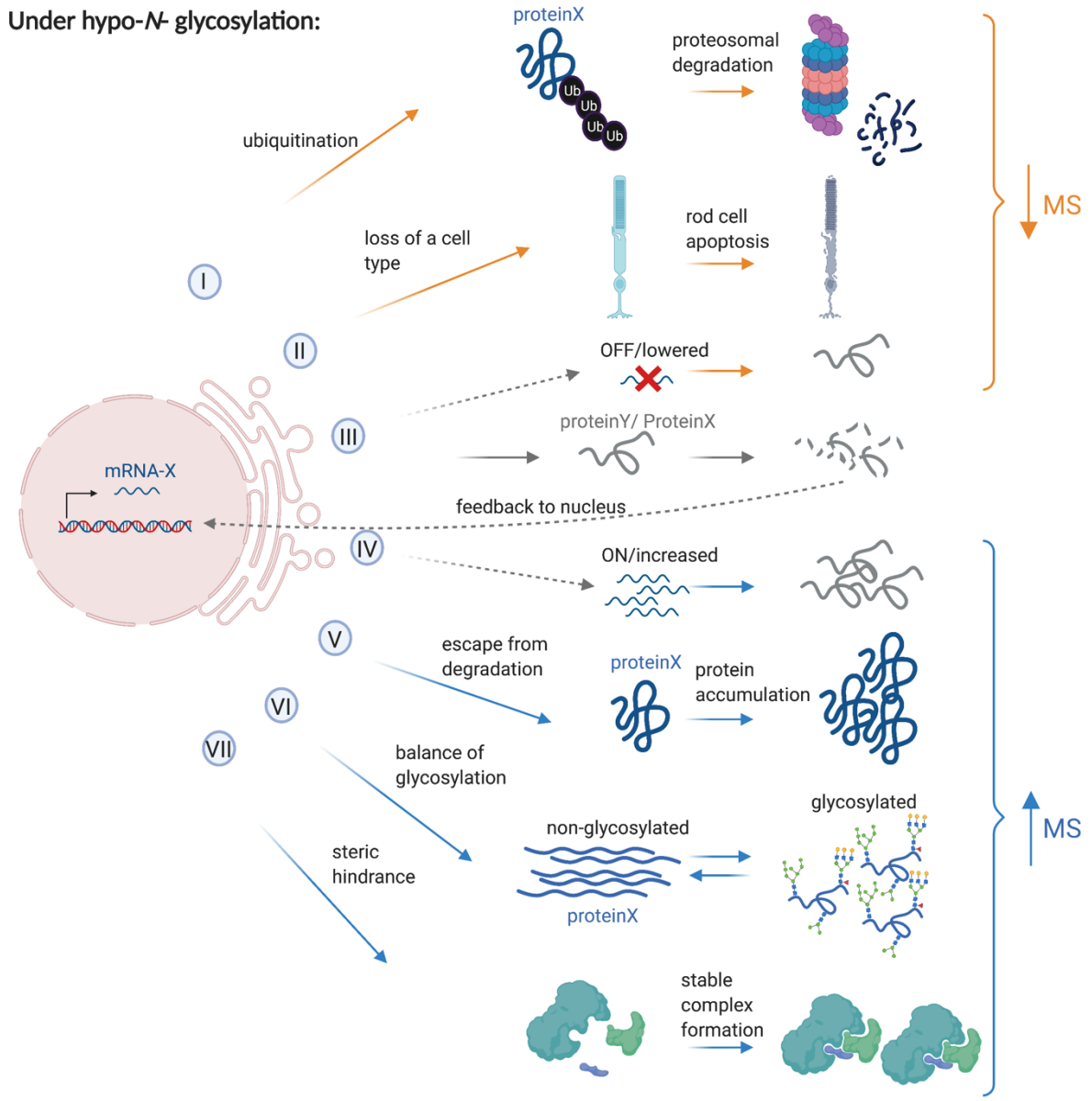

Figure 18: Schematic interpretation of the mass spectrometry data for possible mechanisms explaining up- and downregulation in the proteome under hypo-*N*-glycosylation
(I) Ubiquitination and proteasomal degradation of misfolded proteins
(II) Loss of a cell type (can be both the cause and the result of reduced protein levels)
(III) Transcriptomic regulation by turning OFF or lowering the expression of genes as a response to protein degradation or accumulation
(IV) Transcriptomic regulation by turning ON or increasing the expression of genes as a response to protein degradation or accumulation
(V) Escape of proteins from degradation, possibly via overload of chaperones and proteasomes
(VI) Increase of the non-glycosylated counterpart of a protein with or without changing total protein amounts
(VII) A naturally existing glycosylation site preventing protein aggregation or complex/oligomer formation. Lack of this site would help monomers to collide and form complexes/oligomers.

Mass spectrometry (MS) analysis on whole hatchling samples further revealed downregulation of proteins related to eye and photoreceptor expression and proteins associated with retinitis pigmentosa from mutant samples. This might be due to the fact that at this stage of development,

eyes form a bigger percentage of the body compared to the later stages. MS results combined with immunofluorescence raised the question whether the downregulation in those proteins was simply a result of loss of rod cells (**Figure 18-II**). This point can be argued against since proteins associated to RP might not only be expressed in the rod cells that are in the process of dying, but outside the rod cells, such as Glyr1 and Tbl2. In addition, some of the proteins found to be downregulated are shown to give rise to RP in several animal models, such as Rho (Santhanam et al., 2020), Rom1a (in a mutant background; Conley et al., 2017), and Gnat1 (Calvert et al., 2000) (Collin et al., 2020). Furthermore, the stability of Rhodopsin has been shown to be dependent on its glycosylation at Asn15 for rod photoreceptor stability (Kaushal, Ridge, & Khorana, 1994; Murray et al., 2015). Thus, although loss of rod cells is a relevant argument for downregulation, it is highly likely that hypoglycosylation of proteins associated with RP is a probable cause of the rod cell degradation. One way to assess this hypothesis would be to mutate *N*-glycosylation sites (NXS/T) of selected MS targets via CRISPR/Cas9 targeted genome editing to reproduce RP phenotype. This method can also identify novel proteins, which are responsible from the disease phenotype, but not yet been discovered.

As our MS and IF data revealed a severe loss of rod cells under hypo-*N*-glycosylation, I asked the question whether rod cells failed to differentiate or could not be maintained. To this end, I further checked the stem and progenitor layer and as well as differentiated cell types (Muller glial, bipolar and horizontal cells) in the INL via IF. However, none of these directly showed that at some point in development fish successfully differentiated rod cells. In order to address this issue rod stainings should be repeated during earlier stages of development to capture the beginning of rod cell differentiation, potentially between stage 32 and 39.

3.2.4 Mechanism of rod cell apoptosis is likely via prolonged UPR-response-induced-apoptosis or mannose poisoning

As we could establish that hypoglycosylation is important for rod cell maintenance in the eye, we next sought to shed light on the mechanism by which these cells are maintained and what the downstream targets of hypoglycosylation are. Our MS results revealed one of the *bona fide* markers of the UPR, namely Hspa5, also known as Bip, as upregulated. Moreover, as Hspa5 does not have any *N*-glycosylation motif (**Appendix Table 2a**), the UPR response was likely elevated as a secondary response to hypoglycosylation (as described in **Figure 18**), suggesting that hypoglysosylation led to the misfolding of proteins, which consequently resulted in ER-stress and a prolonged UPR response that eventually led to apoptosis. This hypothesis, however,

needs further orthogonal lines of evidence, such as transcriptomic analysis of UPR associated response genes, i.e. *Bip, Xbp1, Perk, IreI, Atf4* and *Atf6* in combination with *in situ* analyses to pinpoint their spatial localization (Li et al., 2016).

Another possible mechanism for apoptosis induction might be sugar accumulation, for example of mannose-6-phosphate, in the reported mutants, leading to rapid depletion of ATP resources in the body. The drastic effects of sugar accumulation on an organismal level can be fully appreciated in honey bees or cultured rat embryos, in which the increase of sugar levels leads to rapid death, also known as honeybee effect (de la Fuente, Peñas, & Sols, 1986; DeRossi et al., 2006; Freeze & Schachter, 2011; Freinkel et al.,1984). Since Alg2 is the rate-limiting step in substrate dependent pathway of *N*-glycan synthesis, a slowed-down or disrupted enzyme function would presumably lead to sugar accumulation in cells. Overall, both mechanisms of prolonged-UPR-induced- apoptosis or mannose poisoning can be considered as possible explanations of rod cells apoptosis.

3.2.5 Rescue of the symptoms after the disease phenotypes have been developed is the most important step towards clinical trials

The specificity of our genetic approach and the rate-limiting nature of Alg2 in the establishment of hypo-*N*-glycosylation could be confirmed with rescue experiments, in which both human and medaka *alg2* mRNA were injected in 1-cell stage mutant embryos. These experiments served as a stage-setting proof of principle which revealed on the one hand great preservation of ALG2 enzyme function between human and medaka and on the other hand that restoring wild-type Alg2 enzyme levels is sufficient to phenotypically rescue mutant fish. Although gene therapy is already approved for certain diseases, applications of it in human fetus to correct genetic diseases have not found their way to the clinics despite advances in avoiding immune reactions and increased effectiveness of the viral transfection in several animal models were shown (David & Peebles, 2008; Ma et al., 2020; Marktel et al., 2019; Naldini, 2019; Peranteau & Flake, 2020; Waddington et al., 2005). In this line, rescue of alg2^{hypo} fish model after hatch is an important aspect. As a proof of principle experiment, a Ubi::Cre^{ERT2}/LoxP inducible system (LoxP sites flanking a STOP codon upstream of the *alg2* coding sequence; Ubi is ubiquitously and constitutively active promoter; ERT2 is to induce expression only at hatching stage with tamoxifen induction) could be used to induce the overexpression of Alg2 coding sequence only at the hatching stage. Another way would be to transfect medaka with a viral transfection system such as lentivirus or adenoviruses, as both methods have proven to work

either *in vitro* for medaka and both *in vivo* and *in vitro* for zebrafish (Fazio et al., 2017; Kawasaki et al., 2009; Kurita, Burgess, & Sakai, 2004; Zou, De Koninck, Neve, & Friedrich, 2014). Both Cre^{ERT2}/LoxP and viral transfection methods would also allow for organ and cell type specific rescues to test the cell intrinsic and extrinsic nature of glycosylation.

Although injected at 1-cell stage, 100-200ng/ul concentration of mRNA was enough to rescue the survival of the embryos until the end point of the experiment, which was 18dph. Upon reduction of the injection amount (judged by less GFP expression), juveniles started displaying phenotypes at 7dph and could not survive further, arguing for a life-long dependency on functional enzyme, which is not only limited to overcome a developmental bottleneck. Rescue for high dose injections has most likely occurred due to the long half-life of Alg2 protein, which in HeLa cells is reported as 240 days (5776.2 hr) (Zecha et al., 2018). An alternative mechanism of protein stability could be formation of a stable trimeric structure with ALG1 and ALG11 (Gao, Nishikawa, & Dean, 2004).

Currently available therapies for CDG patients include nutritional and mineral supplementation and organ transplantation, which are reported to alleviate symptoms of CDGs (Brasil et al., 2018; Witters et al., 2017). Nutritional therapy *per se* might increase the rate of the reaction by increasing the substrate concentration whereas it cannot change the Km of the enzymatic reaction, which is a measure for the affinity of the enzyme for its substrate (Berg et al., 2002). However, mannose as a nutritional therapy failed in some CDG patients, including PMM2-CDG (Freeze, 2009; Mayatepek & Kohlmuller, 1998), although fibroblast culture supplementation were shown to correct for LLO size and amount of [^{3}H]-mannose transfer (Panneerselvam & Freeze, 1996). One possible explanation for the failure of mannose treatment in patients was suggested to be due to metabolization of mannose-6-phosphate by mannose-6 phosphate isomerase (MPI) for glycolysis (Freeze, 2009). On the other hand, if the enzyme activity level is under a certain level, increased substrate levels might not be enough to elevate the reaction rate. In this line, nutritional supplementation was not enough to reduce the symptoms or improve the survival of $alg2^{hypo}$ model. The C-terminal truncation in *alg2* allele might be increasing Km of the reaction, meaning that it leads to less affinity of enzyme to its substrate. As mentioned above, overdose of mannose is reported to be teratogenic for rat embryos (Buchanan et al., 1985) and honey bees as this feeding regimen is reported to deplete internal ATP resources (Freeze et al., 2017). To this end, our data suggests that nutritional therapies require careful examination of their side effects for the treatment of CDG patients,

especially if the residual enzyme activity is too low. However, other compound treatments are shown to be effective against certain CDG types *in vitro*, such as zaragozic acid A (ZGA), an inhibitor of squalene synthase, which can be used for treatment of *in vivo* models. Squalene synthase catalyzes the first steps of cholesterol and steroid hormones synthesis, inhibition of which leads to the stimulation of prior diverging pathways and, hence, to the increased formation of Dol and Dol-P, which in return decreases the amount of truncated *N*-glycans in CDG fibroblasts (Haeuptle et al., 2011). Moreover, ketoconazole, a cytochrome P450 family 51 (CYP51) inhibitor, also lowers the effects of tunicamycin, which is an inhibitor of Dolichyl-Phosphate *N*-Acetylglucosaminephosphotransferase 1 (DPAGT1) catalyzing formation of $GlcNAc_1$-PP-Dol (Harding et al., 2005). Overall, compounds with known *in vitro* effects are promising candidates for the *in vivo* treatments as future therapy options and $alg2^{hypo}$ model serves a good platform for compound screen for pre-clinical studies.

4

Chapter 2

4.1 Results

This part of the thesis is dedicated to results obtained from my second PhD project. My own text from the below manuscript in preparation was paraphrased:

"Sevinç Gücüm*, Kaisa Pakari*, Thomas Thumberger, Joachim Wittbrodt, manuscript in preparation"

**: authors contributed equally*

Note: Order of the authors is yet to be decided by the corresponding author.

4.1.1 NAA is not toxic to wild-type medaka embryos whereas NAA-sodium salt is toxic in a concentration dependent manner

Degron systems utilizing a fusion of GFP and auxin nanobodies, namely deGradFP, require testing of auxin penetration and toxicity. To this end, wild-type medaka embryos, both rolled on a sandpaper and treated with hatching enzyme, were subjected to different concentrations of synthetic auxin (NAA, 1-Naphthaleneacetic acid) dissolved in 20mM final concentration of NaOH to enhance solubility (**Figure 19A**). NAA was applied at 10mM, 5mM, 1mM, and 0.5mM concentrations, while the highest concentration of NaOH was used for the vehicle control. Although none of the embryos among the vehicle control survived 3 days of treatment, medakas treated at high concentrations of auxin were resistant to the treatment in both groups, indicating that auxin was not toxic to medaka embryos up to 10mM concentration. Although the same concentration of NaOH was used both in vehicle control as well as in 10mM NAA, only the vehicle control was affected.

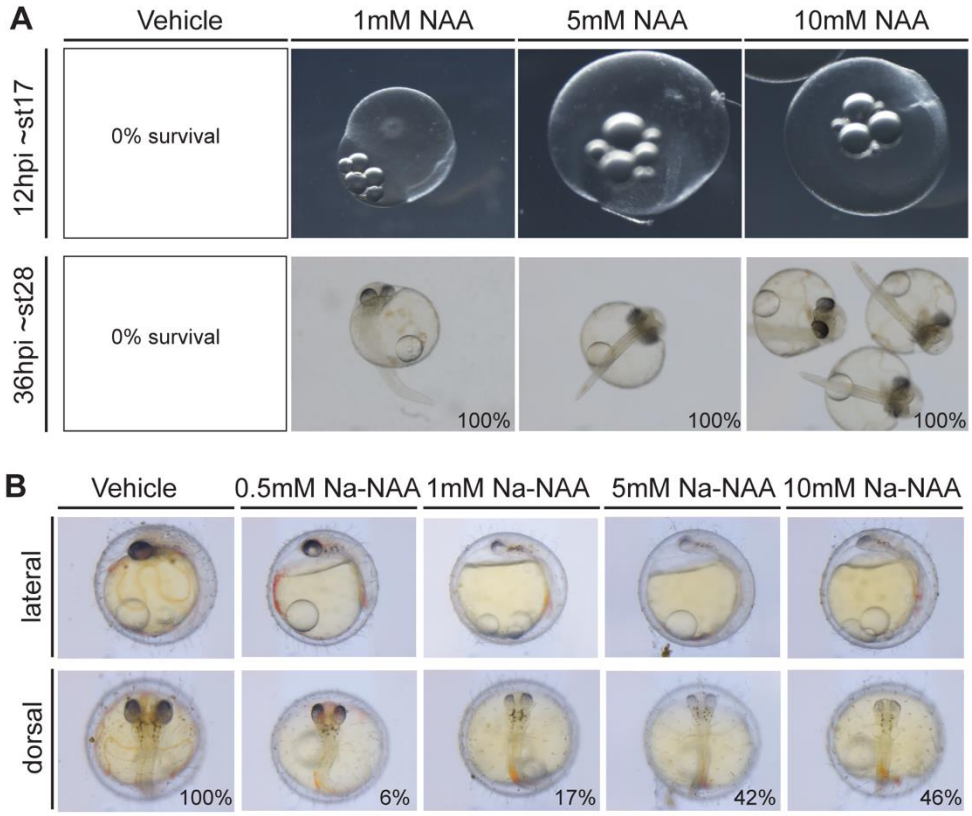

Figure 19: NAA and Na-NAA toxicity test.
(A) Dechorionated embryos were subjected to variant concentrations of NAA.
(B) Embryos were subjected to variant concentrations of NAA-sodium salt (Na-NAA) with intact chorion *(Data produced jointly with Kaisa Pakari).*

The toxicity experiment was repeated with the sodium salt of the same NAA compound, which can be dissolved in water. The results were contradictory to the previously obtained results, since increasing Na-NAA concentrations correlated with the percentage of affected medaka embryos (**Figure 19B**). On the other side, phenotypes such as blood clotting, edema around heart, depigmentation in eye and developmental delays were observed, which were not observed upon Na-NAA induction.

4.1.2 Inducible degradation of GFP in wild-type medaka embryos requires fine-tuning of degron concentration

The components of deGradFP were injected into medaka zygotes together with GFP mRNA. Injected embryos were treated at 0.5 and 1mM NAA concentrations 4 hr post injection (4hpi). GFP and mCherry (injection tracer) signals were assessed under an epifluorescence microscope. GFP signal persisted in the control group with or without auxin induction, indicating that TIR1 complex is not leaky even at high concentrations (50ng/µl) (**Figure 20A**). However, in the experimental group, a reduction of GFP signal was observable without auxin

treatment, pointing towards leakiness of the deGradFP system upon high nanobody concentration (50ng/ul). Reducing nanobody concentration to 4ng/µl or 10ng/µl, respectively, circumvented leakiness of the construct and led to robust GFP degradation upon auxin induction (**Figure 20B**).

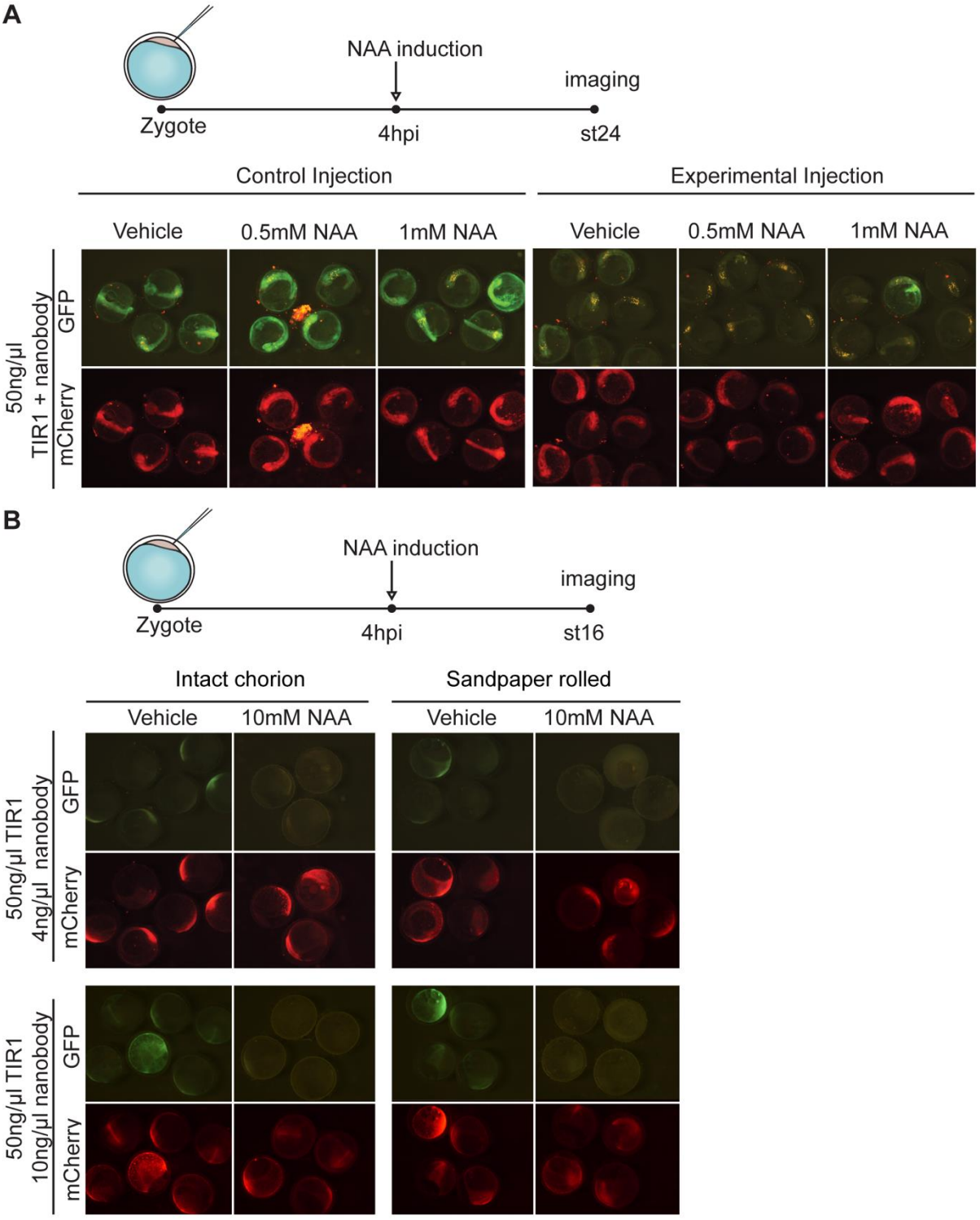

Figure 20: deGradFP injections of wild-type medaka embryos and induction of degradation with NAA. Embryos were injected with TIR1, nanobody, mCherry, and GFP mRNA and induced with NAA at 4hpi **(A)**. Same injections were repeated with lower concentrations of nanobody mRNA to enable NAA inducibility **(B)**.

4.1.3 Pmm2 is expressed ubiquitously and continuously in medaka fish and is maternally contributed at the early stages of development

Endogenous labeling of Pmm2-GFP at the C-terminus was achieved via CRISPR/Cas9 targeted genome editing and homology directed repair with supplied modified PCR product (**Figure 21A and 21B**). The gene insertion was confirmed (**Figure 21C**) and functional expression was observed at the RNA (**Figure 21D**) and at the protein level (**Figure 21E, asterix**). Interestingly, 5' end of the dsDNA with homology flanks was inserted via NHEJ (direct insertion) and the 3' end via HDR when PCR results over gDNA combined with the sequencing results. However, RT-PCR results combined with sequencing revealed splicing of the homology flank at the 5' end, rendering GFP insertion as intended via HDR on the RNA level without any frameshift.

We examined the Pmm2 expression pattern from zygote to adulthood in heterozygote individuals and found dependency on the gender of the parent (**Figure 22A**). When the Pmm2-GFP allele was contributed by the male founder fish (heterozygote male crossed to a wild type female), GFP expression could not be detected under epifluorescence microscope at the zygotic stage, but as early as stage 20 with overall less GFP signal intensity compared to any stage of embryos deriving from a female founder fish. However, when the Pmm2-GFP allele was contributed by a female founder fish (heterozygote female crossed to a wild type male), all of the progeny expressed GFP, in contrast to male contribution of the allele. GFP signal intensity was stable throughout embryonic stages, yet, after approximately stage 29, only 50% of the fish remained GFP positive, whereas the yolk was persistently green. These observations, together with the finding that unfertilized eggs coming from female founder fish displayed GFP signal, strongly suggested early maternal contribution of Pmm2 in medaka embryos. In the adult fish, Pmm2 expression was found to be ubiquitous and continuous with homozygote individuals exhibiting higher expression compared to the heterozygotes on the dorsal and anterior parts of the body (**Figure 22B**). Interestingly, fin-clipped adults showed stronger expression of GFP at the tip of the fin about 1 week after fin-clipping, visible as a strong GFP signal lining the cut fin, hinting towards higher expression of Pmm2 enzyme in dividing or metabolically active cells (data not shown).

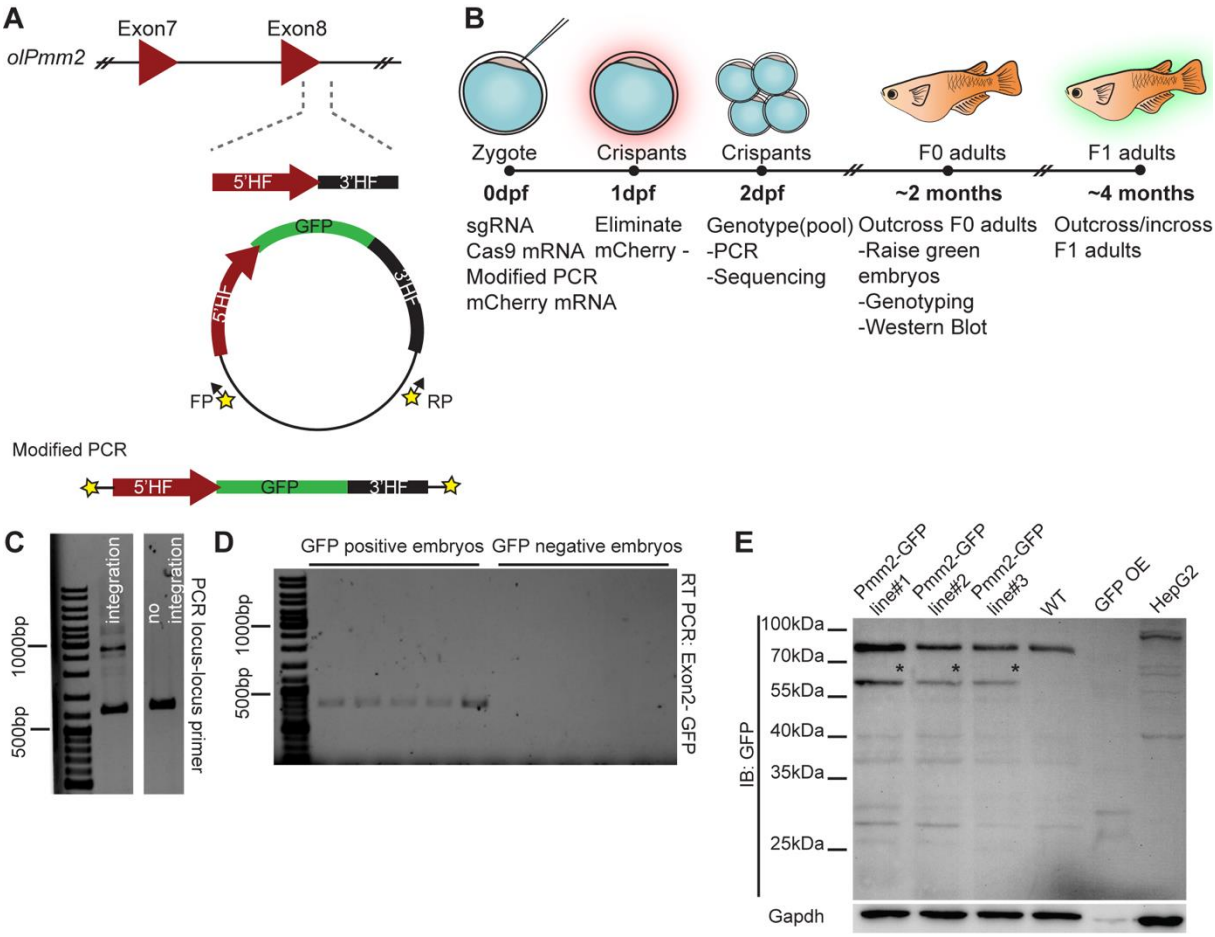

Figure 21: Generation of Pmm2-GFP line.
Modified PCR was produced from a vector containing homology regions to Pmm2 C-terminal end flanking GFP sequence amplified with biotinylated primers **(A)**. Injection and breeding scheme of the medaka embryos and adults, respectively **(B)**. PCR from gDNA **(C)**, RT-PCR from cDNA **(D)** and Western Blotting against GFP antibody **(E)** were performed for validation of the line. *Yellow star: biotin; Asterix: Pmm2-GFP fusion size (Data produced jointly with Simran Panda).*

To test a potential reduction in the Pmm2 enzyme activity upon C-terminal tagging, a pool of stage 40 deyolked hatchlings were subjected to enzyme activity test. Heterozygote Pmm2-GFP fish had 77% and the homozygote had 64% of the enzyme activity levels of the wild-type fish, consistent with the finding that homozygote adults do not display any gross morphological differences or reduced survival compared to wild type siblings (**Figure 22C**). This finding is consistent with previous experiments carried out in patient fibroblasts, in which patients showed PMM2 enzyme activity of up to 47% and the parents, as carriers, showed above 50% compared to that of wild-type allele (Westphal et al., 2001; Yuste-Checa et al., 2015).

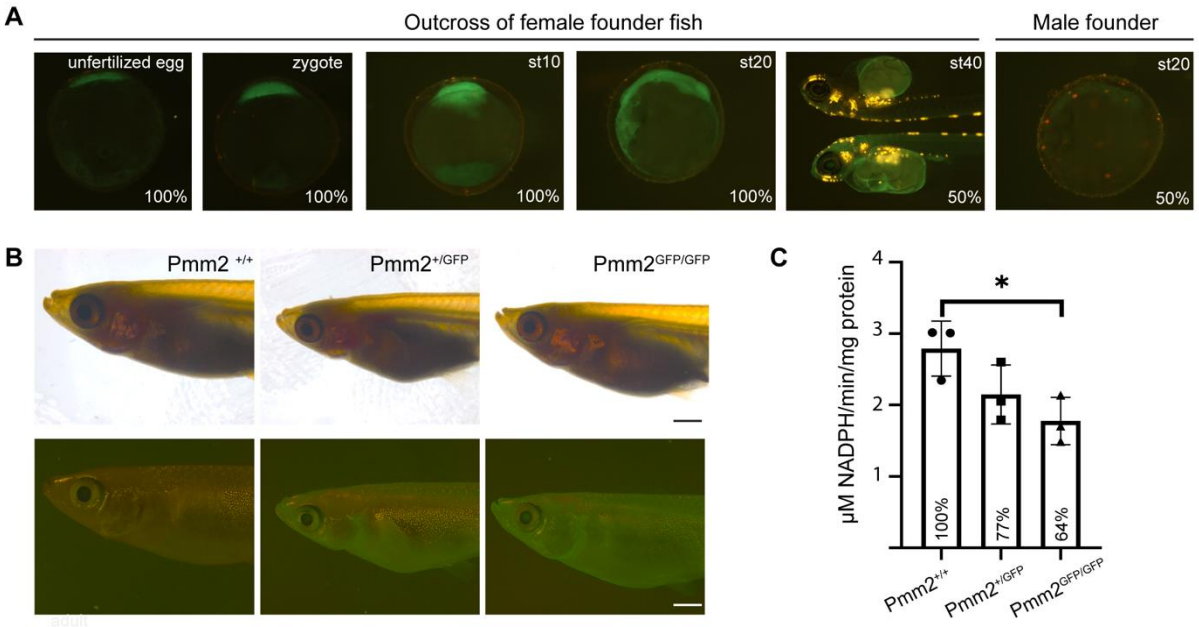

Figure 22: Expression pattern of Pmm2 in Pmm2-GFP line.
(A) Embryos showing endogenous levels of Pmm2 expression with GFP signal from an outcrossed maternal and paternal founder fish is indicating maternal contribution.
(B) Two-month old adults displaying ubiquitous expression of Pmm2 under heterozygosity and homozygosity. *Scale bar: 1mm (Figure was prepared by Kaisa Pakari).*
(C) Pmm2 enzyme activity levels of Pmm2-GFP line compared to wild type siblings. *Two-tailed nonparametric Student's T-test; * <0.05 (Data produced jointly with Lars Beedgen, University Clinic Heidelberg, Germany).*

4.1.4 Pmm2-GFP is successfully degraded with deGradFP

Upon confirming the activity of deGradFP and establishing a Pmm2-GFP tagged line, degradation of endogenous Pmm2 was tested via deGradFP injections into Pmm2-GFP line at zygotic stage. Degradation was induced with 10mM NAA at 6hpi. As a result, all Pmm2-GFP embryos in the experimental group showed reduction or depleted GFP on phenotype, indicating degradation of GFP fused to Pmm2 and suggesting degradation of Pmm2, as well (**Figure 23**) (Note that 100% of the uninjected fish are GFP positive due to maternal contribution within the time period of the injections). To be able to confirm the degradation of Pmm2, injected embryos were subjected to immunoblotting with Pmm2 antibodies. Due to 2 strong Pmm2 isoforms deriving from the yolk of the embryos and masking of the endogenous Pmm2 signal, our results were inconclusive (data not shown). Yet, these preliminary results still suggested that Pmm2 itself is degraded upon deGradFP injection and auxin induction. Moreover, both control and the experimental groups showed multisystemic phenotypes such as edema around the heart, blood clotting, eye pigmentation deficiencies, and developmental delay. These results were side-effects of NAA-sodium salt at 10mM concentration as the phenotypes were also observed

in control injection group (data not shown). Of note, maternal contribution, as evident from the GFP signal of the unfertilized eggs, should be as well degraded by the deGradFP.

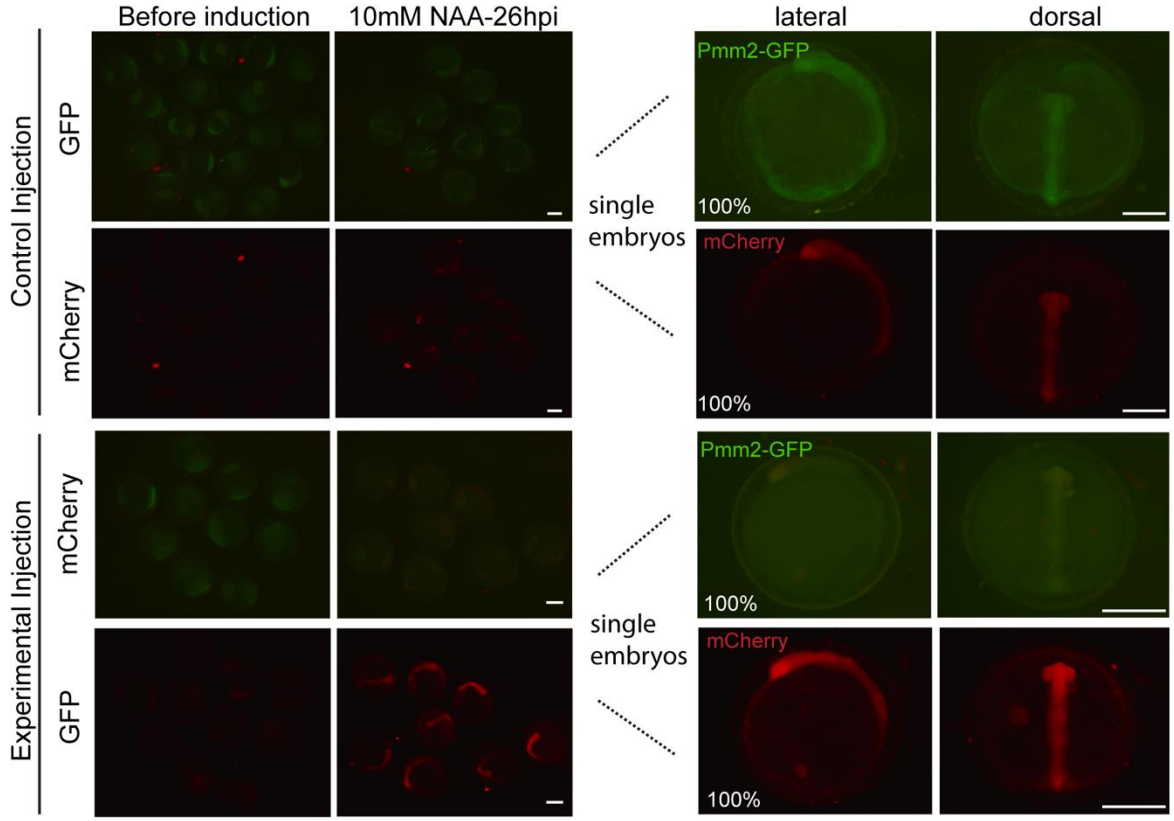

Figure 23: deGradFP injections and NAA induction of Pmm2-GFP fish.
Embryos resulting from an in-cross of Pmm2-GFP heterozygote parents were injected with deGradFP mRNA injection mix and induced with NAA at 6hpi. Experimental injections show reduction of GFP signal compared to the control injection group. *Zoom-in pictures belong to end point. Scale bar: 0.5mm (Data produced jointly with Kaisa Pakari).*

4.2 Discussion

PMM2 is a cytosolic glycosylation enzyme, mutations of which are giving rise to the most common form of CDGs, namely CDG-type Ia (Chang et al., 2018). Instead of introducing a specific patient allele, we took a different approach to create hypomorphic alleles of this gene to have a broader view on the enzyme function at its different levels. Here, we created a system that allows for varying the abundance of WT enzyme by degrading the protein at different rates, rather than altering enzyme function and activity. This was achieved via targeted proteasomal degradation of an endogenously GFP tagged version of Pmm2. The efficiency of GFP integration was high (1/6 couples), most probably due to the use of biotinylated PCR product (Gutierrez-Triana et al., 2018). However, not all the homology flanks were integrated via HDR as proposed by the biotinylation system, but rather upstream HF was integrated via NHEJ whereas downstream HF was integrated via HDR. This is indicating that both HDR and NHEJ repair mechanism might occur in the same dsDNA break repair and probably they are in a competition with each other. Resulting embryos displayed a ubiquitous and continuous expression pattern, as expected from an enzyme serving as a general house keeper protein. The observed maternal contribution in both unfertilized eggs and in yolk indicated a high protection of embryos against loss of this protein at the early stages of development, highlighting its importance and necessity for organismal development.

Injections of Pmm2-GFP heterozygote embryos, which are 100% GFP positive at early embryonic stages, with deGradFP constructs proved that GFP was degraded in all the injected embryos. Although it can be assumed that the fused Pmm2 protein was degraded alongside GFP, further experimental proof, such as immunoblot analysis against Pmm2 for both control and experimental injections is needed to clearly confirm the functionality of the system. Interestingly, the induction of the degradation machinery via auxin was dependent on the injection amount of nanobody (AID-vhhGFP4) mRNA. High concentrations of nanobody (as high as 50ng/ul) resulted in degradation of GFP without auxin induction, indicating that overflow of the cells with both mRNA constructs is leading to higher probability of engineered F-box protein (TIR1) and nanobody to find each other, although TIR1 is a receptor of auxin (Dharmasiri et al., 2005) and helps nanobody to find E3 ubiquitin ligase only when auxin presents. To this end, protein degradation only under auxin induction requires keeping deGradFP components under certain threshold inside the cell.

Several points remain to be addressed to achieve fine-tuning of the system that would allow for varying enzyme levels upon dose-dependent degron induction. Establishing different levels of enzyme quantity to achieve different severity of the disease phenotypes would require either RNA injections of TIR1 and nanobody or generation of transgenic lines expressing those under a ubiquitous (Ubi or β-actin for medaka) promoter. For injections at 1-cell stage, a range of RNA and auxin concentration, which can create different levels of enzyme is necessary. However, at high concentrations the system is saturated at a level that it is insensitive to auxin induction and displays leakiness of the construct. Moreover, 4ng/µl of injection seems to deplete GFP almost completely as measured under epifluorescence microscopy. Reducing the injection amount even further as well as optimization of auxin administration become the bottleneck as we found the sodium-salt of synthetic auxin (Na-NAA) to be toxic at lower concentrations. Furthermore, the homozygote Pmm2-GFP line by default exhibits a reduced level of enzyme activity (64%), which is further restricting the range of degron injection amounts. As a result, Pmm2 protein might be depleted completely if the degron induction cannot be fine-tuned, rendering the hypomorphic model a proxy null allele, which will potentially lead to embryonic lethality.

Since yolk contribution of Pmm2 persists throughout embryonic development until all yolk is digested at stage 40, embryos might be rescued from the complete loss of the enzyme until this stage. Furthermore, injected mRNA does not persist in the cell due to RNA instability and the protein half-life of degron constructs in medaka is not known. As a result, RNA injections of degron components at 1-cell stage might not lead to any phenotypes until stage 40. In line with that, the generation of transgenic lines for a continuous expression of degron components is highly important. However, the strength of the promoter used for a transgenic line should be critically evaluated due to aforementioned reasons. Nevertheless, transgenic lines would also allow for tissue and cell type specific induction of degron system and, hence, for the analysis of cell intrinsic and extrinsic players of glycosylation. Validation of the phenotypes observed from such systems with mutant lines of Pmm2 would also be necessary as a proof of principle.

5

Outlook

The results of this thesis indicate that medaka is a promising organism for disease modelling of CDGs in terms of mimicking human symptoms and for the general study of molecular mechanisms underlying the disorder, which is owed to the high degree of conservation in protein sequence and function of glycosylation enzymes across species. Here, we generated the first vertebrate model of a mannosyltransferase mutant leading to multisystemic phenotypes and reduced glycan occupancy of target proteins, which in turn led to changes in protein abundance. Our approach highlights the validity of modelling patient alleles in fish to delineate molecular determinants of disease phenotypes. As a second strategy, we employed targeted degradation of glycosylation enzymes on the protein level, by using an inducible degron system, allowing for the generation of conditional models of CDGs.

Although this thesis stressed on the importance of generating hypomorphic rather than the complete loss of function alleles, it does not present a direct proof that introduced patient mutations indeed lead to hypomorphism. To address this issue directly, residual enzyme activity could be tested or overexpression of the alg2^{hypo} mutant allele could be used to rescue disease phenotypes after hatching. One mechanism by which the mutants could survive until hatchling in case alg2^{hypo} carries a complete loss of function allele could be via maternal mRNA or yolk protein contribution. However, the mechanisms underlying this process are poorly understood and have not yet been addressed. To this end, tracing tagged versions of maternal glycosylation enzymes with fluorescent proteins under physiological and pathological conditions could shed light on the degree of maternal contribution, as well as give mechanistic insights in how proteins are trafficked from the yolk and taken up by the embryo.

While this thesis emphasized on the establishment and characterization of much needed *in vivo* models of CDGs, the underlying molecular basis of disease manifestation still remains elusive. To this end, further experimental validation of differentially regulated protein groups by mutating Asparagine on *N*-glycosylation motifs will help us to connect disease phenotypes to the disease-causing proteins under hypoglycosylation. Furthermore, the surprising finding of

cell type-specific vulnerabilities to hypo-*N*-glycosylation in eye, and potentially in brain, although glycosylation genes are proposed to be expressed ubiquitously and continuously, needs further clarification. For that, increasing the resolution by means of single cell omics analyses of the alg2^{hypo} model could deepen our understanding of cell-type specific changes and vulnerabilities under reduced glycan occupancy. While single cell approaches are suitable to study cell intrinsic properties, dependencies on secreted factors by the microenvironment could maximally only be inferred. To this end, transplantation of cells at the blastula stage from wild-type embryos into alg2^{hypo} background, or vice versa, could be a promising approach to address this point. Furthermore, it is still unknown why patients with mutations of different glycosylation genes of the same pathway display such variety of phenotypes, feeding into the assumption that cell type vulnerabilities are patient specific. To address that, the generation of fish carrying other CDG patient alleles or using targeted reduction of enzyme quantities in medaka could help to identify "cell type tropism of glycosylation", meaning that certain cell types preferentially use certain routes of glycosylation.

While in this thesis we lay the foundation of studying hypo-*N*-glycosylation in an organismal context, multiple lines of research that should be pursued in follow-up work emerged. As outlined above, these open questions range from immediate translational applications to the most basic biological processes, as of how glycosylation is regulated on the cellular level in a cell type specific manner and how crucial it is for the maintenance of certain cell types. Extended analysis of both models presented in this thesis will help us to uncover above mentioned questions. Eventually, those models will serve as platforms of pre-clinical research such as drug screening and gene therapy for the treatment of CDG symptoms.

6

Materials and Methods

6.1 Materials

6.1.1 Medaka Fish Lines

Table 1: Fish lines used in this thesis. *CR: produced with CRISPR/Cas9; double semi colon: expressed under the promoter of.*

Line Name	References
CR(Alg2: p.(S335Lfs*8))	(Gücüm et al. 2020)
CR(Alg2: p.336G*) or alg2^{hypo}	(Gücüm et al. 2020)
CR(Alg2: p.N334_S335del)	(Gücüm et al. 2020)
CR(Pmm2-GFP)	Gücüm, unpublished
Fli1::GFP	AGCentanin, University of Heidelberg/Germany
Wild-type Cab strain	(Loosli et al., 2000)

6.1.2 Cells

Table 2: Cells and cell lines used in this thesis. *AG: Arbeitsgruppe or The Team of.*

Name	Source
ALG2-CDG patient fibroblast	AGThiel, University Clinic Heidelberg/Germany
HepG2 cell line	AGAugustin, German Cancer Research Center, DKFZ/Germany
Mach1 T1^{R} phage resistant chemically competent *Escherichia coli*	Thermo Fisher Scientific

6.1.3 Plasmids

Table 3: Plasmids used in this thesis with lab specific internal stock numbers when available

Name	Source	Internal Stock Number
Alg2 sgRNA1	This thesis	-
Alg2 sgRNA2	This thesis	-
Alg2_inSitu	This thesis (Gücüm, unpublished)	5582
Cas9	Lab stock	5197
DR274 (sgRNA backbone)	Lab stock	3632
GFP	Lab Stock	-
hsAlg2_full_cDNA	AGThiel, University Clinic Heidelberg	-
mCherry	Lab Stock	-
olalg2_full_cDNA	(Gücüm et al., 2020)	-
pCDNA5FRT/TO_HA-mAID-nanobody	Addgene	117713
pCS2+	Lab Stock	221
pCS2+_Flag-myc-NES-Tir1	Addgene	117717
pGEM-T Easy	Promega	2877
Pmm2 sgRNA1	This thesis	-
Pmm2 sgRNA2	This thesis	-
Pmm2_GG	This thesis	4956
Pmm2_inSitu	This thesis (Gücüm, unpublished)	5583

6.1.4 Primers and sgRNAs

Table 4: Primers and sgRNAs used in this thesis with their nucleotide sequences and internal stock numbers

Name	Sequence (5' to 3')	Source	Internal stock number
Alg2_C_seq_F	TCCACTTGGAGGATTGCGTC	This thesis	JW6284
Alg2_C_seq_R2	CATTTAGCTGGGGATTGGTACAC	This thesis	JW6282

Alg2_ex4_sgRNA1	CCCGTTATTGCCGTCAACTC	This thesis	-
Alg2_ex4_sgRNA2	CCGTTATTGCCGTCAACTCT	This thesis	-
Alg2_ssODN	CCCGTTATTGCCGTCAACTCTTAAGGCCTCTGGAGAGCGTAGCACACGGGGAGACGGGCTTCCTGTGCGAGCCTACGGCTGAGGCGTTCTCCCAGGCCATGGAGAGGCTCATCAGAGACC	This thesis	JW6277
Alg2CDS_F_BamHI	GCCGGATCCATGGCGCGGGTGGTGTTT	This thesis	JW9320
Alg2CDS_R_XbaI	GCCTCTAGATTACTGGCTGAGCATAACTACGT	This thesis	JW9321
Cr - GFP - T3	AAACGCTCGACCAGGATGGGCA	Lab stock	JW1408
EGFPrtPCRfwd	GACGACGGCAACTACAAGAC	Lab stock	JW5006
EGFPrtPCRfwd	GACGACGGCAACTACAAGAC	Lab stock	JW5006
GFP_seq_Frx2	CATCAAGGTGAACTTCAAGATCCG	Lab stock	JW2222
M13 uni-21	TGTAAAACGACGGCCAGT	Eurofins Genomics	-
Modified_PCR_Fwd	CGAGCGCAGCGAGTCAGTGAG	Lab stock	*
Modified_PCR_Rev	CATGTAATACGACTCACTATAG	Lab stock	**
o_GGWassembly_R	TCGACCTCGAGCCTTAGGTAC	Lab stock	JW0276
pmm2_C_seq_F	TGGACGACACAGATGATGCT	This thesis	JW6251
pmm2_C_seq_R	CTCACAGACTGACCCTCACC	This thesis	JW6252
Pmm2_ex8_sgRNA1	TCTTCTTCTGCTGAAGCTACTGG	This thesis	-
Pmm2_ex8_sgRNA2	TCTTCTGCTGAAGCTACTGGAGG	This thesis	-
PMM2_T2_R	AAACGCAGAGGCTCAGGACTCG	Lab stock	JW5908
PMM2fwd	AGTCCATTCAGGCCCACATG	Lab stock	JW5870
PMM2rev	TGAGGTCACATCCCGTGTTG	Lab stock	JW5869

*Shares same sequence with JW5237; biotinylated
**Shares same sequence with JW5238; biotinylated

6.1.5 Antibodies and Lectins

Table 5: Primary antibodies used in this thesis with their types, hosts, dilutions used in respective assays, catalog numbers (Cat No.), and internal stock numbers

Target	Type	Host	Dilution	Source	Cat No.	Internal number
Gapdh(14C10)	monoclonal	rabbit	1:1000	Cell Signaling	2118	-
GFP	polyclonal	chicken	1:500	Life Technologies	A10262	38
GS	monoclonal	mouse	1:500	Chemicon	MAB302	42
HuC/D	monoclonal	mouse	1:500	Life Technologies	A21271	102
PKCα	polyclonal	rabbit	1:200	Santa Cruz	sc-208	72
Rhod	-	rabbit	1:200	Homemade Dr. Hyde	-	164
Rhod(1D4)	monoclonal	mouse	1:100	Millipore,	MABN15	143
Rx2	polyclonal	rabbit	1:500	Homemade (Charles River)	-	165
Zpr1	monoclonal	mouse	1:200	ZIRC	AB_10013803	87
β-actin antibody	monoclonal	mouse	1:10,000	Sigma	A5441	-

Table 6: Secondary antibodies used in this thesis *Cat No.: Catalog Number*

Name	Host	Dilution	Source	Cat No.
anti-chicken AF488	donkey	1:750	Jackson/ Dianova	703-545-155
anti-mouse AF647	donkey	1:750	Invitrogen	A32787
anti-mouse IgG (H+L) AF546	goat	1:750	Life Technologies	A11030
anti-mouse IgG-HRP	goat	1:10,000	Santa Cruz	sc-2005
anti-rabbit AF647	goat	1:750	Thermo LifeTech	A21245

anti-rabbit HRP	goat	1:5000	Agrisera	AS09 602
anti-rabbit IgG AF488	goat	1:750	Life Technologies	A11034
streptavidin-HRP	-	1:10,000	Vector Laboratories	SA-5014-1

Table 7: Lectins used in this thesis *Cat No.: Catalog Number*

Target	Dilution	Source	Cat No.	Internal number
ConA-biotin	1:1000	Vector Laboratories	B-1005-5	-
WGA-biotin	1:1000	Vector Laboratories	B-1025-5	-

5.1.6 Antibiotics

Table 8: Antibodies used in this thesis with their final concentrations

Name	Working concentration	Source
Ampicillin	100 µg/ ml	Roth
Kanamycin	50 µg/ ml	Roth

6.1.7 Kits

Table 9: Commercial kits used in this thesis *(for ingredients please refer to the company)*

Name	Source
glyXprep 16 kit	glyXera, Magdeburg, Germany
In Situ Cell Death Detection Kit, TMR red	Roche
innuPREP Gel Extraction Kit	Analytik Jena
innuPREP PCRpure Kit	Analytik Jena
MEGAscript T7 Transcription Kit	Life Technologies
mMESSAGE mMACHINE Sp6 Transcription Kit	Life Technologies
mMESSAGE mMACHINE™ T7 Transcription Kit	Thermo Fisher Scientific
pGEM-T Easy Vector System	Promega
Pierce™ BCA Protein Assay Kit	Thermo Fisher Scientific
Pierce™ ECL Plus Western Blotting Substrate	Thermo Fisher Scientific
Pierce™ ECL Western Blotting Substrate	Thermo Fisher Scientific
QIAprep Spin Miniprep Kit	Qiagen
Revert-Aid First Strand cDNA Synthesis Kit	Thermo Fisher Scientific

Revert-Aid First Strand cDNA Synthesis Kit	Thermo Fisher Scientific
RNeasy Mini Kit	Qiagen

6.1.8 Enzymes

Table 10: Enzymes used in this thesis. *FD: Fast Digest; HF: high fidelity; U: Unit*

Name	Source
BamHI-HF (20U/µl)	New England Biolabs
BsaI-HF (20U/µl)	New England Biolabs
DraI-FD	Thermo Fisher Scientific
HpaI	New England Biolabs
NotI- HF (20U/µl)	New England Biolabs
NotI-FD	Thermo Fisher Scientific
PauI	New England Biolabs
peptide-*N*-glycosidase F	AGRapp, Max Planck Institute, Magdeburg
Proteinase K (20mg/ml)	Roche
PvuI	New England Biolabs
Q5 Polymerase	New England Biolabs
StuI (10U/µl)	New England Biolabs
T4 DNA ligase (5U/ul)	Thermo Fisher Scientific
T7 endonuclease I	New England Biolabs
Turbo DNase I (2U/µl)	Invitrogen
XbaI	New England Biolabs

6.1.9 Buffers

Table 11: Commercial and in-house made buffers used in this thesis with their ingredients or sources

Name	Source or Ingredient
10X Cut Smart Buffer	New England Biolabs
10X ligase buffer (for T4 ligase (5U/ul))	Thermo Fisher Scientific
10x NEB buffer 2	New England Biolabs

10X PBS	1370 mmol /l NaCl 27 mmol/ l KCl 2.4 g/l KH_2PO_4 14.4 g/l Na_2HPO_4
10X Running Buffer	250 mM Tris 2 M glycine 30 mM SDS in dH_2O pH 8.3
10X Running Buffer	10% v/v 10X Running Buffer in dH_2O
10X TBS	0.15 M Tris-HCl 0.05 M Tris base 1.5 M NaCl in dH_2O adjust pH to 7.6
10X Wet Blotting Buffer	142 mM Glycin powder 250 mM Tris powder in dH_2O
1X PTW	10 % v/v 10x PBS 0.1 % v/v Tween 20
1X TAE buffer	242 g /l Tris base 5.71 % v/v Glacial acetic acid 50 mmol /l EDTA Adjust pH: 8.5
1X TBST	10% v/v 10X TBS 0.1% Tween 20 in dH_2O
1X Wet Blotting Buffer	10% v/v MeOH 0.0375% v/v SDS 10% v/v 10X wet blotting buffer in dH_2O

2.5X Laemli buffer	5% SDS 25% glycerol 156.25 mM Tris-HCl, pH 6.8 0.05% bromophenol blue (0.8mg/ml) in dH_2O 12.5% v/v 2-mercaptoethanol is added freshly when used
2X RNA loading buffer	Life Sciences
4X Separation buffer, pH 8.8	1.5 M Tris pH 8.8 0.4% SDS in dH_2O
4X Stacking Buffer, pH 6.8	0.5 M Tris pH 6.8 0.4% SDS in dH_2O
5X Q5 buffer	New England Biolabs
6x Laemmli buffer	375 mM Tris–HCl pH 6.8 6 % SDS 48 % glycerol 9 % 2-mercaptoethanol 0.03 % bromophenol blue
8 M urea buffer	Urea ≥ 99.5 %, p.a. 100 mM NaCl ≥ 99.5 %, p.a. 50 mM triethylammonium bicarbonate (TEAB) pH 8.5
Buffer A	0.1 % FA 1 % ACN in H_2O
Buffer B	0.1 % *v*/*v* formic acid (FA), 10 % *v*/*v* H_2O in ACN
DNA lysis buffer	Fin Clip Buffer 1mg/ml Proteinase K
FD Green buffer	Thermo Fisher Scientific

Fin clip buffer	0.4 M Tris-HCl pH 8.0 5 mM EDTA pH 8.0 0.15M NaCl 0.1% SDS in dH_2O
Mild stripping buffer	0.5 % glycine (w/v) 0.1% SDS (w/v) 1% Tween20 (w/w), adjust pH 2.2
RIPA buffer	Thermo Fisher Scientific
sgRNA annealing buffer	10mM Tris-HCl 30mM NaCl pH 7.5-8

6.1.10 Solutions

Table 12: Solutions used in this thesis with their ingredients and final concentrations

Name	**Ingredients**	**Final Concentration**
1% agarose (low-melt) In 1X ERM	agarose (low-melt)	1% w/v
1% agarose in TAE	agarose boil in 1X TAE	1% w/v
16% PFA	PFA adjust pH to 7.0	160 g/ l
1x ERM	NaCl KCl $CaCl{\cdot}2H_2O$ $MgSO_4{\cdot}7H_2O$ HEPES pH 7.3 adjust to pH 7	17 mM 0.4 mM 0.27mM 0.66 mM 17 mM
20 x Tricaine	Tricaine $Na_2HPO_4 \cdot H_2O$ in 1x ERM adjust pH to 7-7.5 with 1 N HCl	4 g/ l 10 g/ l

4% PFA/PBS	16% PFA dilute in 1X PBS	25 % v/v
4% PFA/PTW	16% PFA dilute in 1X PTW adjust pH to 7-7.5	25 % v/v
6x Orange G Loading dye	Orange G Glycerol	1.2 mg/ml 20% v/v
Bleaching solution	KOH H_2O_2 in PBS	1 % v/v 3 % v/v
Davidson's fixative	Tap water EtOH Formalin Glacial acetic acid	33% v/v 33% v/v 22% v/v 11% v/v
EtBr bath	EtBr 10 mg/ml in 1x TAE	0.02% v/v
LB medium	Bacto-Tryptone Yeast Extract NaCl	10g/l 5g/l 10g/l
LB Plates	Agar boil in LB medium	15g/l
Medaka hatching solution	Methylene blue in 1x ERM	2 mg/ l
TB medium	Bacto-Tryptone Yeast Extract Glycerol KH_2PO_4 K_2HPO_4	12g/ l 24g/ l 0.4 % v/v 2.13 g /l 12.54 g/ l
1.5% agarose in dH_2O	agarose boil in water	1.5% w/v
1.5% agarose in TAE	agarose boil in 1X TAE	1.5% w/v
1.5% agarose in water	agarose bring to boil	1.5% w/v

6.1.11 Reagents

Table 13: Reagents used in this thesis with their synonyms/abbreviations

Name	Alias	Source
1- Naphthaleneacetic acid	NAA	Sigma
1- Naphthaleneacetic acid-sodium salt	Na-NAA	Santa Cruz
1,1,1,3,3,3-Hexafluoro-2- propanol	-	Sigma-Aldrich
2-Chloroacetamide (≥ 98.0 %)	-	Sigma-Aldrich
2-propanol	Isopropanol	Sigma-Aldrich
2X RNA loading dye	-	Thermo Fisher Scientific
30% Acrylamide (29:1)	-	BioRad
4-(2-Hydroxyethyl)piperazine-1-ethanesulfonic acid	HEPES	Roth/ZBT
4',6-diamidino-2-phenylindole	DAPI	Sigma-Aldrich
8-aminopyrene-1,3,6-trisulfonic acid	APTS	Sigma-Aldrich
Acetonitrile, UPLC grade	ACN	Biosolve
Agar	-	Roth
Agarose	-	Sigma-Aldrich
Alcian Blue 8GX	-	Sigma Aldrich
Ammonium persulfate	APS	Sigma-Aldrich
Asialofetuin	-	AGRapp, Max Planck Institute-Magdeburg
Benzonase Nuclease	-	Millipore
Bovine Serum Albumin	BSA	
Bromophenol blue	-	Sigma-Aldrich
Calcium chloride dihydrate	$CaCl_2 \cdot 2H_2O$	AppliChem
Chloroform	-	Sigma-Aldrich
cOmplete™ EDTA-free Protease Inhibitor Cocktail	-	Roche
D-glucose	-	Sigma-Aldrich
D-mannose	-	Sigma-Aldrich
Deoxynucleotide triphosphates	dNTPs	Sigma-Aldrich
Dimethyl sulfoxide	DMSO	Roth

Dimethyl, heavy	C_2H_6O	Sigma- Aldrich
Dimethyl, light	C_2H_6O	Sigma- Aldrich
Disodium phosphate	Na_2HPO_4	Sigma-Aldrich
Dulbecco's modified Eagle's medium	DMEM	Life Technologies
Eosin	-	Waldeck
Ethanol	EtOH	Sigma-Aldrich
Ethydium bromide	EtBr	Sigma-Aldrich
Ethylenediaminetetraacetic acid	EDTA	Roth
Ethylenediaminetetraacetic acid	EDTA	Roth
Eukitt® Quick-hardening mounting medium	-	Sigma-Aldrich
Fetal calf serum	FCS	PAN Biotech
Formalin (37−40% Formaldehyde)	-	Roth
formic acid	FA	Proteochem
GeneRulerDNALadderMix	-	Thermo Fisher Scientific
Glacial acetic acid	-	Merck
Glucose-1-phosphate	-	AGThiel, University Clinic Heidelberg
Glycerol	-	Applichem
Glycine	-	Applichem
Glycogen (1 mg/ml)	-	Merck
Hematoxylin	-	Roth
Hydrogen chloride	HCl	Merck
Hydrogen peroxide	H_2O_2	Sigma-Aldrich
Low melting agarose	-	Roth
Lysyl Endopeptidase®, MS grade	-	Wako Chemicals
Magnesium chloride	$MgCl_2$	Merck
Magnesium chloride	$MgCl_2$	AGThiel, University Clinic Heidelberg
Magnesium sulphate heptahydrate	$MgSO_4.7H_2O$	Merck
Mannose-6 phosphate isomerase	MPI	AGThiel, University Clinic Heidelberg
Methanol	MeOH	Roth
Methanol, MS grade	MeOH	Carl Roth

Methylcellulose	-	Sigma Aldrich
MS-222	Tricaine	Sigma-Aldrich
Nicotinamide adenine dinucleotide phosphate	NADP	AGThiel, University Clinic Heidelberg
Normal goat serum	NGS	Sigma-Aldrich
Orange G	-	Sigma-Aldrich
Paraffin	-	AGJLohmann, University of Heidelberg
Paraformaldehyde	PFA	Sigma-Aldrich
PEG4000	-	Merck
Penicillin/Streptomycin	Pen/Strep	AGThiel, University Clinic Heidelberg
Phosphoglucose Isomerase	PGI	AGThiel, University Clinic Heidelberg
Pierce™ ECL Western Blotting Substrate		Thermo Scientific
Potassium chloride	KCl	AppliChem
Potassium dihydrogen phosphate	KH_2PO_4	Merck
Potassium dihydrogen phosphate	KH_2PO_4	Merck
Potassium hydrogen phosphate	K_2HPO_4	Merck
Potassium hydroxide	KOH	Merck
Skim milk powder	-	Sigma-Aldrich
Sodium chloride	NaCl	Sigma-Aldrich
Sodium chloride, ≥ 99.5 %, p.a.	NaCl	Applichem
Sodium dodecyl sulphate	SDS	Serva
Sodium hydrogen phosphate dihydrate	$Na_2HPO_4.H_2O$	Sigma-Aldrich
Sodium hydroxide	NaOH	Sigma-Aldrich
Sodium tetraborate	Borax	Fluka
Streptavidin solution	-	Vector Laboratories
Sucrose	Saccharide	Roth
Tetramethylethylenediamine	TEMED	Roth
Tissue Freezing Medium	TFM	Leica
triethylammonium bicarbonate	TEAB	Sigma-Aldrich
Trifluoroacetic acid, ≥ 99.0 %	TFA	Sigma-Aldrich

Tris hydrochloride	Tris-HCl	Sigma-Aldrich
Tris(2-carboxyethyl)phospin	-	Carl Roth
TRIzol™ Reagent	-	Thermo Fisher Scientific
Trypsin, MS grade	-	Thermo Fisher Scientific
Tween 20	-	Sigma-Aldrich
Urea, ≥ 99.5 %, p.a.	-	Carl Roth
Water, MS grade	H_2O	Biosolve
Xylene	Xylol	Merck
Yeast Extract	-	Roth

6.1.12 Consumables

Table 14: Consumables used in this thesis with the provider company/source

Name	**Source**
3M™ Empore™ C18 Extraction Disks	Thermo Fisher Scientific
Aluminium foil	Paclan
Borosilicate glass capillaries GC100F-10	Harvard apparatus
C18 StageTips	Thermo Fisher Scientific
Cell scraper	AGThiel, University Clinic Heidelberg
Filter tips 10 µl, 20 µl, 200 µl, 1.25 ml	STARLAB
Folded filter paper	Sartorius
Glass beads	Roth
Glass bottom dishes	MatTek
Glass slides for H&E samples	AGJLohmann, University of Heidelberg
Latex gloves	Semperguard
Low-binding tubes, 1.5 ml	Thermo Fisher Scientific
Low-binding tubes, 2 ml	Thermo Fisher Scientific
Microloader tips 10 µl	Eppendorf
Molding cup trays 6 mm x 12 mm x 5 mm	Polysciences
Nail polish	Rival De Loop
Needle, 20G	AGThiel, University Clinic Heidelberg
Nitrile gloves	STARLAB

Nitrocellulose membrane	GE Healthcare
Paper napkins	Kammerer
Parafilm M® All-Purpose Laboratory Film	Bemis
Pasteur pipettes	Sarstedt
Petri dishes	Greiner
Phase-lock heavy gel tubes, 2 ml	Quantabio
Pipette tips 10 µl, 200 µl, 1 ml	Steinbrenner
PVDF membrane- Immobilion P	Merck
Reaction tubes 1.5 ml, 2 ml	Eppendorf
Reaction tubes 1.5 ml, 2 ml (safe-lock)	Eppendorf
Reaction tubes for polymerase chain reaction	Sarstedt
ReprosilPur-AQ 120 C18 material	Dr. Maisch
Scalpel	Schreiber Instrumente
Six-well plates	Böttger
Superfrost plus microscope slides	Thermo Fisher Scientific
Tubes 15 ml, 50 ml	Sarstedt
Tubes for bacterial cultures, 13 ml	Sarstedt
Whatman paper	Whatman

6.1.13 Equipment

Table 15: Equipment used in this thesis with the provider company/source

Name	**Source**
Acclaim PepMap300 C18, Trapping cartridge	Thermo Fisher Scientific
Analytical column	In-house made (AGRuppert, Heidelberg University/Germany)
Bacterial Shaker INNOVA 44	New Brunswick Scientific
Blot Documentation System	Intas
Centrifuge 5417 C	Eppendorf
Centrifuge 5425	Eppendorf
Centrifuge 5430	Eppendorf
Centrifuge 5430 R	Eppendorf
Centrifuge for PCR tubes	Steinbrenner Laborsysteme
Centrifuge MC 6	Sarstedt

Cryostat CM 3050S	Leica
DIC microscope DB5000	Leica
Fish incubator	Heraeus instruments
Fish incubator	RuMed
Forceps 5, 55 Inox stainless steel	Dumont
Freezer -20˚C	Liebherr
Freezer -80˚C	Thermo Scientific
Fridge 4˚C	Liebherr
Gel chamber	peqLab and custom-made
Incubator 37˚C, 60˚C	BINDER
Leica TCS SP8 (confocal microscope)	Leica
Microinjector 5242	Eppendorf
Microtome	AGJLohmann, University of Heidelberg
Microwave R-939	Sharp
Mini Trans-Blot® Cell	Bio-Rad
Mini-PROTEAN® Tetra Handcast Systems	Bio-Rad
nanoEase MZ Peptide analytical column	BEH
nanoEase MZ Peptide analytical column	Waters
Needle puller P-30	Sutter Instrument Co USA
Nikon AZ100	Nikon
Nikon DS-Ri1 camera	Nikon
Nikon SMZ18	Nikon
pH-meter	Sartorius
Pipetboy acu	Integra biosciences
Pipettes (10 µl, 20 µl, 200 µl, 1 ml)	ErgoOne, Starlab
Power supply PowerPac Basic	Bio-Rad
Q-Exactive HF mass spectrometer	Thermo Fisher Scientific
Q-Exactive HF-X mass spectrometer	Thermo Fisher Scientific
Qiagen TissueRuptor II	Qiagen
ReprosilPur-AQ 120 C18 material	Dr. Maisch
Rocking shaker DRS-12	neoLab
Scale EW 2200-2NM	KERN
Spectrophotometer DS-11+	DeNovix

Staining container for immunofluorescence on cryosections	Custom-made
Stereomicroscope Nikon SMZ18	Nikon
Stereomicroscope Zeiss Stemi 2000	Zeiss
Stereomicroscope Zeiss Stemi SV11	Zeiss
Thermocycler	Bio-Rad
Thermomixer Compact	Eppendorf
Thermomixer F1.5	Eppendorf
Tube revolver	Thermo Fisher Scientific
Ultimate 3000 UPLC	Thermo Fisher Scientific
UV table	Vilber Lourmat
UV-Gel Documentation System	Intas
Vortex	Scientific Industries
Water bath	GFL

6.1.14 Softwares

Table 16: Softwares used in this thesis

Name	Reference
Adobe Illustrator version 16.0.0	Adobe
Fiji	(Schindelin et al., 2012)
FileMaker Pro	FileMaker, Inc.
Geneious Prime	Biomatters Limited
glyXtool™ software	glyXera, Magdeburg, Germany
MaxQuant version 1.6.12.0	(Cox & Mann, 2008)
Mendeley version 1.19.4	Elsevier Solutions
Perseus version 1.5.6.0	(Tyanova et al., 2016)
Prism 6	GraphPad
RStudio version 1.2.5042	(R Core Team. 2018; RStudio Team)

6.1.15 Online tools

Table 17: Online tools used in this thesis with their internet links

Name	Use	Link
Biorender	Drawing figures	https://biorender.com/ *(used to make Figure 1 and 18 of this thesis)*

CCTop	sgRNA design	https://cctop.cos.uni-heidelberg.de:8043/
eLabFTW	Data storage	https://elabftw.cos.uni-heidelberg.de:444/experiments.php
Ensembl	Gene, RNA, and protein information	https://www.ensembl.org/index.html
Ensembl (BioMart)	Finding human orthologs of medaka genes	https://www.ensembl.org/biomart/martview/4a0df1fafe645f876cecc7e8a8e05f02
GeneCards	MS data analysis	https://www.genecards.org/
Poly Peak Parser	Finding mutations upon CRISPR/Cas9	http://yosttools.genetics.utah.edu/PolyPeakParser/
Primer3	Primer design	https://bioinfo.ut.ee/primer3-0.4.0/
Uniprot (Retrieve/ID Mapping)	MS data analysis	https://www.uniprot.org/uploadlists/

6.2 Methods

This part of the thesis describes the experiments performed to reach the "Results" section. Please note that the parts in quotation mark means that these parts were paraphrased from my own publication with the following citation:

Gücüm et al. (2020) "The medaka *alg2* mutant is a model for hypo-*N*-glycosylation-associated retinitis pigmentosa". BioRxiv. doi: https://doi.org/10.1101/2020.08.20.260430

Please also refer to the "Contributions" section of this thesis for details of the contributions of other people to the experiments performed below.

6.2.1 Animal Husbandry

″ Medaka (*Oryzias latipes*) Cab strain used in this study were kept as closed stocks in accordance to Tierschutzgesetz §11, Abs. 1, Nr. 1 and with European Union animal welfare guidelines. Fish were maintained in a constant recirculating system at 28°C on a 14 h light/10 h dark cycle (Zucht- und Haltungserlaubnis AZ35-9185.64/BH). Written informed consent was obtained for the analysis of patient-derived material. This study was approved by the Ethics Committee of the Medical Faculty Heidelberg.″

6.2.2 Medaka Microinjections

-Generation of CR(Alg2:p.G336) and CR(Pmm2-GFP) Lines*

Female and male adults were separated the night before the injections and in the morning placed into the same fish tank for mating. The fertilized eggs (zygotes) were collected 15 minutes later, placed in an ice-cold dish with 1X ERM, separated from each other, and placed in a 1.5% agarose (in water) gel mold. Fish were injected with the respective injection mixtures in the cytosol via a capillary glass needle. Injection amounts were not equal due to unequal opening of each glass needle and unequal air pressure or time of injection.

-GFP degradation in wild-type and Pmm2-GFP lines

Freshly fertilized medaka embryos were collected from either wild-type or $Pmm2^{+/GFP}$ lines. The wild-type embryos were injected with 50ng/ul TIR1 mRNA; 4ng/ul, 10ng/ul or 50ng/ul nanobody mRNA (*mAID-vhhGFP4)*; 10ng/ul mCherry mRNA and 10ng/ul and GFP mRNA with the help of a glass needle at 1-2 cell stage as described above. Control injections lacked

nanobody mRNA. Embryos were incubated at 28 °C for around 4 hr. Dead and mCherry negative embryos were removed prior to NAA induction. At around st9, half of the samples were rolled on sandpaper. NAA induction (10mM) started at st9 and lasted until stage 24.
Pmm2-GFP embryos were injected with 100 ng/µl or 50 ng/µl TIR1 mRNA, 10 ng/µl mCherry mRNA and 10 ng/µl or 20 ng/µl nanobody mRNA. The control injection lacked nanobody mRNA. Embryos were incubated at 26 °C for about 6 hr and induced with 10mM NAA at 32 °C for about 24 hr. mCherry negative embryos were removed from the analysis. Finally, the images were acquired for both green and red channels under epifluorescence microscope (Nikon SMZ18).

6.2.3 Genomic DNA Extraction

DNA was extracted from several different samples including embryos, hatchling eyes or fins, and adult fins. For all samples a lysis buffer (fin-clip buffer with Proteinase K (20 mg/ml, 1µl per 100µl buffer)) was used. For single embryos 20 µl, for pool of embryos (up to 10) 100µl, for hatchling eyes or fins 20 µl, and for individual fins 100 µl lysis buffer was used. Embryos were ground with the help of a pestle inside lysis buffer whereas other type of samples did not need grinding. All samples were incubated at 60-65 °C overnight. Samples were quickly spinned down in a table top centrifuge, distilled water was added in 2-times of the buffer volume and samples were incubated at 95 °C for 15 min to inactivate Proteinase K. Samples were centrifuged at 4 °C, 10000g for 10 min. One µl of DNA was used for PCR genotyping.

6.2.4 alg2^{hypo} Line Generation

-Microinjections
Microinjections were performed as mentioned in "6.2.2. Medaka Microinjection" section to wild-type zygote medakas. Injection mixture contained 2 sgRNAs at 15ng/µl, 150ng/µl Cas9 mRNA, 25 ng/µl ssODN and 10 ng/µl GFP mRNA as injection tracer (for sequences refer to Materials). Next day, dead and GFP negative embryos were eliminated. At 2dpi, 5 or 10 embryos were pooled together in a 1.5 ml Eppendorf tube and lysed inside DNA lysis buffer for DNA extraction (refer to "6.2.3 Genomic DNA Extraction").

-PCR
PCR was performed with with the PCR mixture prepared according to **Table 18**. PCR was run in thermal cycler according to **Table 19**. Primers with forward 5'-

TCCACTTGGAGGATTGCGTC, reverse 5'- CATTTAGCTGGGGATTGGTACAC sequences were used. PCR product (5-10 µl) was run in 1% agarose gel in TAE buffer to test PCR amplification.

Table 18: Ingredients of PCR for genotyping of *alg2* mutant lines

Ingredients	**1X (µl)**
dH_2O	35.8
5X Q5 buffer	10
10 mM dNTP	1
10 µM FP (JW6282)	1
10 µM RP (JW6284)	1
Q5 polymerase (2U/ µl)	0.2
DNA	1

Table 19: PCR cycle of reaction in Table 18

Temperature	**Time**	
98 °C	2 min	
98 °C	20 sec	30 cycles
67 °C	30 sec	
72 °C	25 sec	
72 °C	4 min	
10 °C	10 min	

-*Surveyor assay*

Efficiency of sgRNA cut was tested with T7 endonuclease I assay (Surveyor Assay). Accordingly, 10 µl PCR product, 2 µl 10x NEB buffer 2, and 7.5 µl dH2O were incubated in thermal cycler according to **Table 20**. Then, 0.5 µl of T7 Endonuclease I was added and samples were incubated at 37 °C for 30min. Samples were size separated via 1.5% agarose gel in TAE buffer electrophoresis.

Table 20: Thermal cycle of the Surveyor Assay for dsDNA denaturation and re-annealing

Step	**Temperature**	**Ramp rate**	**Time**
Initial denaturation	95 °C	-	5 min
Annealing	95-85 °C	-2 °C /sec	10 sec
Annealing	85-25 °C	-0.1 °C/sec	20 min
Hold	4 °C	-	15 min

-StuI test digest

Samples were further subjected to StuI restriction test digest to detect successful ssODN integration. First, PCR samples were cleaned up with Analytik Jena PCR clean up kit according to manufacturer's instructions (Analytik Jena, 2017a). Cleaned up PCR product was eluted in 30 µl distilled water and mixed with 5 µl 10X Cut Smart Buffer (NEB), 0.2 µl StuI (NEB), and distilled water up to 50 µl. Mixture was incubated at 37 °C for 2 hr and size separated with 1.5% agarose gel in TAE buffer.

-Breeding

Integration of ssODN was not detected in the F0 injected generation from pooled embryos. Nevertheless, F0 fish were raised to adulthood and outcrossed to wild-type adults. Resulting F1 generation embryos were collected and raised to adulthood. A small sample of fin from each adult was taken to repeat each step of the genotyping as mentioned above. Successful germline transmission of the ssODN inserted lines were outcrossed and raised to adulthood, giving rise to F2 generation. *alg2*$^{+/-}$ adults were incrossed and phenotypes were assessed until hatching. Hatchlings with multisystemic phenotypes and their healthy age-matched siblings were counted for phenotypic Mendelian segregation. Fish with phenotypes were genotypes for homozygosity as mentioned above. Fish carrying ssODN insertion as well as other mutant alleles were sequenced with JW6284 primer at Eurofins Genomics and mutant alleles were analyzed on Geneious Prime® 2019.2.1 and Poly Peak Parser (Hill et al., 2014).

6.2.5 Pmm2-GFP Line Generation

GFP sequence flanked by 5' and 3' homology flanks (HFs) to the Pmm2 C-terminus sequence was created with Golden-Gate cloning. Biotinylated primers (5'-CGAGCGCAGCGAGTCAGTGAG-3' and 5'-CATGTAATACGACTCACTATAG-3') amplifying this sequence were used to produce a modified PCR product according to **Table 21 and Table 22**.

Table 21: Ingredients of PCR for generation of modified PCR product with biotinylated primers

Ingredients	1X (µl)
dH_2O	35.8
5X Q5 buffer	10
10 mM dNTPs	1
10 µM FP (Modified_PCR_Fwd)	1
10 µM RP (Modified_PCR_Rev)	1
Q5 polymerase (2U/ µl)	0.2
Plasmid 4956 (1 ng)	1

Table 22: PCR cycle of reaction in Table 21

Temperature	Time	
98 °C	2 min	
98 °C	20 sec	35 cycles
57 °C	30 sec	
72 °C	80 sec	
72 °C	4 min	
10 °C	10 min	

Wild-type medaka zygotes were injected with 15 ng/µl sgRNAs (5' TCTTCTTCTGCTGAAGCTACTGG 3' and 5' TCTTCTGCTGAAGCTACTGGAGG 3') targeting Pmm2 C-terminus locus, 150 ng/µl Cas9 mRNA, 5 ng/µl Modified PCR product and 10ng/µl mCherry mRNA. mCherry negative embryos were eliminated the next day. Early stage injected embryos were genotyped via conventional PCR as well as RT-PCR to test integration of modified PCR into the locus. Accordingly, Pmm2-GFP line was genotyped either from embryo or adult fin-clip lysates as described in **Table 23 and Table 24**.

Table 23: Ingredients of PCR for genotyping of Pmm2-GFP line

Ingredients	1X (µl)
dH_2O	35.8
5X Q5 buffer	10
10 mM dNTPs	1
10 µM FP (JW6251)	1
10 µM RP (JW6252)	1
Q5 polymerase (2U/ µl)	0.2
DNA	1

Table 24: PCR cycle of reaction in Table 23

Temperature	Time	
98 °C	2 min	
98 °C	20 sec	30 cycles
59 °C	30 sec	
72 °C	1min 50 sec	
72 °C	4 min	
10 °C	10 min	

RNA extraction was performed from individual GFP screened embryos as described in "6.2.9 Reverse Transcription PCR (RT-PCR)"**.** RT-PCR settings for genotyping were 98°C initial denaturation for 2 min, followed by 35 cycles of 98 °C denaturation for 20sec, 59 °C annealing for 30 sec, 72 °C extension for 50sec (Primers: 5' AAACGCAGAGGCTCAGGACTCG 3' and 5' AAACGCTCGACCAGGATGGGCA 3'). All PCR reactions were analysed with 1.5% agarose gel. Upon confirmation of successful integration, the rest of the injected embryos that have ubiquitous GFP expression were raised to adulthood. Adult F0 fish were outcrossed to wild-type medakas and resulting generation was again screened for ubiquitous GFP expression. Successful candidates were genotyped via conventional PCR, RT-PCR and Western Blot as in "6.2.14 Western Blots".

6.2.6 Fibroblast Culture Maintenance

″ Patient and control fibroblasts were cultured in Dulbecco's modified Eagle's medium (high glucose; Life Technologies) supplemented with 1 % FCS (PAN Biotech) and 1 % Pen/Strep with 5 % CO2 at 37 °C. Medium was replaced every 72 hr. ″

6.2.7 Cas9 mRNA Production

Cas9 messenger RNA (mRNA) was transcribed from NotI- HF-linearised plasmids (in-house) using the mMESSAGE mMACHINE Sp6 Transcription Kit according to the manufacturer's instructions (Ambion by life technologies, 2012a).

6.2.8 sgRNA Production

- *Cloning*

DR274 plasmid was digested with BsaI-HF (NEB) at 37 °C overnight according to **Table 25**. Digested product was run on 1% agarose gel electrophoresis and 2147bp band was gel purified

with Analytic Jena gel purification kit according to manufacturer's protocol (Analytik Jena, 2017b). Ordered single stranded oligos targeting region of interest were annealed in sgRNA annealing buffer (10mM Tris-HCl pH 7.5-8. 30mM NaCl) from 95 to 10 °C with 0.1 °C reduction.

Table 25: Reaction for linearization of DR274, sgRNA backbone

Ingredient	Volume/Amount
Vector plasmid (DR274)	8.0 µg
BsaI-HF (NEB)	0.5 µl
10X Cut Smart Buffer	5.0 µl
dH_2O	Up to 50 µl

Annealed product was diluted 1:33 (v/v) in distilled water and ligated to the gel-extracted backbone at RT for 10 min according to **Table 26**.

Table 26: Reaction for ligation of sgRNA backbone and target sequences

Ingredients	Volume
dH_2O	5 µl
10X ligase buffer	1 µl
PEG4000	1 µl
DR274 (40ng, 0.025pmol vector)	1 µl
Insert oligo (0.075pmol insert)	1 µl
T4 DNA ligase (5U/ul)	1 µl

MachT1^{TM} T1^{R} phage resistant chemically competent *Escherichia coli* (Thermo Fisher Scientific) were transfected with ligated product, plated on LB plates with (1:1000) Kanamycin, and incubated at 37 °C overnight. Next day, resistant colonies were picked and bacteria were grown either 5 hr or overnight at 37 °C. Plasmid extraction was done with an adjusted protocol of Qiagen Miniprep (Qiagen, 2020). Accordingly, cells were centrifuged at 12000g for 3min and supernatant was removed. Cells were resuspended in P1 buffer, digested with P2 and P3 buffers, and was centrifuged at 12000g for 15min. Supernatant was taken into a new tube and 500 µl of isopropanol was added to precipitate DNA by centrifuging at 12000g for 15 min. Samples were washed with 500 µl 70% EtOH and left to air dry. DNA was resuspended in distilled water. Plasmid was tested with BsaI and PvuI test digest in FD Green buffer (Thermo Fisher Scientific) for transfection of correctly ligated plasmid. DNA bands were checked on 1% agarose gel via electrophoresis and sequenced with M13 uni-21 primer at Eurofins Genomics. Bacterial culture with the correct plasmids were used to inoculate 20ml LB medium with (1:1000) Kanamycin, which was incubated at 37 °C overnight. Total of 8 ml culture was

precipitated with centrifuge at 10000g for 2min. DNA was extracted with Qiagen Miniprep kit according to manufacturer's protocol (Qiagen, 2020).

-Linearization of sgRNA plasmids

Plasmid from previous step was linearized by incubating the reaction mixture from **Table 27.** at 37 °C overnight. Digested product was size separated on 1.5% agarose gel via electrophoresis and 300bp band was excised and purified according to manufacturer's protocol (Analytik Jena, 2017b). Concentration of the elute was measured on Spectrophotometer DS-11+ (DeNovix).

Table 27: Linearization reaction of sgRNA vector for *in vitro* RNA synthesis

Ingredients	Volume/Amount
10X FD Green Buffer	6 µl
Plasmid DNA	10 µg
DraI-FD	3 µl
dH_2O	Up to 60 µl

-in vitro Transcription

MEGAscript T7 Transcription Kit (Life Technologies) was used according to manufacturer's instructions (Ambion by life technologies, 2012b). Template DNA of 200 ng eluted plasmid from previous step was used. Sample was incubated overnight at 37 °C. For digestion of DNA, samples were incubated with 1 µl Turbo DNase I (stock 2U/µl) at 37 °C for 15 min. Samples were cleaned up with RNeasy Mini Kit (Qiagen) according to manufacturer's instruction (Qiagen, 2019). The concentration was measured with Spectrophotometer DS-11+ (DeNovix). Clarity of the extraction was judged by the following parameters: $OD^{260/280} > 2$ and $OD^{260/230} >2$. RNA (around 200ng) was also run on 1.5% agarose gel in 1X TAE buffer with 2X RNA loading buffer (Ambion). Prior to gel loading, sample was denaturated at 80 °C for 10min.

6.2.9 Reverse Transcription PCR (RT-PCR)

This assay was used to confirm the expression of $alg2^{hypo}$ and Pmm2-GFP alleles in transcript level.

-RNA Extraction

Embryos or hatchlings were transferred to 2 ml low-binding tubes (Thermo Fisher Scientific) and washed several times in ice-cold PBS and lysed directly inside TRIzol™ Reagent (Thermo

Fisher Scientific) with pestle under a fume hood. Yolk was not removed. Samples were lysed with Qiagen TissueRuptor II. If needed, samples were snap frozen inside liquid nitrogen and kept at -80 °C freezer at this step. Otherwise, samples were incubated at RT for 5 min and centrifuged at 12000g at 10 °C for 2 min. Meantime phase-lock heavy gel (Quantabio) tubes were spinned down at 12000g for 30 sec. Supernatant was transferred to phase-lock heavy tubes and 200 µl RNase-free water and 100 µl chloroform was added. Samples were shaken up and down for 50 sec and incubated at RT for 2 min. Samples were centrifuged at 12000g at 4 °C for 15 min. Transparent upper phase was taken into 1.5 ml fresh low-binding tubes and 0.8-times volume of isopropanol and 1 ul glycogen (1 mg/ml) were added and mixed with a pipette up and down. Samples were incubated on ice for 10 min and centrifuged at 12000g at 4 °C for 10 min. Supernatant was trashed and 700 µl 70% EtOH was added to the pellet. Samples were centrifuged at 8000g at 4 °C for 5 min. Supernatant was trashed and pellet was air dried at RT for 5 min. About 12 µl of RNase-free dH_2O was used for resuspension of RNA. Samples were digested with DNaseI and test gel was performed as described in "6.2.8 sgRNA Production" section. Concentration was measured and samples with $OD^{260/230}$ >2 was accepted clean.

-cDNA Conversion

To inactivate the DNase I from previous step, 5 µl 50 mM EDTA (about 5mM final concentration) was added and samples were incubated at 65 °C for 10 min. cDNA synthesis reaction mixture was prepared from Revert-Aid First Strand cDNA Synthesis Kit (Thermo Fisher Scientific) according to manufacturer's instruction (**Table 28**) and incubated at 65 °C for 5 min.

Table 28: Oligo dT annealing for cDNA conversion

Ingredients	Volume/ Amount
RNA	About 50 ng
Oligo dT	1 µl
dH_2O	Up to 12 µl

Upon oligo dT annealing, synthesis reaction mixture was prepared as in **Table 29** and incubated at RT for 5 min, then 42 °C for 1 hr and 70 °C 5 min. cDNA was kept at -20 °C.

Table 29: Reverse transcription reaction

Ingredients	Volume
5X RT Buffer	4 µl
Ribolock (20U/µl)	1 µl
10mM dNTP	2 µl
RTase (5U/µl)	1 µl
RNA annealed to Oligo dT	12 µl

- *RT-PCR*

RT-PCR for CR(Alg2: p.G336*) line was performed with the reaction mixture of **Table 18** with JW6282 and JW6284 primers (refer to materials for details). Reaction was run according to **Table 19.** As a control of DNA contamination, also RNA samples were directly used in a separate set of PCR reaction.

RT-PCR reaction mixture of Pmm2-GFP line was prepared according to **Table 18** with JW5908 (anneals to exon2 of *olPmm2* allele) and JW1408 (anneals to *GFP*) primers. Reaction was run in a thermal cycler according to **Table 30.**

Table 30: RT-PCR cycle of Pmm2-GFP line validation

Temperature	Time	
98 °C	2 min	
98 °C	20 sec	30 cycles
59 °C	30 sec	
72 °C	50 sec	
72 °C	4 min	
10 °C	10 min	

6.2.10 Hematoxylin and Eosin (H&E) Staining

″ Stage 40 (9 dpf at 26°C) medaka hatchlings were fixed in Davidson's fixative (3 parts tap water, 3 parts EtOH, 2 parts formalin, 1 part 98 % acetic acid) overnight at 4 °C. Samples were dehydrated in series of 70 % - 90 % - 100 % EtOH and xylene. Dehydrated hatchlings were incubated in paraffin for 1 hr at 60 °C. All samples were embedded in paraffin blocks at RT and sectioned on microtome with 7 µm thickness and mounted on glass slides. Samples were incubated at 42 °C overnight and rehydrated in a stepwise manner in xylene-100 % - 90 % - 70 % - 50 % EtOH series. Slides were stained in hematoxylin for 10 min, washed with tap water for 40 min and stained with eosin for 2 min at RT. Upon staining, samples were dehydrated again with 70 % - 90 % - 100 % EtOH and xylene series. Samples were mounted with Eukitt® Quick-hardening mounting medium (Sigma-Aldrich). Images were taken under DIC microscope (Leica DB5000).″

6.2.11 Alcian Blue Staining

″ Stage 40 (9 dpf at 26 °C) medaka hatchlings were anaesthetized with 1X Tricane (Sigma-Aldrich). Tail of each fish was clipped and processed for PCR-genotyping as decribed in "6.2.4 alg2^{hypo} Line Generation" Specimens were fixed in 4% PFA in PBS overnight at 4 °C. Next day, samples were dehydrated in 50% and 70% EtOH for 15 min at RT, respectively. Cartilages were stained in 0.02 % Alcian Blue 8GX (Sigma Aldrich) in 70 % EtOH and 60 mM $MgCl_2$ overnight at RT. Hatchlings were rehydated for depigmentation of eyes. Accordingly, samples were washed once in 70% and 50% EtOH and eye pigments were bleached in 1 % KOH, 3 % H_2O_2 in PBS for 30 min at RT. Hatchlings were washed once with 50% EtOH and imaged under Nikon SMZ18 in 3 % methylcellulose. For long term storage, samples were dehydrated in 100 % EtOH and kept at -20°C. Analysis of the cartilage lengths were performed on Fiji by measuring the distance between the beginning and the end of the cartilages (euclidean distance) and lengths were normalized to standard length (SL), which is the distance between the center of lenses, as decribed in (Cline et al., 2012). Two-tailed nonparametric Student's T-test was performed as statistical analysis.″

6.2.12 Live Imaging of *Fli1::GFP, alg2^{hypo}* Line

alg2$^{+/-}$ adults were crossed to *Fli1::GFP* line (Kindly provided by AGCentanin, COS, Heidelberg University). Resulting progeny was raised, screened for GFP expression in the vessels and GFP positive ones were raised to adulthood. Adults were genotyped as described in "6.2.4 alg2^{hypo} Line Generation". Heterozygote individuals were incrossed and resulting progeny was raised until st40. Fish were anesthetized with 1X Tricane in ERM and mounted in 1% low melting agarose in glass bottom dishes (MatTek). Once the agarose hardened, the dish was covered with 1X ERM. Images were acquired under Leica TCS SP8 inverted confocal laser scanning microscope at 488 nm wavelength.

6.2.13 Lectin Blots

-Medaka samples

Proteins from a pool of hatchlings (n=10-20) were lysed with the help of Qiagen Tissue Ruptor II in RIPA buffer (Thermo Scientific) with cOmplete^{TM} EDTA-free Protease Inhibitor Cocktail (Roche) in 2 ml low binding tubes (Thermo Fisher Scientific). Samples were incubated on ice for 30 min and centrifuged at 12000g at 4 °C for 10 min. Supernatant was taken to a fresh 1.5

ml low binding tube. Concentration of each sample was measured with Pierce™ BCA Protein Assay Kit (Thermo Fisher Scientific) according to manufacturer's instruction with microplate procedure (Thermo Fisher Scientific, 2020). Total of 10 µg protein was mixed with 2.5X Laemli buffer and dH_2O up to 20 µl. Samples were boiled at 95 °C for 15 min prior to loading. 10% SDS gel was prepared according to **Table 31.**

Table 31: Recipe of 10% SDS separation gel (For 2 gels)

Ingredients (For 2 gels)	**Volume**	**Final concentration**
H_2O	4.09 ml	-
30% Acrylamide (29:1) (BioRad)	3.3 ml	10%
4X Separation buffer, pH 8.8	2.5 ml	1X
20% APS	100 µl	0.2%
TEMED	10 µl	0.1%

Before the 10% gel hardened between vertical glass plates (BioRad), isopropanol was poured to avoid air bubbles. Once the gel hardened, 4% stacking gel was prepared according to **Table 32**.

Table 32: Recipe of 4% SDS stacking gel (For 2 gels)

Ingredients (For 2 gels)	**Volume**	**Final concentration**
H_2O	2.945 ml	-
30% Acrylamide (29:1) (BioRad)	0.75 ml	4.5%
4X Stacking Buffer, pH 6.8	1.25 ml	1X
20% APS	50 µl	0.2%
TEMED	5 µl	0.1%

Samples were run at 60V for 30 min and 100V for about 1.5 hr in 1X SDS running buffer until the gel front runs out. Proteins were blotted on a MeOH-activated-PVDF membrane (Millipore Immobilon-P) with wet blotting technique from Mini Trans-Blot® Cell (Bio-Rad, n.d.) inside 1X wet blotting buffer at 350mA for 1 hr at 4 °C. A cooling pack was used to prevent overheating. Membrane was blocked with 5 % BSA in 1X TBST (TBS with 0.1 % Tween) for 1 hr at RT. As an internal control, anti-Gapdh rabbit monoclonal antibody (Cell Signaling(14C10)) was used in 1:1000 dilution in blocking buffer (5 % BSA in 1X TBST) for 1 hr at RT. Goat anti-rabbit HRP (Agrisera) was used in 1:5000 concentration as a secondary

antibody. After developing signal with Pierce™ ECL Western Blotting Substrate (Thermo Scientific), the blot was stripped in mild stripping buffer (1.5 % glycine (*w*/*v*), 0.1 % SDS (*w*/*v*), 1 % Tween20 (*w*/*w*), pH 2.2). Blots were incubated in streptavidin solution (1 drop in 10 ml TBST, Vector laboratories) for 15 min at RT to block internal biotin signal of the fish. Blots were incubated with either biotinylated Concanavalin A (Con A, Vector Laboratories) or biotinylated Wheat Germ Agglutinin (WGA, Vector Laboratories) at 1:1000 dilution in TBST 2.5 hr at RT. Streptavidin- Horseradish Peroxidase (Vector Laboratories) was used at 1:10000 dilution for 30 min at RT. Signal was developed with Pierce™ ECL Western Blotting Substrate (Thermo Scientific).

"-Fibroblast samples

ALG2-CDG patient and control fibroblasts were washed with ice-cold PBS and harvested by cell scraper and lysed for 30 min in RIPA buffer (Thermo Fisher Scientific) on ice by pasing the samples 20 times through a 20G needle. Samples were centrifuged for 30 min at 13000 rpm at 4 °C. Total protein of 10 µg both from control and patient fibroblast were used for gel loading. Samples were mixed with 6x Laemmli buffer (375 mM Tris–HCl, pH 6.8, 6 % SDS, 48 % glycerol, 9 % 2-mercaptoethanol, 0.03 % bromophenol blue) and denatured at 95 °C for 5 min. Proteins were size separated on a 12.5 % SDS-PAGE and blotted onto a nitrocellulose membrane (GE Healthcare) by a semi-dry electrophoretic transfer. The membrane was blocked for 1 hr at RT with 5 % milk powder in PBST (0.1 % Tween20 in PBS). After blocking, the membrane was washed and incubated with the primary antibodies against β -actin antibody (1:10,000, Sigma) overnight at 4 °C. Membrane was washed with 1X TBST several times and incubated with secondary antibody anti-mouse IgG-conjugated with horseradish peroxidase (1:10,000, Santa Cruz) for 45 min at RT. Pierce™ enhanced chemiluminescence reagent (ECL) plus western blot analysis substrate (ThermoFisher Scientific) was used for signal detection. Blots were stipped with 10 % acetic acid for 12 min at RT for lectin incubation. The membrane was blocked with 5 % BSA in TBST (0.5 % Tween20 in TBS) for 1 hr. Membranes were incubated with the biotinylated lectins ConA and WGA (Vector Laboratories) at 1:1000 dilution in TBST for 2 hr at RT. The membranes were subsequently incubated with horseradish peroxidase streptavidin (Vector Laboratories) for 30 min at RT and signal was detected with PierceECL plus assay kit (ThermoFisher Scientific). ″

-Analysis of lectin blots

The signal strength from each lane was measured in Fiji. All lanes were selected and the pixel intensities were calculated. Along the lanes, a non-loaded part of the membrane was also

selected as a region of interest and the pixel intesity of the background was calculated, as well. Always a background closer to the lane of interest was chosen. Background signals were removed both from the lectin blots and the Gapdh internal control signal. Signal intensity of lectins were normalized to their respective Gapdh intensity. Finally, all internally normalized samples were normalized to their wild-type counterparts for percentage normalization. As wild-type samples were normalized to themselves, they were always represented as 100%.

6.2.14 Western Blots

Sample lysis, measurement of concentration, preparation of SDS-gels, electrophoresis, blotting, and incubation of Gapdh antibody were done according to section "6.2.13 Lectin Blots- Medaka Samples" Samples were 3 different Pmm2-GFP medaka lines at st40, wild-type age matched medaka hatchlings, GFP mRNA injected medaka embryos to see the size of GFP and HepG2 cell line as a positive control of Pmm2 expression. After Gapdh signal development, blot was stripped with mild stripping buffer and blocked with 5% milk for 1 hr at RT. Blot was incubated with anti-GFP antibody (A11122, Invitrogen, 1:500) in 5% milk ON at 4 °C. Other blots loaded with the same samples were blocked with 5% BSA for 1 hr at RT and incubated with anti-Pmm2 (10666-1-AP, Proteintech or HPA040852, Sigma-Aldrich) at 1:500 in 5% BSA overnight at 4 °C. Goat anti-rabbit HRP (Agrisera) was used in 1:5000 in 1X TBST as a secondary antibody for 1 hr at RT. Signal was developed with Pierce™ ECL Western Blotting Substrate (Thermo Scientific).

6.2.15 Multiplexed Capillary Gel Electrophoresis with Laser Induced Fluorescence (xCGE-LIF)

″ Samples were prepared and quantitative analysis was performed by xCGE-LIF according to a modified version of previously described protocols (Hennig et al., 2016; Thiesler et al., 2016). Accordingly, a pool of medaka hatclings (n=20) at st40 and human fibroblasts ($7x10^5$ cells) were lysed with RIPA Lysis and Extraction Buffer (Thermo Scientific). Purification of the samples were performed with a methanol/chloroform protein extraction protocol according to a previously published protocol (Wessel & Flügge, 1984). Further processing of samples were performed with the glyXprep 16 kit (glyXera, Magdeburg, Germany). *N*-glycans were released from solubilized proteins using peptide-*N*-glycosidase F and fluorescently labeled with 8-aminopyrene-1,3,6-trisulfonic acid (APTS). Hydrophilic interaction liquid chromatography-solid phase extraction (HILIC-SPE) was used to remove excessive fluorescent dye. The purified APTS-labeled *N*-glycans were analyzed by xCGE-LIF. Data processing and normalization of

migration times to an internal standard were performed with glyXtoolTM software (glyXera, Magdeburg, Germany). An in-house *N*-glycan database (glyXbase^{TM}) and exoglycosidase sequencing was used to annotate *N*-glycan fingerprints (normalized electropherograms) based on migration time matching. The symbolic representations were drawn with GlycoWorkbench (Ceroni et al., 2008) according to the guideline of the Consortium for Functional Glycomics (Varki et al., 2009). To facilitate the quantitative inter-sample comparison, an aliquot of each sample was spiked in with 1 µg of a bovine asialofetuin as an internal standard prior to methanol/chloroform protein extraction. A unique and asialofetuin-derived *N*-glycan peak was used to quantitatively normalize peak intensities. The quantitative normalization was then applied to the standard *N*- glycan fingerprints using mannose-6 as a transfer peak as explained in Appendix Figure 1. "

6.2.16 Mass Spectrometry

"-Sample preparation and protein precipitation

Mass spectrometry (MS) was performed on whole deyolked st40 hatchlings as well as st40 eyes. For the whole organism, st40 hatchlings were euthanized with tricane, deyolked, washed a couple of times in ice-cold PBS, pooled (n=3 biological replicates, n=6 fish each), snap frozen in liquid nitrogen and kept at -80 °C until lysis. For the measurement of eyes, both left and right eyes were dissected from 15 fish per biological replicate (n=4 biological replicates, 30 eyes each), washed a couple of times in ice-cold PBS, and snap frozen in liquid nitrogen.

Sample lysis and measurement of concentration steps were performed similar to "6.2.13 Lectin Blots". Accordingly, samples were lysed with 100-150 µl of RIPA Lysis and Extraction Buffer (Thermo Scientific) including cOmpleteTM EDTA-free Protease Inhibitor Cocktail (Roche) with the help of Qiagen TissueRaptor II. Protein lysis was incubated on ice with 50 U of Benzonase Nuclease (Millipore) for 20 min and at 37 °C for 5 min. Samples were then centrifuged at 12000 g for 10 min at 4 °C. Supernatant was taken into fresh tubes and protein concentration was assessed via Pierce^{TM} BCA Protein Assay Kit (Thermo Fisher Scientific). 100 ug and 30 ug of total protein for whole hatchling and eyes, respectively, were used for protein precipitation. Samples were precipitated with methanol / chloroform protocol according to (Wessel & Flügge, 1984).

-In-solution digestion

For in-solution digestion, pellets of precipitated proteins were resuspended in 20 µl of in-house made 8M urea buffer. Cysteine thiols were subsequently reduced and alkylated by adding

Tris(2-carboxyethyl)phospin (Carl Roth) to a final concentration of 10 mM and 2-Chloroacetamide (≥ 98.0 %, Sigma-Aldrich) to a final concentration of 40 mM, respectively. The solution was incubated for 30 min at RT. Sample predigestion was performed with Lysyl Endopeptidase® (MS grade, Wako Chemicals), which was added in an enzyme:protein ratio of 1:40 (*w*/*w*) and the samples were incubated for 4 hr at 37 °C. After diluting the urea concentration to 2 M by adding 50 mM TEAB buffer, trypsin (MS grade, Thermo) was added in an enzyme:protein ratio of 1:100 (*w*/*w*) and incubated for 16 hr at 37 °C.

-Dimethyl labeling

Dimethyl duplex labeling was performed bound to C18 material according to previously pulished standard protocol (Boersema et al., 2009). Briefly, digestion reaction was stopped by reducing the pH < 2 through the addition of trifluoroacetic acid (TFA, ≥ 99.0 %, Sigma-Aldrich) to a final concentration of 0.4 % (v/v) and samples were centrifuged for 10 min at 2500 g at RT. Supernatants' volume corresponding to 20 µg of total tryptic peptides per sample were loaded onto C18 StageTips containing 3 disks of Empore C18 material (3M). Prior to sample loading, StageTip material was successively equilibrated with 20 µl of methanol (MS grade, Carl Roth), followed by 20 µl of 50 % (*v*/*v*) acetonitrile (ACN, UPLC grade, Biosolve) in 0.1 % (*v*/*v*) TFA and by 20 µl of 0.1 % (*v*/*v*) TFA with centrifuging at 1500 g for 1 min after each equilibration step. Loaded peptide samples were washed with 20 µl of 100 mM TEAB, to shift pH for labeling and were tagged with stable-isotope dimethyl labels comprising regular formaldehyde and cyanoborohydride (28 Da shift, designated "light label") or deuterated formaldehyde and regular cyanoborohydride (32 Da shift, designated "heavy label") (all reagents from Sigma- Aldrich). Wild-type samples were tagged with light labels and alg2^{hypo} mutant samples were tagged with heavy labels, including a label swap for one of the four eye sample replicates. Labeled peptides were washed with 20 µl of 0.1 % TFA and eluted from StageTip material by adding 10 µl of 50 % ACN in 0.1 % TFA twice with subsequent centrifugation for 1 min at 1500g after each step. Differentially labeled samples were mixed in equal amounts, dried in a vacuum centrifuge and stored at -20 °C until LC-MS analysis.

-LC-MS measurements

For technical reasons, whole hatchling and eye samples were analyzed using slightly different LC-MS setups. Approx. 5 and 8.3 µg of tryptic peptides per LC-MS injection were analyzed for hatchling samples (two technical replicate measurements per biological replicate with different amounts, respectively) and approx. 2 µg of tryptic peptides were analyzed for eye

samples. A precursor ions inclusion list was used to improve run-to-run reproducibility for all samples. All used solvents were UPLC grade.

Whole hatchling samples were resuspended after vacuum centrifuge in 20 % ACN / 0.1 % TFA and incubated for 5 min at RT. Samples were diluted 10-fold in 0.1 % TFA prior to LC-MS measurement, which was conducted using an Ultimate 3000 UPLC (Thermo Fisher Scientific) coupled to a Q-Exactive HF mass spectrometer (Thermo Fisher Scientific). Analytical LC separation was performed using an in-house packed analytical column (20 cm length, 75 µm inner diameter; CS – Chromatographie Service GmbH) filled with 1.9 µm particle size, 120 Å pore size ReprosilPur-AQ 120 C18 material (Dr. Maisch) and carried out for 160 min total analysis time. The chromatographic method consisted of a linear gradient of buffer B (0.1 % *v*/*v* formic acid (FA), Proteochem, 10 % *v*/*v* H_2O, Biosolve in ACN) in buffer A (0.1 % FA, 1 % ACN in H_2O) from 3 to 40% B in 120 min with a flow rate of 300 nl /min, followed by a washing (95 % B) and an equilibration step. Prior to the gradient, samples were loaded to the analytical column for 20 min with 3% B at 550 nl/min flow rate. Eluting peptides were analyzed online by a coupled Q-Exactive-HF mass spectrometer running in DDA mode. Full scans were performed at 60 000 (m/z 200) resolution for a mass range covering 400-1600 m/z for 3e6 ions or up to a max IT of 45 ms. The full scan was followed by up to 15 MS/MS scans at 15 000 resolution with a max IT of 50 ms for up to 1e5 ions (AGC target). Precursors were isolated with a window of 1.6 m/z and fragmented with a collision energy of 27 (NCE). Unassigned and singly charged peptides were excluded from fragmentation and dynamic exclusion was set to 35 sec.

For eye samples, dried peptides were resuspended in 2.5 % 1,1,1,3,3,3-Hexafluoro-2- propanol (Sigma-Aldrich) / 0.1% TFA prior to LC-MS measurement, which was conducted using an Ultimate 3000 UPLC (Thermo Fisher Scientific) coupled to a Q-Exactive HF-X mass spectrometer (Thermo Fisher Scientific). During the LC separation, peptides were first loaded onto a trapping cartridge (Acclaim PepMap300 C18, 5 µm particle size, 300 Å pore size, Thermo Fisher Scientific) and washed for 3 min with 0.1 % TFA. Analytical separation was performed using a nanoEase MZ Peptide analytical column (BEH, 20 cm length, 75 µm inner diameter, 1.7 µm particle size, 300 Å pore size, Waters) and carried out for 150 min total analysis time. The chromatographic method consisted of a linear gradient of buffer B (0.1 % FA, 19.9 % H_2O, Biosolve in ACN) in buffer A (0.1 % FA in H_2O) from 5 to 38 % B in 132 min with a flow rate of 300 nL / min, followed by a washing (95% B) and an equilibration step. Eluting peptides were analyzed online by a coupled Q-Exactive-HF-X mass spectrometer

running in DDA mode. Full scans were performed at 60 000 resolution for a mass range covering 350-1500 m/z for 3e6 ions or up to a max IT of 45 ms. The full scan was followed by up to 20 MS/MS scans at 15 000 resolution with a max IT of 22 ms for up to 1e5 ions (AGC target). Precursors were isolated with a window of 1.6 m/z and fragmented with a collision energy of 27 (NCE). Unassigned and singly charged peptides were excluded from fragmentation and dynamic exclusion was set to 35 sec.

-Protein identification and relative quantification with MaxQuant

Raw files were processed using MaxQuant v1.6.12.0 (Cox & Mann, 2008) for protein identification and quantification. MS / MS spectra were searched against the Uniprot Oryzias latipes database (retrieved in February 2020, last edited in November 2019), common contaminants and an additional fasta file containing the amino acid sequence of the usherin protein (Uniprot ID: U3R8H7) by Andromeda search engine with the following parameters: Carbamidomethylation of cysteine residues as fixed modification and Acetyl (Protein *N*-term), Oxidation (M) as variable modifications, trypsin/P as the proteolytic enzyme with up to two missed cleavages allowed. The maximum false discovery rate for proteins and peptides was 0.01 and a minimum peptide length of 7 amino acids was required. Match between runs and requantify options were disabled. Quantification mode was with the dimethyl Lys 0 and *N*-term 0 as light labels and dimethyl Lys 4 and *N*-term 4 as heavy labels. All other parameters were default parameters of MaxQuant. Quantitative normalized ratios were calculated by MaxQuant and used for further data analysis.

-Statistical analysis of MS data

Perseus software v1.5.6.0 was used (Tyanova et al., 2016). For the volcano plots in Figure 10, MaxQuant normalized (total protein normalization) and log2 transformed data were filtered (at least two razor or unique peptides per protein group required) and technical replicate values were averaged, if available. One-sample t-test (comparison to 0, p-value 0.05, -1< t-test difference< 1) was then performed and plots were produced with R and RStudio version 1.2.5042. For exclusive protein groups (only wild-type or only mutant), the raw intensity values for each biological replicate were normalized to the mean of unnormalized Gapdh ratios from all replicates and log2 transformed so that the proteins were plotted on the y axis according to their Gapdh normalized intensities for representation only. Exclusive hits were only considered when present in at least two biological replicates."

6.2.17 Immunofluorescence

Sample fixations were done at the indicated stage of medaka (in the figures) in 4 % PFA in 1X PTW (PBS, 0.4 % Tween) overnight at 4°C on a rotator. Next day, samples were washed in 1X PTW at RT several times and incubated at least once overnight in 30 % sucrose in PTW and at least once in Tissue Freezing Medium (Leica, #14020108926): 30 % Sucrose in PTW (1:1, v/v). Samples were embedded in the same Tissue Freezing Medium and snap frozen inside liquid nitrogen. Samples were sectioned with 16 µm thickness on a cryostat (Leica CM 3050S) and dried on Superfrost plus microscope slides (Thermo Fisher Scientific) overnight at 4 °C. Next day, slides were washed with 1X PTW for rehydration. Antigen retrieval step was applied to the slides that will be stained with the following antibodies: rabbit anti-PKCα antibody (1:200, Santa Cruz, #sc-208), mouse anti-HuC/D (1:500, Life Technologies, #A21271), anti-mouse Rhod (1:200, Millipore, #MABN15). Accordingly, slides were re-fixed with 4% PFA/PTW for 30 min and washed 3 times for 5 min in 1X PTW. Slides were incubated in HCl for 60 min at 37°C (2N HCl, 0.5% TritonX) and slides were washed 3 times for 5 min in 1X PTW. For pH recovery, slides were incubate in Borax-PTW dilution for 15 min and washed in 1X PTW for 5 min. Both antigen-retrieval and non-retrieval samples continued as follows: Slides were blocked with 10% normal goat serum (NGS) in 1X PTW for 2 hr at RT while covered with parafilm (Bemis). Samples were stained with anti-Rhodopsin rabbit and mouse antibodies (1:200, home- made and 1:200, Millipore, #MABN15), anti-Zpr1 mouse antibody (1:200, ZIRC, #AB_10013803), anti-Rx2 rabbit antibody (1:200, (Reinhardt et al., 2015)), and anti-GS mouse antibody (1:500, Merck #MAB302), chicken anti-GFP antibody (1:500, Life Technologies, #A10262), rabbit anti-PKCα antibody (1:200, Santa Cruz, #sc-208), mouse anti-HuC/D (1:500, Life Technologies, #A21271) in 1 % NGS overnight at 4 °C. Goat anti-mouse IgG (H+L) Alexa Fluor 546 (Life Technologies, #A11030) and goat anti-rabbit IgG Alexa Fluor 488 (Life Technologies, #A11034), and donkey anti-mouse 647 (Invitrogen, #A32787), goat anti-rabbit 647 (Thermo LifeTech, #A21245), donkey anti-chicken AF488 (Jackson/ Dianova, #703-545-155) were used in 1:750 dilution as secondary antibodies together with DAPI (10 µg/ml) in 1 % NGS for 2 hr at 37 °C. When combined with TUNEL staining, *In Situ* Cell Death Detection Kit, TMR red (Roche, #12156792910) was used according to the manufacturer's instruction (Roche, 2016). Samples were mounted in 60% glycerol in 1X PTW and were imaged on a Leica SP8 confocal microscope. Image analysis was performed with Fiji (Schindelin et al., 2012).

6.2.18 mRNA Rescue Injections

" -Cloning of olalg2 cDNA and mRNA synthesis

alg2 cDNA was amplified with RT-PCR from the cDNA of wild-type *Oryzias latipes* Cab strain stage 18 embryos with Q5® High-Fidelity DNA Polymerase (New England Biolabs) by using primers with BamHI-HF (New England Biolabs, 20U/ml, #R3136S) and XbaI (New England Biolabs, 20U/ml, #R0145S) recognition sequence extensions, 5' -GCCGGATCCATGGCGCGGGTGGTGTTT-3' and 5'-GCCTCTAGATTACTGGCTGAGCATAACTACGT -3' (98 °C denaturation for 20 sec, 58°C annealing for 30 sec, 70 °C extension for 40 sec, 35 cycles). Both RT-PCR product and pCS2+ vector (Rupp et al., 1994) were digested with BamHI-HF and XbaI restriction enzymes and cleaned up from agarose gel with innuPREP Gel Extraction Kit (Analytik Jena, 2017b). Ligation of digested PCR product and backbone was performed with 0.5 µl T4 DNA ligase (Thermo Scientific, 5U/ml) in 1x ligase buffer with 10 µl end volume for 15 min at RT. Cloned vector was transformed into Mach1-T1 *E. coli* cells (ThermoFisher Scientific) via heat shock induction at 42 °C for 45 sec and snap cooling on ice. Transformed cells were added 300 µl TB and incubated for 45 min at 37 °C. Cloned vector (100 µl) was plated on LB plates with Ampicillin resistance for overnight incubation at 37 °C. Next day, individual clones were inoculated into LB medium containing Ampicillin (100 µg/ml) and plasmids were extracted from bacteria culture with QIAprep Spin Miniprep Kit (Qiagen) according to manufacturer's instructions (Qiagen, 2020). One clone with a successful integration was used to perform *in vitro* mRNA synthesis with mMESSAGE mMACHINE^{TM} SP6 Transcription Kit (ThermoFischer Scientific) (Ambion by life technologies, 2012a) upon NotI-HF (New England Biosciences) linearization and gel purification with innuPREP Gel Extraction Kit (Analytik Jena). Plasmid in the RNA reaction was digested with 1 µl TURBO DNase I (2 U/µl, ThermoFisher Scientific) for 15 min at 37 °C. RNA was cleaned up with RNeasy Mini Kit (Qiagen, 74104) and quality of RNA was confirmed with agarose gel electrophoresis and Spectrophotometer DS-11+ (DeNovix).

-Cloning of hsAlg2 cDNA and mRNA synthesis

The plasmid containing the whole cDNA of healthy human was kindly provided by Christian Thiel (University Clinic, Heidelberg University, Germany). The RNA was synthesized *in vitro* with mMESSAGE mMACHINETM T7 Kit according to manufacturer's instructions (Ambion by life technologies, 2012a) on HpaI linearized and gel purified (InnuPrep, AnalytikJena) plasmid DNA.

-Injections into medaka

Adults *alg2*$^{+/-}$ medaka were crossed and offspring was injected at the one-cell stage with 100 - 200 ng/µl medaka *alg2 (olalg2)* or 34 ng/µl of human *Alg2 (hsAlg* mRNA and both together with *GFP* mRNA (10 ng/µl) as injection tracer. As injection control, offspring of the same crossing scheme was used for *GFP* mRNA injection only. Embryos were kept at 28 °C. GFP negative embryos were discarded. Genotyping of the embryos was performed from the fin clip biopsies with Q5® High-Fidelity DNA Polymerase (New England Biolabs) as menationed in "6.2.4 alg2^{hypo} Line Generation" section. Remainder of the sample was used either for Alcian Blue staining or antibody staining as mentioned above. ″

6.2.19 D-mannose Supplementation

-Toxicity test on wild-type medaka

Wild-type medaka adults were mated and embryos were collected at 1-cell stage. Half of the embryos were rolled on sand paper until they lost the hair on the chorion. For serial dilutios, 500mM D-mannose stock was prepared by dissolving 0.9 gr D-mannose in 10 ml ERM. Embryos were incubated in D-mannose (Sigma-Aldrich) at 50, 100, 250, and 500 mM concentrations in 1X ERM (solubility in water is 50mg/ml). Treatment of embryos started around st8/9 (6 hpf at RT) and embryos were kept in 24-well plates with 2.5 ml of respective D-mannose solution. Vehicle control had only in 1X ERM. Embryos were kept at 26 °C. Medium was refreshed every 24 hr and treatment continued for 72 hr. Viability and the phenotypes were observed under binocular.

-Treatment of alg2^{hypo} line

alg2$^{+/-}$ adults were incrossed and embryos were treated with 50 mM D-mannose (or 50mM D-glucose) similar to described above: Embryos were not dechorionated, treatment started at st8/9, medium was refreshed every 24 hr, and the treatment continued until around 5 dph. Each day number of survivors were noted.

6.2.20 NAA and Na-NAA Toxicity Tests

NAA (Sigma, N0640-25G) was dissolved in 1N NaOH to prepare stock solution (For 0.5M Stock, 0.465g NAA was dissolved in 5ml of 1N NaOH). A working concentration of 10 mM was prepared from the NAA stock by diluting it directly in 1X ERM and 1M HEPES (final concentration of 5mM). Other dilutions were prepared from a dilution series. Embryos were

collected from freshly mated wild-type Cab strain medaka adults and dechorionated around stage8. Embryos were incubated in the respective concentrations for 3 days. Solutions were refreshed every 24 hr. Tests were repeated with Sodium 1-Naphthaleneacetate (Santa Cruz) that can be solved directly in water. Chorion was kept intact. A stock concentration of 0.5mM of Na-NAA was prepared by directly dissolving in 1X ERM and serial dilutions were prepared from the stock in 1X ERM.

6.2.21 Pmm2 Enzyme Activity Test of Pmm2-GFP Line

-Sample preparation

Heterozygote Pmm2-GFP ($Pmm2^{+/GFP}$) F2 generation fish were incrossed. Resulting progeny were euthanized with 1X Tricane at st40 (1-5dph at 26 degree). Left eyes were removed for genotyping and fish were deyolked. Genotyping was performed according to section "6.2.5 Pmm2-GFP Line Generation". The rest of the body was snap frozen in liquid nitrogen for enzyme activity test. Fish were submitted to University Clinic, University of Heidelberg, AGThiel group for protein lysis and activity test on dry ice. Briefly, the pool of st40 embryos were lysed in an extraction buffer containing protease inhibitors without any detergent. Total protein amount was measured with PierceTM BCA Protein Assay Kit (Thermo Fisher Scientific).

-Enzyme activity measurement

Thirty µg of protein per well in ninety-six well plate was placed. Hundred µmol of NADP per well (Chemical mix NADP, $MgCl_2$(cofactor), glucose-1-phosphate (activator)), oversaturated Mannose-6 phosphate isomerase (MPI) and phosphoglucose isomerase (PGI)) was added to the reaction mix. These two enzymes were oversaturated to have endogenous Pmm2 as a rate limiting step. Resulting NADPH concentration was measured at 340nm for 3 hr. The background signal was removed from the wells containing protein mix, chemical mix, and the enzyme mix.

6.2.22 TIR1 and AID-nanobody mRNA Production for Microinjections

AID-nanobody (plasmid number 117713) was cloned into PCS2+ vector for *in vitro* mRNA synthesis whereas TIR1 vector (plasmid number 117717) was obtained already inside PCS2+ vector. Accordingly, AID-nanobody and PCS2+ plasmids were digested with DraI-FD and XbaI in 10X Cut Smart Buffer (NEB) at 37 °C for 1 hr and enzymes were inactivated at 65 °C

for 10 min. Digested product was size separated on 1.5 % agarose gel and 700 bp band of AID-nanobody and 4kb band of PCS2+ vector were excised and cleaned up with Analytik Jene gel extraction kit according to manufacturer's instructions (Analytik Jena, 2017b). Cleaned up products were ligated with T4 DNA ligase (insertion : backbone = 3 : 1 mol ratio) and transfected to Mach1-T1 cells (Thermo Fisher Scientific) with heat shock at 42 °C for 45 sec and incubation of samples on ice. Cells were incubated in TB medium for 1 hr at 37 °C, inoculated on agar plates with Ampicillin (1:1000) and incubated overnight at 37 °C. Next day, one positive colony was incubated in 3 ml LB medium with Ampicillin (1:1000) overnight at 37 °C and plasmids were extracted with an adjusted version of Qiagen Miniprep protocol as mentioned in "6.2.8 sgRNA Production". Test digest was performed with NotI-FD (Thermo Fisher Scientific) in FD Green Buffer 1 hr at RT. Positive colonies from AID-nanobody-PCS2+ and TIR1 plasmid were used to expand the plasmids via Qiagen Miniprep (Qiagen, 2020) according to manufacturer's instruction from 8 ml inoculated LB medium + Ampicillin (1:1000) for *in vitro* mRNA synthesis. AID-nanobody vector was linearized with PauI (NEB) and TIR1 plasmid was linearized with NotI-HF (NEB). Linearized products were gel purified as mentioned above. *In vitro* mRNA synthesis was performed with mMESSAGE mMACHINE Sp6 Transcription Kit (Ambion by life technologies, 2012a) and RNAs were cleaned up with RNeasy Mini Kit (Qiagen, 2019) according to the manufacturers' instructions. Quality of RNA was assessed via agarose gel electrophoresis and spectrophotometer as mentioned in "6.2.8 sgRNA Production".

Appendix

Appendix Table 1: Peak numbers of xCGE-LIF (Figure 8 and 9), their abbreviations and structures

Number	Abbreviation	Structure
1	A3[2,4]S1(2,6)G1(3)[3,4]G2(4)S2(2,6)S1(2,3)[3,4]	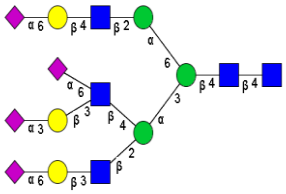
2	A3[2,4]S1(2,6)G1(3)[3,4]G2(4)S2(2,3)S1(2,6)[3,2]	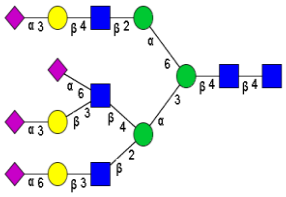
3	A3[2,4]S1(2,6)G1(3)[3,4]G2(4)S2(2,6)[3,2;6,2]	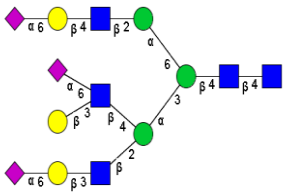
4	A3G3S3(2,6)	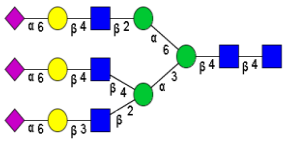
5	A3G3S1(2,3)[3,4]S2(2,6)	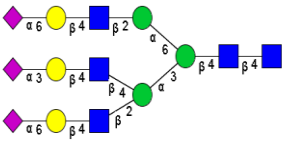
6	A2G2S2(2,6)	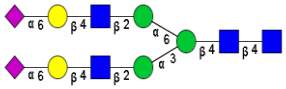
7	A3G3S2(2,3)S1(2,6)[3,2]	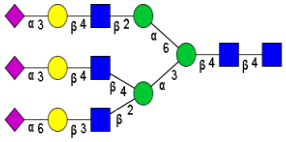

8	FA2G2S2(2,6)	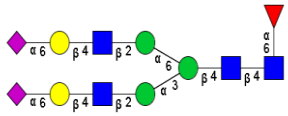
9	A2G2S2(2,3)	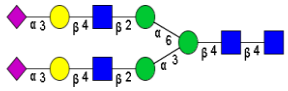
10	FA2BG2S2(2,6)	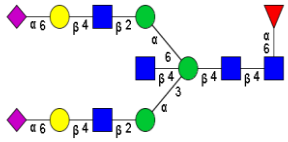
11	A1G1S1(2,3)[3]	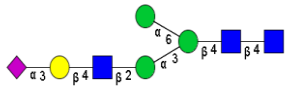
12	FA2G2S2(2,3)	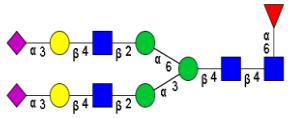
13	A3[2,4]S1(2,6)G1(3)[3,4]G2(4)S1(2,6)[3,2]	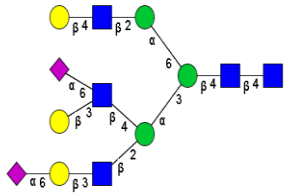
14	FA2F1(1,3)G2S2(2,3)	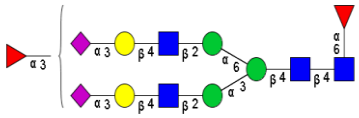
15	FMan3	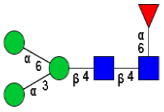

16	A3G3S1(2,3)S1(2,6)	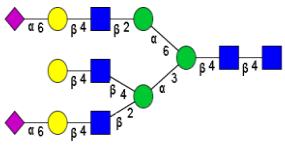
17	FA2BG1S1(2,6)[6]	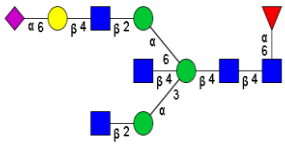
18	A2G2S1(2,6)	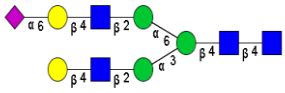
19	A2G2S1(2,3)[3]	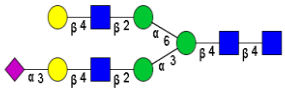
20	FA2G2S1(2,6)	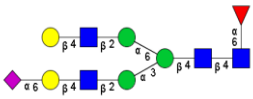
21	Man5	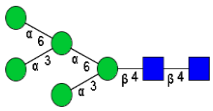
22	FA2G2S1(2,3)[6]	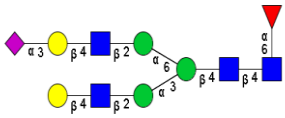
23	FA2G2S1(2,3)[3]	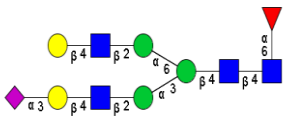

24	FA4G4S2(2,3)	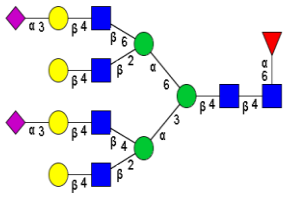
25	Man6	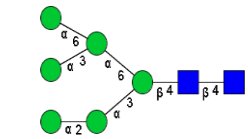
26	A2G1[3]	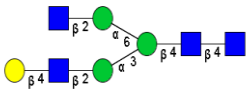
27	FA3G3S1(2,3)[2,6]	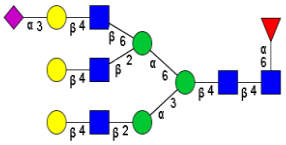
28	Man7[D1]	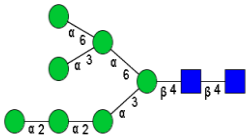
29	Man7[D3]	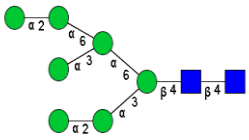
30	FA2BG1[6]	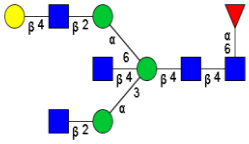
31	A2G2	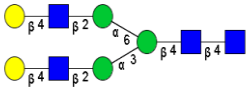

32	Man8	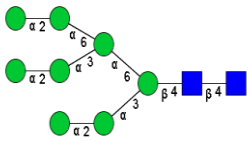
33	FA3G1[2,6]	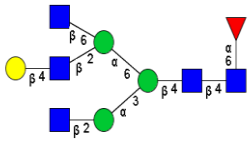
34	Man9	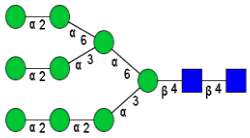
35	FA2G2	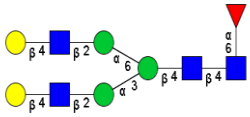
36	FA2BG2	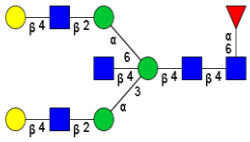
37	Man8-Glc	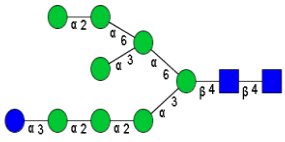
38	Man9-Glc	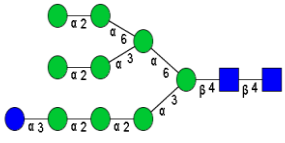

39	FA4G2	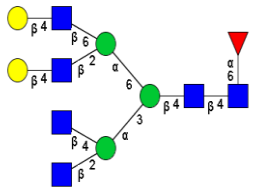
40	FA3G3[2,6]	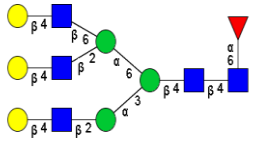
41	FA3[2,4]G3	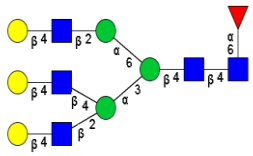
42	A4G3	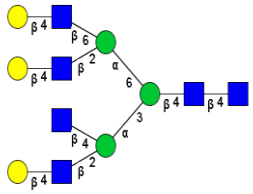

Appendix Table 2a: Differentially upregulated and exclusive (in mutant) protein groups according to MS of eye samples, their human orthologs, number of *N*-glycosylation motifs and subcellular localization (orange: no *N*-glycosylation motif predicted, green: existence of *N*-glycosylation motif predicted as well as reported to localize to membrane or to be secreted on uniprot.org)

Regulation	Medaka Gene Name	Medaka Gene stable ID	Human gene name	Human gene stable ID	Number of N-glyc motif	Number of predicted N-glyc site	Subcellular Localization	UniProt ID
up	gale	ENSORLG00000017448	GALE	ENSG00000117308	4	4	Cytosol	H2MSS6
up	sec22bb	ENSORLG00000004111	SEC22B	ENSG00000265808	1	1	ER-Golgi	A0A3B3H3F1
up	apoeb	ENSORLG00000013886	APOE	ENSG00000130203	0	0	Extracellular -secreted	H2MG05
up	hspa5	ENSORLG00000006886	HSPA5	ENSG00000044574	0	0	ER	H2LRF2
up	gfpt1	ENSORLG00000011306	GFPT1	ENSG00000198380	2	2	x	A0A3B3HEB0;A0A3B3HFC7
up	p4ha1b	ENSORLG00000005147	P4HA1	ENSG00000122884	1	1	ER	A0A3B3HZS5;H2MJ53
up	ago2	ENSORLG00000004615	AGO2	ENSG00000123908	4	3	P body	H2LIH8
up	calub	ENSORLG00000023455	CALU	ENSG00000128595	1	0	ER-Golgi-Extracellular-secreted	A0A3B3IHZ0
up	hsp90b1	ENSORLG00000004360	HSP90B1	ENSG00000166598	4	4	ER	H2LHK4
up	prkcsh	ENSORLG00000005398	PRKCSH	ENSG00000130175	3	2	ER	H2LL89
up	Arf5	ENSORLG00000020571	ARF5	ENSG00000004059	0	0	Plasma membrane	H2N213
up	ganab	ENSORLG00000002721	GANAB	ENSG00000089597	0	0	x	A0A3B3I6F1
up	pmm2	ENSORLG00000030353	PMM2	ENSG00000140650	1	0	Cytosol	A0A3B3IBB4
up	-	ENSORLG00000025745	none	none	0	0	Cytosol	Q8AYQ6
up	-	ENSORLG00000030133	none	none	0	0	Cytosol	Q8AYQ5
only mutant	lman1	ENSORLG00000006066	LMAN1	ENSG00000074695	0	0	ER-Golgi	H2LNJ7
only mutant	arhgef2	ENSORLG00000019404	ARHGEF2	ENSG00000116584	4	3	Cytosol	A0A3B3H269
only mutant	alg5	ENSORLG00000003991	ALG5	ENSG00000120697	1	1	ER	H2LG98
only mutant	hce	ENSORLG00000014846	none	none	1	1	Secretory vesicles	P31580;H2MIY0;H2MIZ4;P31581
only mutant	arf4	ENSORLG00000017377	none	none	1	1	Plasma membrane	H2MSI7
only mutant	zgc:114181	ENSORLG00000003701	none	none	1	1	Cytosol	H2LF82
only mutant	-	ENSORLG00000022891	MYH9	ENSG00000100345	2	2	Cytoskeleton	A0A3B3IMD1
only mutant	LOC101158738	ENSORLG00000010644	CALD1	ENSG00000122786	4	3	Cytoskeleton	H2M4H8
only mutant	col18a1a	ENSORLG00000014422	COL18A1	ENSG00000182871	5	4	Extracellular -secreted	H2MHG7
only mutant	-	ENSORLG00000017308	FLNB	ENSG00000136068	1	1	x	H2MSC4
only mutant	Pdcl3	ENSORLG00000009325	PDCL3	ENSG00000115539	1	1	x	H2LZX0
only mutant	atp6ap2	ENSORLG00000011684	ATP6AP2	ENSG00000182220	0	0	ER and cell membrane	H2M835
only mutant	eif2b3	ENSORLG00000016154	EIF2B3	ENSG00000070785	3	2	x	H2MNB4
only mutant	-	ENSORLG00000029511	GOLGA4	ENSG00000144674	1	1	x	A0A3B3HDP6
only mutant	rbm39a	ENSORLG00000009919	none	none	4	2	Nucleus	H2M208
only mutant	sec23a	ENSORLG00000020123	SEC23A	ENSG00000100934	4	3	Cytosol	H2N0Q7
only mutant	mogs	ENSORLG00000026440	MOGS	ENSG00000115275	5	4	ER	A0A3B3I7U8
only mutant	glyr1	ENSORLG00000017440	GLYR1	ENSG00000140632	2	1	x	H2MSR5
only mutant	c12orf57	ENSORLG00000024125	C12orf57	ENSG00000111678	0	0	Cytosol	H2M6T8

Appendix Table 2b: Differentially downregulated and exclusive (in wild-type) protein groups according to MS of eye samples, their human orthologs, number of *N*-glycosylation motifs and subcellular localization (orange: no *N*-glycosylation motif predicted, green: existence of *N*-glycosylation motif predicted as well as reported to localize to membrane or to be secreted on uniprot.org)

Regulation	Medaka Gene Name	Medaka Gene stable ID	Human gene name	Human gene stable ID	Number of N-glyc motif	Number of predicted N-glyc site	Subcellular Localization	UniProt ID
down	sv2ba	ENSORLG00000014648	SV2B	ENSG00000185518	3	1	x	H2MI91
down	marcksb	ENSORLG00000013439	none	none	1	1	Membrane	H2ME50
down	adh5	ENSORLG00000017646	none	none	1	1	x	H2MTT4;H2MTT3;H2MZR4
down	tpi1a	ENSORLG00000006391	TPI1	ENSG00000111669	1	1	Cytosol	H2LPP4;Q589R5
down	opn1sw	ENSORLG00000019293	OPN1SW	ENSG00000128617	2	2	Membrane	P87368;Q2L6A1
down	gnb1	ENSORLG00000003613	GNB1	ENSG00000078369	0	0	x	H2LEX4
down	zgc:109982	ENSORLG00000013730	RDH8	ENSG00000080511	2	1	Membrane	H2MF51
down	rom1a	ENSORLG00000010774	ROM1	ENSG00000149489	1	0	Membrane	H2M4Z1
down	rcvrna	ENSORLG00000001318	none	none	1	1	x	H2L718
down	kfharr-r2	ENSORLG00000006701	SAG	ENSG00000130561	4	2	x	Q9W7R1
down	gnat1	ENSORLG00000018998	GNAT1	ENSG00000114349	1	0	x	H2MXN0
down	rho	ENSORLG00000010979	RHO	ENSG00000163914	3	3	Membrane	P87369;H2M4C4
only wt	slc44a2	ENSORLG00000028411	SLC44A2	ENSG00000129353	6	3	Membrane	A0A3B3HLZ3
only wt	si:ch211-113g11.6	ENSORLG00000027544	none	none	6	2	x	A0A3B3HNH0
only wt	sypa	ENSORLG00000025491	SYP	ENSG00000102003	2	2	Membrane	A0A3B3I291
only wt	slc4a10a	ENSORLG00000002809	SLC4A10	ENSG00000144290	6	6	Membrane	A0A3B3I626;H2MRC5
only wt	nfu1	ENSORLG00000011320	none	none	0	0	x	H2M6T4
only wt	atp6v0a1	ENSORLG00000014447	ATP6V0A1	ENSG00000033627	3	3	Membrane	H2MHJ5
only wt	cpsf3	ENSORLG00000018854	CPSF3	ENSG00000119203	3	2	Nucleus	H2MX86

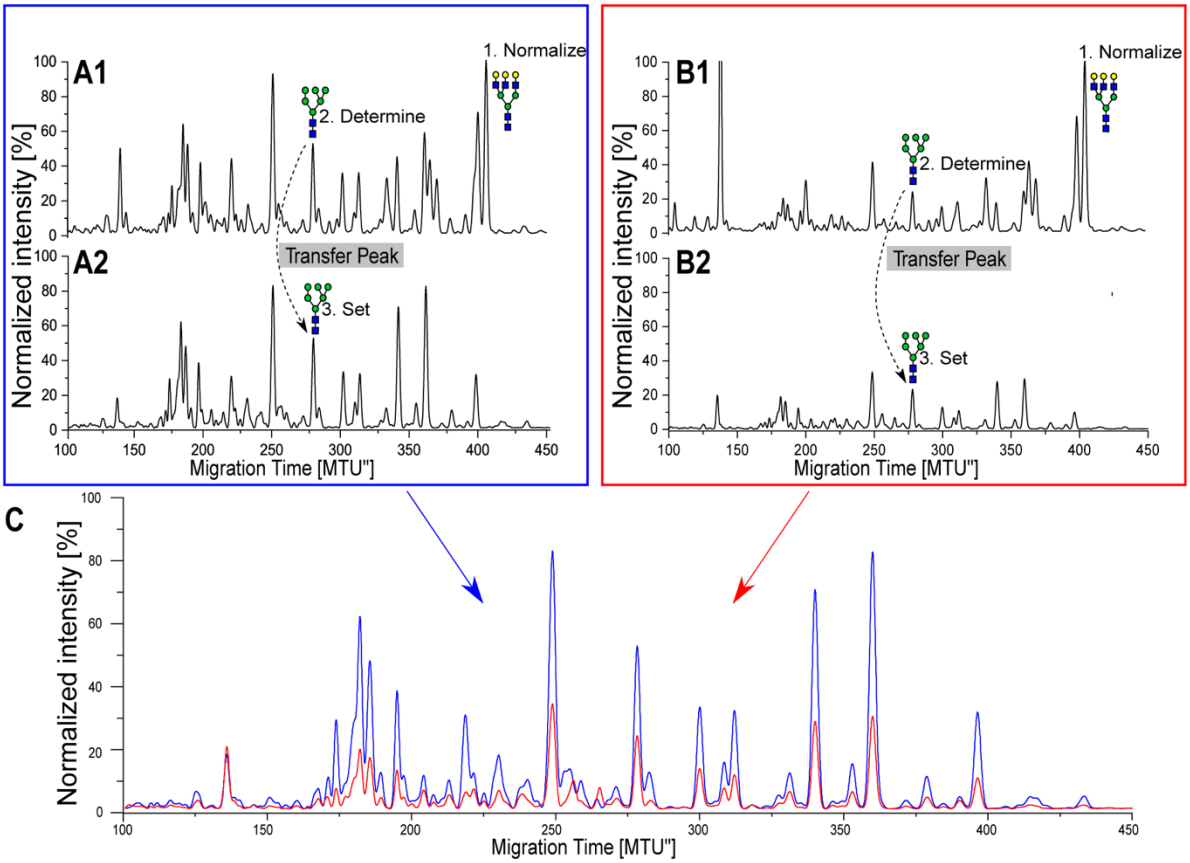

Appendix Figure 1: Normalization of the xCGE-LIF data for comparison of samples acquired independently

(A-B) A1 and A2 or B1 and B2 represents 2 different measurements from the same sample. Prior to obtaining results from A1 or B1, the samples were spiked in with asialofetuin (1. Normalize), whereas A2 and B2 were left without a spike-in-control. Additionally, A2 and B2 were treated with oligohexosidases to clean up the sample. The comparison of all the peaks between the A1/A2 and B1/B2 showed that Man6 peak remained unaltered (2. Determine and 3. Set). Thus, Man6 peak was chosen for the normalization of both samples. In this sense all the graphs were normalized, but A1 and B1 were normalized to asialofetuin, which is 100%.

(C) Combined results of the samples from A and B after both x- and y-axis normalization.

Contributions

This section is dedicated to the contributions that were made to this thesis.

Alicia Perez-Saturnino cloned the Pmm2-GFP plasmid for the production of modified PCR.

Elena Tonin performed the cloning of TIR1 and AID-nanobody into PCS2+ vector for *in vitro* mRNA synthesis

Kaisa Pakari performed the injections of TIR1 and AID-nanobody mRNA for degradation of Pmm2 in Pmm2-GFP line. She also performed toxicity test of Na-NAA.

Lars Beedgen cultured the ALG2-CDG patient fibroblasts, submitted the cell extracts for xCGE-LIF, performed lectin blots from patient samples, and measured the enzyme activity of Pmm2-CDG medaka hatchlings.

Nicole Lübbehusen performed chemical labeling of MS samples.

Oi Pui Hoang performed the injections for the alg2^{hypo} fish F0 generation.

Rachel Müller fin-clipped and genotyped some of the adult alg2^{hypo} line for stock maintenance.

Roman Sakson ran the MS samples and helped with the data analysis.

Simran Panda screened phenotype and genotype of the Pmm2-GFP line for the founder fish.

Tanja Kellner produced the sgRNA and Cas9 mRNA for the alg2^{hypo} line.

Thomas Thumberger designed the sgRNA constructs to target the *alg2* locus.

Valerian Grote and **Marcus Hoffmann** ran the samples on xCGE-LIF and analyzed the data.

Acknowledgements

I would like to thank Jochen for enabling me to work in his lab and in this interesting project. I would also like to thank Thomas, the TT, for his close supervision and support. I would like to thank Prof. Dr. Sabine Strahl, Prof. Dr. Bernd Bukau and Dr. Sergio Acebrón for their detailed feedback and support during the Thesis Advisory Committee (TAC) meetings. I also thank Prof. Dr. Ingrid Lohmann for accepting to be in my defense committee as my primary supervisor and examiner and for evaluating my thesis.

I have to thank my boyfriend Moritz for supporting me throughout my PhD, engaging in countless discussions about my project until late in the night, reading my thesis and giving me detailed feedback to improve the quality of my thesis, supporting me unconditionally, always being patient with me, and helping me to grow both scientifically and personally.

I would also like to thank my mother for reminding me how much more money I can earn once I finish my PhD and, therefore, convincing me to complete my PhD as soon as possible. I love you Mom…

I have to thank my best friends, Marie and Umut, for always supporting me in any topic in life, as well as throughout my PhD with any of the problems I faced.

I owe a special thanks to my lab members Jørgen, Omar, Risa, Karen, Erika, and Bettina for making the lab a warm and friendly environment. I also want to thank everybody in the lab for valuable scientific discussions at all times.

I want to thank my grandfather, who unfortunately passed away due to Covid19, for always being like a father to me and supporting me in every step of my life. With that, I would also like to express my gratitude for all the healthcare workers worldwide who have been fighting against Coronavirus.

Lastly, I thank my beloved rabbit Loca, my Minnoş, for always being cute and making my day with her fluffy fur. I also owe thanks to my hamster Balduin who never stopped running late into the night with his mouth full of nuts, which motivated me to keep working until late hours.

Publications

Gücüm, S., Sakson, R., Hoffmann, M., Grote, V., Beedgen, L., Thiel, C., Rapp E., Ruppert T., Wittbrodt J., Thumberger, T. (2020). The medaka alg2 mutant is a model for hypo-*N*-glycosylation-associated retinitis pigmentosa. *BioRxiv*. https://doi.org/https://doi.org/10.1101/2020.08.20.260430
(currently in revision in Development)

References

Alloway, P. G., Howard, L., & Dolph, P. J. (2000). The formation of stable rhodopsin-arrestin complexes induces apoptosis and photoreceptor cell degeneration. *Neuron*, *28*(1), 129–138. https://doi.org/10.1016/S0896-6273(00)00091-X

Ambion by life technologies. (2012a). *mMESSAGE mMACHINE ® Kit*. Retrieved from https://www.thermofisher.com/document-connect/document-connect.html?url=https%3A%2F%2Fassets.thermofisher.com%2FTFS-Assets%2FLSG%2Fmanuals%2Fcms_055516.pdf&title=VXNlciBHdWlkZTogbU1FU1NBR0UgbU1BQ0hJTkUmcmVnOyBLaXQgLSBIaWdoIFlpZWxkIENhcHBlZCBSTkEgVHJhbnNjc

Ambion by life technologies. (2012b). *MEGAscript® Kit User Guide (Pub. no. 1330M Rev. G)*. (1330M). Retrieved from https://www.thermofisher.com/document-connect/document-connect.html?url=https%3A%2F%2Fassets.thermofisher.com%2FTFS-Assets%2FLSG%2Fmanuals%2F1330M_G.pdf&title=TUVHQXNjcmlwdCZ0cmFkZTsgS2l0IEluc3RydWN0aW9uIE1hbnVhbA==

Analytik Jena. (2017a). *Instructions for Use Life Science Kits & Assays innuPREP PCRpure Kit*. Retrieved from https://www.analytik-jena.kr/fileadmin/content/pdf_life_science/Manual/Manual_KS-5010_innuPREP_PCRpure_Kit_e_170505_WEB_geschuetzt.pdf

Analytik Jena. (2017b). *Instructions for Use Life Science Kits & Assays innuPREP Gel Exraction Kit*. Retrieved from https://www.analytik-jena.kr/fileadmin/content/pdf_life_science/Manual/Manual_innuPREP_Gel_Extraction_Kit.pdf

Andergassen, D., Dotter, C. P., Wenzel, D., Sigl, V., Bammer, P. C., Muckenhuber, M., … Hudson, Q. J. (2017). Mapping the mouse Allelome reveals tissue-specific regulation of allelic expression. *ELife*, *6*(Xci), 1–29. https://doi.org/10.7554/eLife.25125

Ansai, S., & Kinoshita, M. (2014). Targeted mutagenesis using CRISPR/Cas system in medaka. *Biology Open*, *3*(5), 362–371. https://doi.org/10.1242/bio.20148177

Apweiler, R., Hermjakob, H., & Sharon, N. (1999). On the frequency of protein glycosylation, as deduced from analysis of the SWISS-PROT database. *Biochimica et Biophysica Acta - General Subjects*, *1473*(1), 4–8. https://doi.org/10.1016/S0304-4165(99)00165-8

Baker, K. E., & Parker, R. (2004). Nonsense-mediated mRNA decay: Terminating erroneous gene expression. *Current Opinion in Cell Biology*, *16*(3), 293–299. https://doi.org/10.1016/j.ceb.2004.03.003

Balakrishnan, B., Verheijen, J., Lupo, A., Raymond, K., Turgeon, C., Yang, Y., … Lai, K. (2019). A novel phosphoglucomutase-deficient mouse model reveals aberrant glycosylation and early embryonic lethality. *Journal of Inherited Metabolic Disease*, *42*(5), 998–1007. https://doi.org/10.1002/jimd.12110

Bateman, A. (2019). UniProt: A worldwide hub of protein knowledge. *Nucleic Acids Research*, *47*(D1), D506–D515. https://doi.org/10.1093/nar/gky1049

Becker, C., Lust, K., & Wittbrodt, J. (2021). Igf signaling couples retina growth with body growth by modulating progenitor cell division. *Development*. https://doi.org/10.1242/dev.199133

Berg, J., Tymoczko, J., & Stryer, L. (2002). Section 8.4, The Michaelis-Menten Model Accounts for the Kinetic Properties of Many Enzymes. *Biochemistry. 5th Edition. New York: W H Freeman*. https://doi.org/10.1088/1751-8113/44/8/085201

Bio-Rad. (n.d.). Mini Trans-Blot® Electrophoretic Transfer Cell. *Bio-Rad*. Retrieved from https://www.bio-rad.com/webroot/web/pdf/lsr/literature/M1703930.pdf

Boersema, P. J., Raijmakers, R., Lemeer, S., Mohammed, S., & Heck, A. J. R. (2009). Multiplex peptide stable isotope dimethyl labeling for quantitative proteomics. *Nature Protocols*, *4*(4), 484–494. https://doi.org/10.1038/nprot.2009.21

Bogdańska, A., Lipiński, P., Szymańska-Rożek, P., Jezela-Stanek, A., Rokicki, D., Socha, P., & Tylki-Szymańska, A. (2021). Clinical, biochemical and molecular phenotype of congenital disorders of glycosylation: long-term follow-up. *Orphanet Journal of Rare Diseases*, *16*(1), 1–11. https://doi.org/10.1186/s13023-020-01657-5

Boon Ng, G. H., & Gong, Z. (2011). Maize Ac/Ds transposon system leads to highly efficient germline transmission of transgenes in medaka (Oryzias latipes). *Biochimie*, *93*(10), 1858–1864. https://doi.org/10.1016/j.biochi.2011.07.006

Brasil, S., Pascoal, C., Francisco, R., Marques-da-silva, D., Id, G. A., Videira, P. A., … Ferreira, R. (2018). *CDG Therapies : From Bench to Bedside*. (c), 1–47. https://doi.org/10.3390/ijms19051304

Brooks, S., Tyler, C. R., & Sumpter, J. P. (1997). Egg quality in fish: What makes a good egg? *Reviews in Fish Biology and Fisheries*, *7*(4), 387–416. https://doi.org/10.1023/A:1018400130692

Brum, J. M. (2013). Clinical and Molecular Features of Patients with Congenital Disorders of

Glycosylation in Brazil. *Pediatrics & Therapeutics*, *03*(03). https://doi.org/10.4172/2161-0665.s3-001

Buchanan, T., Freinkel, N., Lewis, N. J., Metzger, B. E., & Akazawa, S. (1985). Fuel-mediated teratogenesis. Use of D-mannose to modify organogenesis in the rat embryo in vivo. *Journal of Clinical Investigation*, *75*(6), 1927–1934. https://doi.org/10.1172/JCI111908

Butler, M., Quelhas, D., Critchley, A. J., Carchon, H., Hebestreit, H. F., Hibbert, R. G., … Rudd, P. M. (2003). Detailed glycan analysis of serum glycoproteins of patients with congenital disorders of glycosylation indicates the specific defective glycan processing step and provides an insight into pathogenesis. *Glycobiology*, *13*(9), 601–622. https://doi.org/10.1093/glycob/cwg079

Calvert, P. D., Krasnoperova, N. V., Lyubarsky, A. L., Isayama, T., Nicoló, M., Kosaras, B., … Lem, J. (2000). Phototransduction in transgenic mice after targeted deletion of the rod transducin α-subunit. *Proceedings of the National Academy of Sciences of the United States of America*, *97*(25), 13913–13918. https://doi.org/10.1073/pnas.250478897

Carl, M., Loosli, F., & Wittbrodt, J. (2002). Six3 inactivation reveals its essential role for the formation and patterning of the vertebrate eye. *Development*, *129*(17), 4057–4063.

Carrigan, M., Duignan, E., Humphries, P., Palfi, A., Kenna, P. F., & Farrar, G. J. (2016). A novel homozygous truncating GNAT1 mutation implicated in retinal degeneration. *The British Journal of Ophthalmology*, *100*(4), 495–500. https://doi.org/10.1136/bjophthalmol-2015-306939

Caussinus, E., Kanca, O., & Affolter, M. (2011). Fluorescent fusion protein knockout mediated by anti-GFP nanobody. *Nature Publishing Group*, *19*(1), 117–121. https://doi.org/10.1038/nsmb.2180

Ceroni, A., Maass, K., Geyer, H., Geyer, R., Dell, A., & Haslam, S. M. (2008). GlycoWorkbench: A tool for the computer-assisted annotation of mass spectra of glycans. *Journal of Proteome Research*, *7*(4), 1650–1659. https://doi.org/10.1021/pr7008252

Chan, B., Clasquin, M., Smolen, G. A., Histen, G., Powe, J., Chen, Y., … Jin, S. (2016). A mouse model of a human congenital disorder of glycosylation caused by loss of PMM2. *Human Molecular Genetics*, *25*(11), 2182–2193. https://doi.org/10.1093/hmg/ddw085

Chang, I. J., He, M., & Lam, C. T. (2018). Congenital disorders of glycosylation. *Annals of Translational Medicine*, *6*(24). https://doi.org/http://dx.doi.org/10.21037/atm.2018.10.45

Chen, J., Shi, G., Concepcion, F. A., Xie, G., Oprian, D., & Chen, J. (2006). Stable

rhodopsin/arrestin complex leads to retinal degeneration in a transgenic mouse model of autosomal dominant retinitis pigmentosa. *Journal of Neuroscience*, *26*(46), 11929–11937. https://doi.org/10.1523/JNEUROSCI.3212-06.2006

Chu, J., Mir, A., Gao, N., Rosa, S., Monson, C., Sharma, V., … Sadler, K. C. (2013). A zebrafish model of congenital disorders of glycosylation with phosphomannose isomerase deficiency reveals an early opportunity for corrective mannose supplementation. *Disease Models & Mechanisms*, *6*(1), 95–105. https://doi.org/10.1242/dmm.010116

Clement, E., Mercuri, E., Godfrey, C., Smith, J., Robb, S., Kinali, M., … Muntoni, F. (2008). Brain involvement in muscular dystrophies with defective dystroglycan glycosylation. *Annals of Neurology*, *64*(5), 573–582. https://doi.org/10.1002/ana.21482

Cline, A., Gao, N., Flanagan-Steet, H., Sharma, V., Rosa, S., Sonon, R., … Steet, R. (2012). A zebrafish model of PMM2-CDG reveals altered neurogenesis and a substrate-accumulation mechanism for N-linked glycosylation deficiency. *Molecular Biology of the Cell*, *23*(21), 4175–4187. https://doi.org/10.1091/mbc.e12-05-0411

Coddeville, B., Carchon, H., Jaeken, J., Briand, G., & Spik, G. (1998). Determination of glycan structures and molecular masses of the glycovariants of serum transferrin from a patient with carbohydrate deficient syndrome type II. *Glycoconjugate Journal*, *15*(3), 265–273. https://doi.org/10.1023/A:1006997012617

Collin, G. B., Gogna, N., Chang, B., Damkham, N., Pinkney, J., Hyde, L. F., … Krebs, M. P. (2020). Mouse Models of Inherited Retinal Degeneration with Photoreceptor Cell Loss. *Cells*, *9*(4), 1–67. https://doi.org/10.3390/cells9040931

Conley, S. M., Stuck, M. W., Watson, J. N., & Naash, M. I. (2017). Rom1 converts Y141C-Prph2-associated pattern dystrophy to retinitis pigmentosa. *Human Molecular Genetics*, *26*(3), 509–518. https://doi.org/10.1093/hmg/ddw408

Corey, D. R., & Abrams, J. M. (2001). Morpholino antisense oligonucleotides: Tools for investigating vertebrate development. *Genome Biology*, *2*(5), 3–5. https://doi.org/10.1186/gb-2001-2-5-reviews1015

Cossins, J., Belaya, K., Hicks, D., Salih, M. A., Finlayson, S., Carboni, N., … Beeson, D. (2013). Congenital myasthenic syndromes due to mutations in ALG2 and ALG14. *Brain*, *136*(3), 944–956. https://doi.org/10.1093/brain/awt010

Cox, J., & Mann, M. (2008). MaxQuant enables high peptide identification rates, individualized p.p.b.-range mass accuracies and proteome-wide protein quantification. *Nature Biotechnology*, *26*(12), 1367–1372. https://doi.org/10.1038/nbt.1511

Cylwik, B., Lipartowska, K., Chrostek, L., & Gruszewska, E. (2013). Congenital disorders of glycosylation. Part II. Defects of protein o-glycosylation. *Acta Biochimica Polonica*, *60*(3), 361–368.

Daenzer, J. M. I., Sanders, R. D., Hang, D., & Fridovich-Keil, J. L. (2012). UDP-Galactose 4′-epimerase activities toward UDP-Gal and UDP-GaLNAc play different roles in the development of Drosophila melanogaster. *PLoS Genetics*, *8*(5), 1–9. https://doi.org/10.1371/journal.pgen.1002721

Daniel, K., Icha, J., Horenburg, C., Müller, D., Norden, C., & Mansfeld, J. (2018). Conditional control of fluorescent protein degradation by an auxin-dependent nanobody. *Nature Communications*, *9*(1). https://doi.org/10.1038/s41467-018-05855-5

David, A. L., & Peebles, D. (2008). Gene therapy for the fetus: is there a future? *Best Practice and Research in Clinical Obstetrics and Gynaecology*, *22*(1), 203–218. https://doi.org/10.1016/j.bpobgyn.2007.08.008

de la Fuente, M., Peñas, P. F., & Sols, A. (1986). Mechanism of mannose toxicity. *Biochemical and Biophysical Research Communications*, *140*(1), 51–55. https://doi.org/10.1016/0006-291X(86)91056-9

DeRossi, C., Bode, L., Eklund, E. A., Zhang, F., Davis, J. A., Westphal, V., … Freeze, H. H. (2006). Ablation of mouse phosphomannose isomerase (Mpi) causes mannose 6-phosphate accumulation, toxicity, and embryonic lethality. *Journal of Biological Chemistry*, *281*(9), 5916–5927. https://doi.org/10.1074/jbc.M511982200

Dharmasiri, N., Dharmasiri, S., & Estelle, M. (2005). The F-box protein TIR1 is an auxin receptor. *Nature*, *435*(7041), 441–445. https://doi.org/10.1038/nature03543

Dryja, T. P. (1990). Mutations Within The Rhodopsin Gene In Patients With Autosomal Dominant Retinitis Pigmentosa. *The New England Journal of Medicine*, 1302–1307.

Dupré, T., Vuillaumier-Barrot, S., Chantret, I., Yayé, H. S., Le Bizec, C., Afenjar, A., … Moore, S. E. H. (2010). Guanosine diphosphate-mannose: GlcNAc2-PP-dolichol mannosyltransferase deficiency (congenital disorders of glycosylation type Ik): Five new patients and seven novel mutations. *Journal of Medical Genetics*, *47*(11), 729–735. https://doi.org/10.1136/jmg.2009.072504

El-Brolosy, M. A., Kontarakis, Z., Rossi, A., Kuenne, C., Günther, S., Fukuda, N., … Stainier, D. Y. R. (2019). Genetic compensation triggered by mutant mRNA degradation. *Nature*, *568*(7751), 193–197. https://doi.org/10.1038/s41586-019-1064-z

Engel, A. G. (2018). Congenital Myasthenic Syndromes in 2018. *Current Neurology and Neuroscience Reports*. https://doi.org/10.1007/s11910-018-0852-4

Fazio, M., Avagyan, S., Van Rooijen, E., Mannherz, W., Kaufman, C. K., Lobbardi, R., … Zon, L. I. (2017). Efficient Transduction of Zebrafish Melanoma Cell Lines and Embryos Using Lentiviral Vectors. *Zebrafish*, *14*(4), 379–382. https://doi.org/10.1089/zeb.2017.1434

Frank, C. G., Grubenmann, C. E., Eyaid, W., Berger, E. G., Aebi, M., & Hennet, T. (2004). Identification and functional analysis of a defect in the human ALG9 gene: Definition of congenital disorder of glycosylation type IL. *American Journal of Human Genetics*, *75*(1), 146–150. https://doi.org/10.1086/422367

Freeze, H. H. (2002). Human disorders in N-glycosylation and animal models. *Biochimica et Biophysica Acta - General Subjects*, *1573*(3), 388–393. https://doi.org/10.1016/S0304-4165(02)00408-7

Freeze, H. H. (2007). Congenital Disorders of Glycosylation : CDG-I , CDG-II , and Beyond. *Current Molecular Medicine*, *7*(4), 389–396.

Freeze, H. H. (2009). Towards a therapy for phosphomannomutase 2 deficiency, the defect in CDG-Ia patients. *Biochimica et Biophysica Acta - Molecular Basis of Disease*, *1792*(9), 835–840. https://doi.org/10.1016/j.bbadis.2009.01.004

Freeze, H. H., Eklund, E. A., Ng, B. G., & Patterson, M. C. (2012). Neurology of inherited glycosylation disorders. *The Lancet Neurology*, *11*(5), 453–466. https://doi.org/10.1016/S1474-4422(12)70040-6

Freeze, H. H., Schachter, H., & Kinoshita, T. (2017). Chapter 45-Genetic Disorders of Glycosylation. In *Essentials of Glycobiology, 3rd edition*. https://doi.org/10.1101/glycobiology.3e.045

Freinkel, N., Lewis, N. J., Akazawa, S., Roth, S. I., & Gorman, L. (1984). The Honeybee Syndrome-Implications of the Teratogenicity of MAnnose in Rat Embryo Culture. *The New England Journal of Medicine*.

Fribley, A., Zhang, K., & Kaufman, R. J. (2009). Regulation of apoptosis by the unfolded protein response. *Methods Mol Biol.*, *559*, 191–204. https://doi.org/10.1007/978-1-60327-017-5_14

Fricker, M., Tolkovsky, A. M., Borutaite, V., Coleman, M., & Brown, G. C. (2018). Neuronal cell death. *Physiological Reviews*, *98*(2), 813–880. https://doi.org/10.1152/physrev.00011.2017

Froschauer, A., Sprott, D., Gerwien, F., Henker, Y., Rudolph, F., Pfennig, F., & Gutzeit, H. O. (2012). Effective generation of transgenic reporter and gene trap lines of the medaka (Oryzias latipes) using the Ac/Ds transposon system. *Transgenic Research*, *21*(1), 149–

162. https://doi.org/10.1007/s11248-011-9514-x

Gámez, A., Serrano, M., Gallego, D., Vilas, A., & Pérez, B. (2020). New and potential strategies for the treatment of PMM2-CDG. *Biochimica et Biophysica Acta - General Subjects*, *1864*(11), 129686. https://doi.org/10.1016/j.bbagen.2020.129686

Gao, X. D., Nishikawa, A., & Dean, N. (2004). Physical interactions between the Alg1, Alg2, and Alg11 mannosyltransferases of the endoplasmic reticulum. *Glycobiology*, *14*(6), 559–570. https://doi.org/10.1093/glycob/cwh072

Godfrey, C., Foley, A. R., Clement, E., & Muntoni, F. (2011). Dystroglycanopathies: Coming into focus. *Current Opinion in Genetics and Development*, *21*(3), 278–285. https://doi.org/10.1016/j.gde.2011.02.001

Goreta, S. S., Dabelic, S., & Dumic, J. (2012). Insights into complexity of congenital disorders of glycosylation. *Biochemia Medica*, *22*(2), 156–170. https://doi.org/10.11613/bm.2012.019

Gotte, G., Libonati, M., & Laurents, D. V. (2003). Glycosylation and Specific Deamidation of Ribonuclease B Affect the Formation of Three-dimensional Domain-swapped Oligomers. *Journal of Biological Chemistry*, *278*(47), 46241–46251. https://doi.org/10.1074/jbc.M308470200

Grabher, C., Henrich, T., Sasado, T., Arenz, A., Wittbrodt, J., & Furutani-Seiki, M. (2003). Transposon-mediated enhancer trapping in medaka. *Gene*, *322*(1–2), 57–66. https://doi.org/10.1016/j.gene.2003.09.009

Grabher, C., & Wittbrodt, J. (2007). Meganuclease and transposon mediated transgenesis in medaka. *Genome Biology*, *8(Suppl 1)*(S10). https://doi.org/10.1186/gb-2007-8-s1-s10

Grünewald, S. (2009). The clinical spectrum of phosphomannomutase 2 deficiency (CDG-Ia). *Biochimica et Biophysica Acta - Molecular Basis of Disease*, *1792*(9), 827–834. https://doi.org/10.1016/j.bbadis.2009.01.003

Guan, G., Zhang, X., Naruse, K., Nagahama, Y., & Hong, Y. (2014). Gene Replacement by Zinc Finger Nucleases in Medaka Embryos. *Marine Biotechnology*, *16*(6), 739–747. https://doi.org/10.1007/s10126-014-9587-7

Gücüm, S., Sakson, R., Hoffmann, M., Grote, V., Beedgen, L., Thiel, C., … Thumberger, T. (2020). The medaka alg2 mutant is a model for hypo-N-glycosylation-associated retinitis pigmentosa. *BioRxiv*. https://doi.org/https://doi.org/10.1101/2020.08.20.260430

Gutierrez-Triana, J. A., Tavhelidse, T., Thumberger, T., Thomas, I., Wittbrodt, B., Kellner, T., … Wittbrodt, J. (2018). Efficient single-copy HDR by 5’ modified long dsDNA donors. *ELife*, *7*. https://doi.org/10.7554/eLife.39468

Haeuptle, M. A., & Hennet, T. (2009). Congenital disorders of glycosylation: An update on defects affecting the biosynthesis of dolichol-linked oligosaccharides. *Human Mutation*, *30*(12), 1628–1641. https://doi.org/10.1002/humu.21126

Haeuptle, M. A., Welti, M., Troxler, H., Hülsmeier, A. J., Imbach, T., & Hennet, T. (2011). Improvement of dolichol-linked oligosaccharide biosynthesis by the squalene synthase inhibitor zaragozic acid. *Journal of Biological Chemistry*, *286*(8), 6085–6091. https://doi.org/10.1074/jbc.M110.165795

Harding, H. P., Zhang, Y., Khersonsky, S., Marciniak, S., Scheuner, D., Kaufman, R. J., … Ron, D. (2005). Bioactive small molecules reveal antagonism between the integrated stress response and sterol-regulated gene expression. *Cell Metabolism*, *2*(6), 361–371. https://doi.org/10.1016/j.cmet.2005.11.005

Hashimoto, H., Miyamoto, R., Watanabe, N., Shiba, D., Ozato, K., Inoue, C., … Wakamatsu, Y. (2009). Polycystic kidney disease in the medaka (Oryzias latipes) pc mutant caused by a mutation in the Gli-similar3 (glis3) gene. *PLoS ONE*, *4*(7), 9–12. https://doi.org/10.1371/journal.pone.0006299

Haynes, P. A. (1998). Phosphoglycosylation: A new structural class of glycosylation? *Glycobiology*, *8*(1), 1–5. https://doi.org/10.1093/glycob/8.1.1

Helenius, A., & Aebi, M. (2004). Roles of N-linked glycans in the endoplasmic reticulum. *Annual Review of Biochemistry*, *73*, 1019–1049. https://doi.org/10.1146/annurev.biochem.73.011303.073752

Hennet, T., & Cabalzar, J. (2015). Congenital disorders of glycosylation: A concise chart of glycocalyx dysfunction. *Trends in Biochemical Sciences*, *40*(7), 377–384. https://doi.org/10.1016/j.tibs.2015.03.002

Hennig, R., Cajic, S., Borowiak, M., Hoffmann, M., Kottler, R., Reichl, U., & Rapp, E. (2016). Towards personalized diagnostics via longitudinal study of the human plasma N-glycome. *Biochimica et Biophysica Acta - General Subjects*, Vol. 1860, pp. 1728–1738. https://doi.org/10.1016/j.bbagen.2016.03.035

Hetz, C. (2012). The unfolded protein response: Controlling cell fate decisions under ER stress and beyond. *Nature Reviews Molecular Cell Biology*, *13*(2), 89–102. https://doi.org/10.1038/nrm3270

Hill, J. T., Demarest, B. L., Bisgrove, B. W., Su, Y. C., Smith, M., & Yost, H. J. (2014). Poly peak parser: Method and software for identification of unknown indels using sanger sequencing of polymerase chain reaction products. *Developmental Dynamics*, *243*(12), 1632–1636. https://doi.org/10.1002/dvdy.24183

Hülsmeier, A. J., Tobler, M., Burda, P., & Hennet, T. (2016). Glycosylation site occupancy in health, congenital disorder of glycosylation and fatty liver disease. *Scientific Reports*, *6*(October), 1–12. https://doi.org/10.1038/srep33927

Imtiaz, F., Worthington, V., Champion, M., Beesley, C., Charlwood, J., Clayton, P., … Winchester, B. (2000). Genotypes and phenotypes of patients in the UK with carbohydrate-deficient glycoprotein syndrome type 1. *Journal of Inherited Metabolic Disease*, *23*(2), 162–174. https://doi.org/10.1023/A:1005669900330

Ioffe, E., & Stanley, P. (1994). Mice lacking N-acetylglucosaminyltransferase I activity die at mid-gestation , revealing an essential role for complex or hybrid N-linked carbohydrates. *Proc. Natl. Acad. Sci. USA*, *91*(January), 728–732.

Iwamatsu, T. (2004). Stages of normal development in the medaka Oryzias latipes. *Mechanisms of Development*, *121*(7–8), 605–618. https://doi.org/10.1016/J.MOD.2004.03.012

Jaeken, J. (2003). Komrower Lecture. Congenital disorders of glycosylation (CDG): it's all in it! *Journal of Inherited Metabolic Disease*, *26*(2–3), 99–118. https://doi.org/10.1007/s10545-011-9299-3

Jaeken, J. (2010). Congenital disorders of glycosylation. *Annals of The New York Academy of Sciences*, *1214*, 190–198. https://doi.org/doi: 10.1111/j.1749-6632.2010.05840.x

Jaeken, J., & Carchon, H. (2001). Congenital disorders of glycosylation: The rapidly growing tip of the iceberg. *Current Opinion in Neurology*, *14*(6), 811–815. https://doi.org/10.1097/00019052-200112000-00021

Jayaprakash, N. G., & Surolia, A. (2017). Role of glycosylation in nucleating protein folding and stability. *Biochemical Journal*, *474*(14), 2333–2347. https://doi.org/10.1042/BCJ20170111

Jinek, M., Chylinski, K., Fonfara, I., Hauer, M., Doudna, J. A., & Charpentier, E. (2012). A programmable dual-RNA-guided DNA endonuclease in adaptive bacterial immunity. *Science*, *337*(6096), 816–821. https://doi.org/10.1126/science.1225829

Kamler, E. (2008). Resource allocation in yolk-feeding fish. *Reviews in Fish Biology and Fisheries*, *18*(2), 143–200. https://doi.org/10.1007/s11160-007-9070-x

Kämpf, M., Absmanner, B., Schwarz, M., & Lehle, L. (2009). Biochemical characterization and membrane topology of Alg2 from Saccharomyces cerevisiae as a bifunctional α1,3- and 1,6-mannosyltransferase involved in lipid-linked oligosaccharide biosynthesis. *Journal of Biological Chemistry*, *284*(18), 11900–11912. https://doi.org/10.1074/jbc.M806416200

Kaushal, S., Ridge, K. D., & Khorana, H. G. (1994). Structure and function in rhodopsin: The role of asparagine-linked glycosylation. *Proceedings of the National Academy of Sciences of the United States of America*, *91*(9), 4024–4028. https://doi.org/10.1073/pnas.91.9.4024

Kawasaki, T., Saito, K., Mitsui, K., Ikawa, M., Yamashita, M., Taniguchi, Y., … Sakai, N. (2009). *Introduction of a Foreign Gene into Zebrafish and Medaka Cells Using Adenoviral Vectors Toshihiro*. *6*. https://doi.org/10.1089=zeb.2009.0596 Original

Kjaergaard, S., Schwartz, M., & Skovby, F. (2001). Congenital disorder of glycosylation type Ia (CDG-Ia): Phenotypic spectrum of the R141H/F119L genotype. *Archives of Disease in Childhood*, *85*(3), 236–239. https://doi.org/10.1136/adc.85.3.236

Kleijer, W. J., van der Sterre, M. L. T., Garritsen, V. H., Raams, A., & Jaspers, N. G. J. (2011). Evolution of prenatal detection of neural tube defects in the pregnant population of the city of Barcelona from 1992 to 2006. *Prenatal Diagnosis*, *31*(10), 1184–1188. https://doi.org/10.1002/pd

Congenital Disorders of Glycosylation [Internet Source] (2015). Retrieved January 21, 2021 from https://rarediseases.org/rare-diseases/congenital-disorders-of-glycosylation/

Kurita, K., Burgess, S. M., & Sakai, N. (2004). Transgenic zebrafish produced by retroviral infection of in vitro-cultured sperm. *Proceedings of the National Academy of Sciences of the United States of America*, *101*(5), 1263–1267. https://doi.org/10.1073/pnas.0304265101

Lam, B. L., Züchner, S. L., Dallman, J., Wen, R., Alfonso, E. C., Vance, J. M., & Peričak-Vance, M. A. (2014). Mutation K42E in dehydrodolichol diphosphate synthase (DHDDS) causes recessive retinitis pigmentosa. *Advances in Experimental Medicine and Biology*, *801*, 165–170. https://doi.org/10.1007/978-1-4614-3209-8_21

Li, S. T., Wang, N., Xu, X. X., Fujita, M., Nakanishi, H., Kitajima, T., … Gao, X. D. (2018). Alternative routes for synthesis of N-linked glycans by Alg2 mannosyltransferase. *FASEB Journal*, *32*(5), 2492–2506. https://doi.org/10.1096/fj.201701267R

Li, Y. H., Tardif, G., Hum, D., Kapoor, M., Fahmi, H., Pelletier, J. P., & Martel-Pelletier, J. (2016). The unfolded protein response genes in human osteoarthritic chondrocytes: PERK emerges as a potential therapeutic target. *Arthritis Research and Therapy*, *18*(1), 1–12. https://doi.org/10.1186/s13075-016-1070-6

Lindahl, U., Couchman, J., Kimata, K., & Esko, J. D. (2009). Chapter 17: Proteoglycans and Sulfated Glycosaminoglycans. In *Essentials of Glycobiology, 3rd edition*. https://doi.org/10.1101/glycobiology.3e.017

Loosli, F., Köster, R. W., Carl, M., Kühnlein, R., Henrich, T., Mücke, M., … Wittbrodt, J. (2000). A genetic screen for mutations affecting embryonic development in medaka fish (Oryzias latipes). *Mechanisms of Development*, *97*(1–2), 133–139. https://doi.org/10.1016/S0925-4773(00)00406-8

Luderman, L. N., Unlu, G., & Knapik, E. W. (2017). Zebrafish Developmental Models of Skeletal Diseases. In *Current Topics in Developmental Biology* (1st ed., Vol. 124). https://doi.org/10.1016/bs.ctdb.2016.11.004

Ma, C. C., Wang, Z. L., Xu, T., He, Z. Y., & Wei, Y. Q. (2020). The approved gene therapy drugs worldwide: from 1998 to 2019. *Biotechnology Advances*, *40*(December 2019), 107502. https://doi.org/10.1016/j.biotechadv.2019.107502

Malhotra, A., Pateman, A., Chalmers, R., Coman, D., & Menahem, S. (2009). Prenatal cardiac ultrasound finding in congenital disorder of glycosylation type 1a. *Fetal Diagnosis and Therapy*, *25*(1), 54–57. https://doi.org/10.1159/000196816

Marktel, S., Scaramuzza, S., Cicalese, M. P., Giglio, F., Galimberti, S., Lidonnici, M. R., … Ferrari, G. (2019). Intrabone hematopoietic stem cell gene therapy for adult and pediatric patients affected by transfusion-dependent ß-thalassemia. *Nature Medicine*, *25*(2), 234–241. https://doi.org/10.1038/s41591-018-0301-6

Matsumoto, T., Terai, S., Oishi, T., Kuwashiro, S., Fujisawa, K., Yamamoto, N., … Sakaida, I. (2010). Medaka as a model for human nonalcoholic steatohepatitis. *DMM Disease Models and Mechanisms*, *3*(7–8), 431–440. https://doi.org/10.1242/dmm.002311

Matthijs, G., Schollen, E., Pardon, E., Veiga-da-cunha, M., Jaeken, J., Cassiman, J., & Schaftingen, E. Van. (1997). Mutations in PMM2, a phosphomannomutase gene on chromosome 16p13, in carbohydrate-deficient glycoprotein type I syndrome (Jaeken syndrome). *Nature Genetics*, *16*.

Matthijs, G., Schollen, E., Van Schaftingen, E., Cassiman, J. J., & Jaeken, J. (1998). Lack of homozygotes for the most frequent disease allele in carbohydrate-deficient glycoprotein syndrome type 1A. *American Journal of Human Genetics*, *62*(3), 542–550. https://doi.org/10.1086/301763

Mayatepek, E., & Kohlmuller, D. (1998). Mannose supplementation in carbohydrate-deficient glycoprotein syndrome type I and phosphomannomutase deficiency. *European Journal of Pediatrics*, *157*(7), 605–606. https://doi.org/10.1007/s004310050889

Mills, P. B., Mills, K., Mian, N., Winchester, B. G., & Clayton, P. T. (2003). Mass spectrometric analysis of glycans in elucidating the pathogenesis of CDG type IIx. *Journal of Inherited Metabolic Disease*, *26*(2–3), 119–134.

https://doi.org/10.1023/A:1024476915278

Monies, D. M., Al-Hindi, H. N., Al-Muhaizea, M. A., Jaroudi, D. J., Al-Younes, B., Naim, E. A., … Bohlega, S. (2014). Clinical and pathological heterogeneity of a congenital disorder of glycosylation manifesting as a myasthenic/myopathic syndrome. *Neuromuscular Disorders*, *24*(4), 353–359. https://doi.org/10.1016/j.nmd.2013.12.010

Monin, M. L., Mignot, C., De Lonlay, P., Héron, B., Masurel, A., Mathieu-Dramard, M., … Héron, D. (2014). 29 French adult patients with PMM2-congenital disorder of glycosylation: outcome of the classical pediatric phenotype and depiction of a late-onset phenotype. *Orphanet Journal of Rare Diseases*, *9*, 207. https://doi.org/10.1186/s13023-014-0207-4

Morava, E., Wevers, R. A., Cantagrel, V., Hoefsloot, L. H., Al-Gazali, L., Schoots, J., … Lefeber, D. J. (2010). A novel cerebello-ocular syndrome with abnormal glycosylation due to abnormalities in dolichol metabolism. *Brain*, *133*(11), 3210–3220. https://doi.org/10.1093/brain/awq261

Moremen, K. W., Tiemeyer, M., & Nairn, A. V. (2014). Vertebrate protein glycosylation: diversity, synthesis and function. *Nat Rev Mol Cell Biol*, *13*(7), 448–462. https://doi.org/10.1038/nrm3383

Murray, A. R., Fliesler, S. J., & Al-Ubaidi, M. R. (2009). Rhodopsin: The Functional Significance of Asn Linked Glycosylation and Other Post Translational Modifications. *Ophthalmic Genetics*. https://doi.org/10.1080/13816810902962405

Murray, A. R., Vuong, L., Brobst, D., Fliesler, S. J., Peachey, N. S., Gorbatyuk, M. S., … Al-Ubaidi, M. R. (2015). Glycosylation of rhodopsin is necessary for its stability and incorporation into photoreceptor outer segment discs. *Human Molecular Genetics*, *24*(10), 2709–2723. https://doi.org/10.1093/hmg/ddv031

Naldini, L. (2019). Genetic engineering of hematopoiesis: current stage of clinical translation and future perspectives. *EMBO Molecular Medicine*, *11*(3), 1–12. https://doi.org/10.15252/emmm.201809958

Ng, B. G., & Freeze, H. H. (2018). Perspectives on Glycosylation and Its Congenital Disorders. *Trends in Genetics*, *34*(6), 466–476. https://doi.org/10.1016/j.tig.2018.03.002

Ng, B. G., Shiryaev, S. A., Rymen, D., Eklund, E. A., Raymond, K., Kircher, M., … Freeze, H. H. (2016). ALG1-CDG: Clinical and Molecular Characterization of 39 Unreported Patients. *Human Mutation*, *37*(7), 653–660. https://doi.org/10.1002/humu.22983

Panneerselvam, K., & Freeze, H. H. (1996). Mannose corrects altered N-glycosylation in carbohydrate-deficient glycoprotein syndrome fibroblasts. *Journal of Clinical*

Investigation, *97*(6), 1478–1487. https://doi.org/10.1172/JCI118570

Paprocka, J., Jezela-Stanek, A., Tylki-Szymańska, A., & Grunewald, S. (2021). Congenital disorders of glycosylation from a neurological perspective. *Brain Sciences*, *11*(1), 1–25. https://doi.org/10.3390/brainsci11010088

Péanne, R., de Lonlay, P., Foulquier, F., Kornak, U., Lefeber, D. J., Morava, E., … Jaeken, J. (2018). Congenital disorders of glycosylation (CDG): Quo vadis? *European Journal of Medical Genetics*, *61*(11), 643–663. https://doi.org/10.1016/j.ejmg.2017.10.012

Pengyuan Liu, Lynn A. Beer, Bonnie Ky, Kurt T. Barnhart, and D. W. S. (2017). Quantitative comparisons of large numbers of human plasma samples using TMT10plex labeling. *Methods Mol Biol.* https://doi.org/10.1007/978-1-4939-7057-5_22

Peranteau, W. H., & Flake, A. W. (2020). The Future of In Utero Gene Therapy. *Molecular Diagnosis and Therapy*, *24*(2), 135–142. https://doi.org/10.1007/s40291-020-00445-y

Praissman, J. L., & Wells, L. (2014). Mammalian O-mannosylation pathway: Glycan structures, enzymes, and protein Substrates. *Biochemistry*, *53*(19), 3066–3078. https://doi.org/10.1021/bi500153y

Puig, B., Altmeppen, H., & Glatzel, M. (2014). The GPI-anchoring of PrP Implications in sorting and pathogenesis. *Prion*, *8*(1), 11–18. https://doi.org/10.4161/pri.27892

Qiagen. (2019). *RNeasy Mini Handbook*. Retrieved from https://www.qiagen.com/us/resources/resourcedetail?id=14e7cf6e-521a-4cf7-8cbc-bf9f6fa33e24&lang=en

Qiagen. (2020). *QIAprep Miniprep Handbook*. Retrieved from https://www.qiagen.com/us/resources/download.aspx?id=22df6325-9579-4aa0-819c-788f73d81a09&lang=en

R Core Team. (2018). *R: A language and environment for statistical computing*. Retrieved from https://www.r-project.org/

Rao, R. V., & Bredesen, D. E. (2004). Misfolded proteins, endoplasmic reticulum stress and neurodegeneration. *Current Opinion in Cell Biology*, *16*(6), 653–662. https://doi.org/10.1016/j.ceb.2004.09.012

Reily, C., Stewart, T. J., Renfrow, M. B., & Novak, J. (2019). Glycosylation in health and disease. *Nature Reviews Nephrology*, *15*(6), 346–366. https://doi.org/10.1038/s41581-019-0129-4

Reinhardt, R., Centanin, L., Tavhelidse, T., Inoue, D., Wittbrodt, B., Concordet, J., … Wittbrodt, J. (2015). Sox2, Tlx, Gli3, and Her9 converge on Rx2 to define retinal stem cells in vivo . *The EMBO Journal*, *34*(11), 1572–1588.

https://doi.org/10.15252/embj.201490706

Roche. (2016). *In Situ Cell Death Detection Kit, TMR red*. Retrieved from https://www.sigmaaldrich.com/content/dam/sigma-aldrich/docs/Roche/Bulletin/1/12156792910bul.pdf

Roos, J., Sternglanz, R., & Lennarz, W. J. (1994). A screen for yeast mutants with defects in the dolichol-mediated pathway for N-glycosylation. *Proceedings of the National Academy of Sciences of the United States of America*, *91*(4), 1485–1489. https://doi.org/10.1073/pnas.91.4.1485

Rossi, A., Kontarakis, Z., Gerri, C., Nolte, H., Hölper, S., Krüger, M., & Stainier, D. Y. R. (2015). Genetic compensation induced by deleterious mutations but not gene knockdowns. *Nature*, *524*(7564), 230–233. https://doi.org/10.1038/nature14580

RStudio Team. (n.d.). *RStudio*. Retrieved from https://www.rstudio.com/

Rupp, R. A. W., Snider, L., & Weintraub, H. (1994). Xenopus embryos regulate the nuclear localization of XMyoD. *Genes and Development*, *8*(11), 1311–1323. https://doi.org/10.1101/gad.8.11.1311

Sakson, R., Beedgen, L., Bernhard, P., Alp, K. M., Lübbehusen, N.-C., Röth, R., … Ruppert, T. (2020). Targeted Proteomics Reveals Quantitative Differences in Low Abundance Glycosyltransferases of Patients with Congenital Disorders of Glycosylation. *BioRxiv*, 2020.09.15.291732. Retrieved from https://doi.org/10.1101/2020.09.15.291732

Santhanam, A., Shihabeddin, E., Atkinson, J. A., Nguyen, D., Lin, Y. P., & O'Brien, J. (2020). A Zebrafish Model of Retinitis Pigmentosa Shows Continuous Degeneration and Regeneration of Rod Photoreceptors. *Cells*, *9*(10). https://doi.org/10.3390/cells9102242

Sarkar, M., Leventis, P. A., Silvescu, C. I., Reinhold, V. N., Schachter, H., & Boulianne, G. L. (2006). Null mutations in Drosophila N-acetylglucosaminyltransferase I produce defects in locomotion and a reduced life span. *The Journal of Biological Chemistry*, *281*(18), 12776–12785. https://doi.org/10.1074/jbc.M512769200

Schiller, S., Rosewich, H., Grünewald, S., & Gärtner, J. (2020). Inborn errors of metabolism leading to neuronal migration defects. *Journal of Inherited Metabolic Disease*, *43*(1), 145–155. https://doi.org/10.1002/jimd.12194

Schindelin, J., Arganda-Carreras, I., Frise, E., Kaynig, V., Longair, M., Pietzsch, T., … Cardona, A. (2012). Fiji: An open-source platform for biological-image analysis. *Nature Methods*, *9*(7), 676–682. https://doi.org/10.1038/nmeth.2019

Shi, T., Su, D., Liu, T., Tang, K., Camp, D. G., Qian, W. J., & Smith, R. D. (2012). Advancing the sensitivity of selected reaction monitoring-based targeted quantitative

proteomics. *Proteomics*, *12*(8), 1074–1092. https://doi.org/10.1002/pmic.201100436

Shima, A., & Shimada, A. (1991). Development of a possible nonmammalian test system for radiation-induced germ-cell mutagenesis using a fish, the Japanese medaka (Oryzias latipes). *Proceedings of the National Academy of Sciences of the United States of America*, *88*(6), 2545–2549. https://doi.org/10.1073/pnas.88.6.2545

Shima, A., & Shimada, A. (1994). The Japanese medaka, Oryzias latipes, as a new model organism for studying environmental germ-cell mutagenesis. *Environmental Health Perspectives*, *102*(SUPPL. 12), 33–35. https://doi.org/10.1289/ehp.94102s1233

Sippel, K. C., DeStefano, J. D., Berson, E. L., & Dryja, T. P. (1996). Screen of the human arrestin gene in patients with retinitis pigmentosa and Oguchi disease. *Investigative Ophthalmology and Visual Science*, *37*(3).

Stanley, P. (2016). What Have We Learned from Glycosyltransferase Knockouts in Mice ? *Journal of Molecular Biology*, *428*(16), 3166–3182. https://doi.org/10.1016/j.jmb.2016.03.025

Stelzer, G., Rosen, N., Plaschkes, I., Zimmerman, S., Twik, M., Fishilevich, S., … Lancet, D. (2016). The GeneCards suite: From gene data mining to disease genome sequence analyses. *Current Protocols in Bioinformatics*, *2016*(June), 1.30.1-1.30.33. https://doi.org/10.1002/cpbi.5

Sun, L., Zhao, Y., Zhou, K., Freeze, H. H., Zhang, Y. W., & Xu, H. (2013). Insufficient ER-stress response causes selective mouse cerebellar granule cell degeneration resembling that seen in congenital disorders of glycosylation. *Molecular Brain*, *6*(1), 2–9. https://doi.org/10.1186/1756-6606-6-52

Tadros, W., & Lipshitz, H. D. (2009). The maternal-to-zygotic transition: A play in two acts. *Development*, *136*(18), 3033–3042. https://doi.org/10.1242/dev.033183

Thal, D. R., & Fändrich, M. (2015). Protein aggregation in Alzheimer's disease: Aβ and τ and their potential roles in the pathogenesis of AD. *Acta Neuropathologica*, *129*(2), 163–165. https://doi.org/10.1007/s00401-015-1387-2

Thermo Fisher Scientific. (2020). *Pierce BCA Protein Assay Kit*. Retrieved from https://www.thermofisher.com/document-connect/document-connect.html?url=https%3A%2F%2Fassets.thermofisher.com%2FTFS-Assets%2FLSG%2Fmanuals%2FMAN0011430_Pierce_BCA_Protein_Asy_UG.pdf&title=VXNlciBHdWlkZTogUGllcmNlIEJDQSBQcm90ZWluIEFzc2F5IEtpdA==

Thiel, C., Lubke, T., Matthijs, G., von Figura, K., & Korner, C. (2006). Targeted Disruption of the Mouse Phosphomannomutase 2 Gene Causes Early Embryonic Lethality.

Molecular and Cellular Biology, *26*(15), 5615–5620. https://doi.org/10.1128/mcb.02391-05

Thiel, C., & Körner, C. (2011). Mouse models for congenital disorders of glycosylation. *Journal of Inherited Metabolic Disease*, *34*(4), 879–889. https://doi.org/10.1007/s10545-011-9295-7

Thiel, C., Schwarz, M., Peng, J., Grzmil, M., Hasilik, M., Braulke, T., … Kö, C. (2003). A New Type of Congenital Disorders of Glycosylation (CDG-Ii) Provides New Insights into the Early Steps of Dolichol-linked Oligosaccharide Biosynthesis. *The Journal of Biological Chemistry*, *278*(25), 22498–22505. https://doi.org/10.1074/jbc.M302850200

Thiesler, C. T., Cajic, S., Hoffmann, D., Thiel, C., Van Diepen, L., Hennig, R., … Buettner, F. F. R. (2016). Glycomic characterization of induced pluripotent stem cells derived from a patient suffering from phosphomannomutase 2 congenital disorder of glycosylation (PMM2-CDG). *Molecular and Cellular Proteomics*, *15*(4), 1435–1452. https://doi.org/10.1074/mcp.M115.054122

Thompson, D. A., Lyons, R. J., Russell-Eggitt, I., Liasis, A., Jägle, H., & Grünewald, S. (2013). Retinal characteristics of the congenital disorder of glycosylation PMM2-CDG. *Journal of Inherited Metabolic Disease*, *36*(6), 1039–1047. https://doi.org/10.1007/s10545-013-9594-2

Tsai, Y. H., Liu, X., & Seeberger, P. H. (2012). Chemical biology of glycosylphosphatidylinositol anchors. *Angewandte Chemie - International Edition*, *51*(46), 11438–11456. https://doi.org/10.1002/anie.201203912

Tyanova, S., Temu, T., Sinitcyn, P., Carlson, A., Hein, M. Y., Geiger, T., … Cox, J. (2016). The Perseus computational platform for comprehensive analysis of (prote)omics data. *Nature Methods*, *13*(9), 731–740. https://doi.org/10.1038/nmeth.3901

Uemura, N., Koike, M., Ansai, S., Kinoshita, M., Ishikawa-Fujiwara, T., Matsui, H., … Takahashi, R. (2015). Viable Neuronopathic Gaucher Disease Model in Medaka (Oryzias latipes) Displays Axonal Accumulation of Alpha-Synuclein. *PLoS Genetics*, *11*(4), 1–22. https://doi.org/10.1371/journal.pgen.1005065

Varki, A., Cummings, R. D., Esko, J. D., Freeze, H. H., Stanley, P., Marth, J. D., … Etzler, M. E. (2009). Symbol nomenclature for glycan representation. *Proteomics*, *9*(24), 5398–5399. https://doi.org/10.1002/pmic.200900708

Verbakel, S. K., van Huet, R. A. C., Boon, C. J. F., den Hollander, A. I., Collin, R. W. J., Klaver, C. C. W., … Klevering, B. J. (2018). Non-syndromic retinitis pigmentosa. *Progress in Retinal and Eye Research*, *66*(November 2017), 157–186.

https://doi.org/10.1016/j.preteyeres.2018.03.005

Verheijen, J., Tahata, S., Kozicz, T., Witters, P., & Morava, E. (2020). Therapeutic approaches in Congenital Disorders of Glycosylation (CDG) involving N-linked glycosylation: an update. *Genetics in Medicine*, *22*(2), 268–279. https://doi.org/10.1038/s41436-019-0647-2

Vuillaumier-Barrot, S., Bouchet-Séraphin, C., Chelbi, M., Devisme, L., Quentin, S., Gazal, S., … Seta, N. (2012). Identification of mutations in TMEM5 and ISPD as a cause of severe cobblestone lissencephaly. *American Journal of Human Genetics*, *91*(6), 1135–1143. https://doi.org/10.1016/j.ajhg.2012.10.009

Waddington, S. N., Kramer, M. G., Hernandez-Alcoceba, R., Buckley, S. M. K., Themis, M., Coutelle, C., & Prieto, J. (2005). In utero gene therapy: Current challenges and perspectives. *Molecular Therapy*, *11*(5), 661–676. https://doi.org/10.1016/j.ymthe.2005.01.015

Walker, A. K., Soo, K. Y., Levina, V., H. Talbo, G., & Atkin, J. D. (2012). N–linked glycosylation modulates dimerization of protein disulfide isomerase family A member 2 (PDIA2) Adam. *The FEBS Journal*. https://doi.org/10.1111/febs.12063

Wang, J., Lee, J., Liem, D., & Ping, P. (2017). HSPA5 Gene Encoding Hsp70 Chaperone BiP in the Endoplasmic Reticulum. *Gene*, *618*, 14–23. https://doi.org/10.1016/j.gene.2017.03.005

Wang, S., He, Q., Ye, J., Kang, Z., Zheng, Q., Liu, S., … Sun, L. (2020). N-linked Glycosylation and its Potential Application in Drug Development. *Health Science Journal*, *14*(5), 743. https://doi.org/10.36648/1791-809X.14.5.743

Wessel, D., & Flügge, U. I. (1984). A method for the quantitative recovery of protein in dilute solution in the presence of detergents and lipids. *Analytical Biochemistry*, *138*(1), 141–143. https://doi.org/10.1016/0003-2697(84)90782-6

Westphal, V., Peterson, S., Patterson, M., Tournay, A., Blumenthal, A., Treacy, E. P., & Freeze, H. H. (2001). Functional significance of PMM2 mutations in mildly affected patients with congenital disorders of glycosylation Ia. *Genetics in Medicine*, *3*(6), 393–398. https://doi.org/10.1097/00125817-200111000-00003

White, D. A., Hauswirth, W. W., Kaushal, S., & Lewin, A. S. (2007). Increased sensitivity to light-induced damage in a mouse model of autosomal dominant retinal disease. *Investigative Ophthalmology and Visual Science*, *48*(5), 1942–1951. https://doi.org/10.1167/iovs.06-1131

Wittbrodt, J., Shima, A., & Schartl, M. (2002). Medaka - A model organism from the Far

East. *Nature Reviews Genetics*, *3*(1), 53–64. https://doi.org/10.1038/nrg704

Witters, P., Cassiman, D., & Morava, E. (2017). Nutritional therapies in congenital disorders of glycosylation (CDG). *Nutrients*, *9*(11), 1–10. https://doi.org/10.3390/nu9111222

Yang, H., Ren, S., Yu, S., Pan, H., Li, T., Ge, S., … Xia, N. (2020). Methods favoring homology-directed repair choice in response to crispr/cas9 induced-double strand breaks. *International Journal of Molecular Sciences*, *21*(18), 1–20. https://doi.org/10.3390/ijms21186461

Yau, J. W., Teoh, H., & Verma, S. (2015). Endothelial cell control of thrombosis. *BMC Cardiovascular Disorders*, *15*(1), 1–11. https://doi.org/10.1186/s12872-015-0124-z

Yuste-Checa, P., Gámez, A., Brasil, S., Desviat, L. R., Ugarte, M., Pérez-Cerdá, C., & Pérez, B. (2015). The Effects of PMM2-CDG-Causing Mutations on the Folding, Activity, and Stability of the PMM2 Protein. *Human Mutation*, *36*(9), 851–860. https://doi.org/10.1002/humu.22817

Zecha, J., Meng, C., Zolg, D. P., Samaras, P., Wilhelm, M., & Kuster, B. (2018). Peptide level turnover measurements enable the study of proteoform dynamics. *Molecular and Cellular Proteomics*, *17*(5), 974–992. https://doi.org/10.1074/mcp.RA118.000583

Zhuo, Y., Yang, J. Y., Moremen, K. W., & Prestegard, J. H. (2016). Glycosylation alters dimerization properties of a cell-surface signaling protein, carcinoembryonic antigen-related cell Adhesion Molecule 1 (CEACAM1). *Journal of Biological Chemistry*, *291*(38), 20085–20095. https://doi.org/10.1074/jbc.M116.740050

Zou, M., De Koninck, P., Neve, R. L., & Friedrich, R. W. (2014). Fast gene transfer into the adult zebrafish brain by herpes simplex virus 1 (HSV-1) and electroporation: Methods and optogenetic applications. *Frontiers in Neural Circuits*, *8*(MAY), 1–16. https://doi.org/10.3389/fncir.2014.00041

Züchner, S., Dallman, J., Wen, R., Beecham, G., Naj, A., Farooq, A., … Peričak-Vance, M. A. (2011). Whole-exome sequencing links a variant in DHDDS to retinitis pigmentosa. *American Journal of Human Genetics*, *88*(2), 201–206. https://doi.org/10.1016/j.ajhg.2011.01.001

Declaration

Herewith I declare that I prepared the PhD Thesis "Modeling hypo-*N*-glycosylation in medaka, *Oryzias latipes*, to decipher mechanisms of Congenital Disorders of Glycosylation" on my own and with no other sources and aids than quoted.

Heidelberg, 2021